NASA/TM-2004-213234

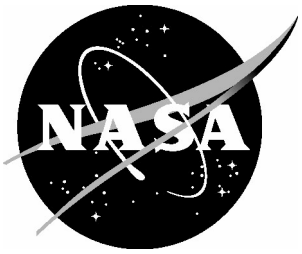

Evaluation and Analysis of F-16XL Wind Tunnel Data From Static and Dynamic Tests

Sungwan Kim and Patrick C. Murphy
Langley Research Center, Hampton, Virginia

Vladislav Klein
The George Washington University
Joint Institute for Advancement of Flight Sciences
Langley Research Center, Hampton, Virginia

June 2004

The NASA STI Program Office . . . in Profile

Since its founding, NASA has been dedicated to the advancement of aeronautics and space science. The NASA Scientific and Technical Information (STI) Program Office plays a key part in helping NASA maintain this important role.

The NASA STI Program Office is operated by Langley Research Center, the lead center for NASA's scientific and technical information. The NASA STI Program Office provides access to the NASA STI Database, the largest collection of aeronautical and space science STI in the world. The Program Office is also NASA's institutional mechanism for disseminating the results of its research and development activities. These results are published by NASA in the NASA STI Report Series, which includes the following report types:

- TECHNICAL PUBLICATION. Reports of completed research or a major significant phase of research that present the results of NASA programs and include extensive data or theoretical analysis. Includes compilations of significant scientific and technical data and information deemed to be of continuing reference value. NASA counterpart of peer-reviewed formal professional papers, but having less stringent limitations on manuscript length and extent of graphic presentations.

- TECHNICAL MEMORANDUM. Scientific and technical findings that are preliminary or of specialized interest, e.g., quick release reports, working papers, and bibliographies that contain minimal annotation. Does not contain extensive analysis.

- CONTRACTOR REPORT. Scientific and technical findings by NASA-sponsored contractors and grantees.

- CONFERENCE PUBLICATION. Collected papers from scientific and technical conferences, symposia, seminars, or other meetings sponsored or co-sponsored by NASA.

- SPECIAL PUBLICATION. Scientific, technical, or historical information from NASA programs, projects, and missions, often concerned with subjects having substantial public interest.

- TECHNICAL TRANSLATION. English-language translations of foreign scientific and technical material pertinent to NASA's mission.

Specialized services that complement the STI Program Office's diverse offerings include creating custom thesauri, building customized databases, organizing and publishing research results ... even providing videos.

For more information about the NASA STI Program Office, see the following:

- Access the NASA STI Program Home Page at ***http://www.sti.nasa.gov***

- E-mail your question via the Internet to help@sti.nasa.gov

- Fax your question to the NASA STI Help Desk at (301) 621-0134

- Phone the NASA STI Help Desk at (301) 621-0390

- Write to:
  NASA STI Help Desk
  NASA Center for AeroSpace Information
  7121 Standard Drive
  Hanover, MD 21076-1320

NASA/TM-2004-213234

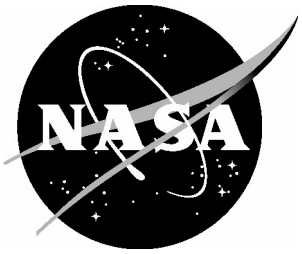

Evaluation and Analysis of F-16XL Wind Tunnel Data From Static and Dynamic Tests

Sungwan Kim and Patrick C. Murphy
Langley Research Center, Hampton, Virginia

Vladislav Klein
The George Washington University
Joint Institute for Advancement of Flight Sciences
Langley Research Center, Hampton, Virginia

National Aeronautics and
Space Administration

Langley Research Center
Hampton, Virginia 23681-2199

June 2004

Available from:

NASA Center for AeroSpace Information (CASI)
7121 Standard Drive
Hanover, MD 21076-1320
(301) 621-0390

National Technical Information Service (NTIS)
5285 Port Royal Road
Springfield, VA 22161-2171
(703) 605-6000

Summary

A series of wind tunnel tests were conducted in the NASA Langley Research Center as part of an ongoing effort to develop and test mathematical models for aircraft rigid-body aerodynamics in nonlinear unsteady flight regimes. Analysis of measurement accuracy, especially for nonlinear dynamic systems that may exhibit complicated behaviors, is an essential component of this ongoing effort. In this report, tools for harmonic analysis of dynamic data and assessing measurement accuracy are presented. A linear aerodynamic model is assumed that is appropriate for conventional forced-oscillation experiments, although more general models can be used with these tools. Application of the tools to experimental data is demonstrated and results indicate the levels of uncertainty in output measurements that can arise from experimental setup, calibration procedures, mechanical limitations, and input errors.

Nomenclature

a_0, a_k, b_k	Fourier coefficients
b	wing span, m
C_L, C_N, C_m	lift, normal force, pitching-moment coefficients
C_D, C_A, C_Y, C_l, C_n	drag, axial, side force, rolling-moment, yawing-moment coefficients
C_{L_α}, C_{L_q}	indicial functions
$\overline{C}_{L_\alpha}, \overline{C}_{L_q}$	in-phase, out-of-phase components of C_L
$\overline{C}_{N_\alpha}, \overline{C}_{N_q}$	in-phase, out-of-phase components of C_N
$\bar{c}$	wing mean aerodynamic chord, m
e	error
f	frequency, Hz
i	time index
k	harmonic analysis index or reduced frequency ($k = \omega\ell / V$)
ℓ	characteristic length, $\ell = \bar{c} / 2$
m	number of harmonics
N	number of measurements
N_r	number of repeated runs
n	time index
n_c	number of cycles
q	pitching velocity, rad/sec
R^2	multiple correlation coefficient
s^2	estimated variance
S	wing area, m^2
T	period, sec
t	time, sec
V	airspeed, m/sec
y	true value
z	measurement

Symbols

α	angle of attack, rad or deg
ε	estimation error
θ	parameter or pitch angle, rad or deg
σ, σ^2	standard deviation, variance
ω	angular frequency, rad/sec
Δ	increment

Superscripts

a	actual value
s	expected value
ˆ	estimated value
.	time derivative
-	mean value
⎯	oscillatory data

Subscripts

A	amplitude
a	actual value
E	Measurement
i	time index
k	harmonic analysis index
M	model
n	time index
s	expected value
0	nominal value

Aerodynamic derivatives

$$C_{L_a}(\infty) \equiv C_{L_a} = \frac{\partial C_L}{\partial a} \quad \text{for } a = \frac{q\bar{c}}{2V}, \frac{\dot{q}\bar{c}^2}{4V^2}, \alpha, \frac{\dot{\alpha}\bar{c}}{2V}$$

1 Introduction

A concern in any scientific experiment is the issue of obtaining sufficient measurement accuracy. In particular, it is a concern when investigating nonlinear dynamic systems since these systems can exhibit behaviors that may substantially complicate responses and model identification. For these experiments the amount of care taken in both experiment design and measurement procedures will be reflected in the final measurement accuracy. Two approaches can be used to estimate measurement accuracy. One approach is to use repeated measurements that allow a statistical estimate of the measurement variance to be made. This approach can be costly and time consuming in some cases; however, it has the advantage of directly reflecting measurement uncertainty. Another approach, based on system identification theory, is to utilize the difference between measured responses and that predicted by an adequate model. The advantage in this case is that repeated measurements are not required, although the presence of any modeling error will increase the residual error. Both approaches are presented and compared in this report.

For the latter approach, a method is presented for harmonic analysis utilizing the least squares principle. In this approach, tools for assessing both accuracy of measured outputs and accuracy of parameter estimates are presented. Application of the tools to both repeated and ensemble-averaged experimental data is demonstrated. In this analysis, a linear aerodynamic model appropriate for conventional forced-oscillation experiments is assumed although more general aerodynamic models can also be used with the tools presented.

In an effort to obtain a more general formulation of the aerodynamic model for aircraft, a series of wind tunnel tests were conducted in the NASA Langley Research Center (LaRC) 12-Foot Low-Speed Tunnel using a 10% scale model of the F-16XL. Two tunnel tests, conducted in 1996 and 2000, provided static and dynamic data for nonlinear modeling research. Initial studies identifying unsteady aerodynamic models from these data were reported[1-3]. During both the 1996 and 2000 experiments, for certain test conditions and signals, forced oscillation measurements did not reflect the expected harmonic motion related to the input signal. Single-run time histories and ensemble-averaged time histories were used to determine the final experimental results, namely, non-dimensional static forces, static moments, and stability derivatives. Combinations of stability derivatives were estimated in the conventional form of in-phase and out-of-phase components. No evaluation of the measurement data (before averaging) was done to test repeatability of the 1996 data. During the 2000 experiment, to reduce ensemble average errors and to enhance measurement accuracy analysis, each test was repeated 10 times. As part of a review process for these experiments, an initial evaluation of measurement accuracy for the 2000 experiment has been done and is presented in this report.

Many problems that occur in testing can be quickly removed through careful monitoring by test engineers. However, in modern test facilities there is always a desire to automate systems to achieve greater production with fewer errors. This may tend to remove the test engineer from close observation of the experiment. Also, some measurement error may not be immediately observable without analysis. In any case data with greater error than desired may be produced even when experimentalists exercise significant care. In this report, examples of problem data that can occur during testing are provided and then procedures to reduce these problems, in an automated testing environment, are suggested.

The uncertainty of an experimental measurement is a combination of bias error and precision error. The squared sum of these terms is often used although other formulations are sometimes used[4]. In order to eliminate systematic errors or bias errors, careful calibration and attention to environmental variables are required. Bias errors can be difficult and in some cases impossible to estimate and remove from the data after the experiment is performed. Therefore in this report only precision of the output measurements and estimated parameters will be evaluated. Also no attempt is made to separate contributions to uncertainty from other factors such as scale effects or wind-tunnel turbulence. Since rigid body dynamics are assumed for this work and the dynamic rig is assumed to be rigid, aeroelastic or structural responses of the scale model and dynamic rig are not investigated.

This report presents both static and dynamic data that have been obtained from single frequency forced-oscillation tests in the LaRC 12-Foot Tunnel. Analysis is limited to static and small amplitude dynamic data in order to limit nonlinear responses contained in the measurements. The approach for harmonic analysis described in this report facilitates testing this assumption as part of the analysis. Model description, test conditions, and measurement parameters are described in Section 2. In Section 3, tools for analysis are presented. Application of the tools to estimate accuracy of output measurements and model parameter estimates is provided in Section 4. Concluding remarks provide an overall assessment of the analysis tools and measurement accuracy of the 2000 data.

2 Model and Tests

The same 10% scale model of an F-16XL was tested in the LaRC 12-Foot Low-Speed Tunnel during both the 1996 and 2000 experiments. A three-dimensional view of the model is shown in Figure 1. The model was mounted on a dynamic test rig through a six-component strain-gauge balance. The dynamic test rig is a computer controlled hydraulically actuated system that was sting-mounted on a C-strut support system. The mounting arrangement rotated the model about the reference center of gravity location of $0.558\,\bar{c}$, over an angle of attack range of -5° to 80°. The maximum capability of the dynamic test rig was 260 deg/sec pitch rate and 2,290 deg/sec^2 pitch

acceleration. Further description of the dynamic test rig may be found in Ref. [5]. The tests were conducted at a dynamic pressure of 192 Pa (= 4 psf) producing an equivalent wind speed of V=17.52 m/sec and a Reynolds number of 10^6 based on the mean aerodynamic chord.

During dynamic tests, pitch angle readings were made with a Linear Variable Differential Transformer (LVDT), six-component force and moment data (C_A, C_N, C_m, C_Y, C_l, and C_n) were obtained from a strain-gauge balance, and wind tunnel dynamic pressure measurements were obtained from pressure transducer. Data were sampled at 100 Hz with an in-line 100 Hz low-pass filter. To compensate the effect of gravitational force and inertial effects wind-off tares were made for each test and subtracted from wind-on measurements. Repeated runs were made at the same test conditions and ensemble averages over the repeated runs were computed. After obtaining the ensemble average, all data channels were subsequently filtered using a digital 6 Hz low-pass filter.

For the 2000 experiment, all test data were obtained at zero sideslip, zero deflection of leading-edge flaps, and zero deflection of trailing-edges surfaces (flaperons and elevons). Static data were obtained for angles of attack from -2° to 70° and single frequency forced oscillations data were obtained at 5 different frequencies (0.5, 0.9, 1.1, 1.5, and 2.0 Hz) and 13 different values of the initial angle of attack (α_0 = 2, 5, 10, 15, 20, 25, 30, 35, 40, 45, 50, 55, and 60 degrees) with amplitude of ±5°.

3 Theoretical Tools

Analysis and evaluation methods, metrics to assess measurement accuracy, and procedures that may help to identify and reduce measurement error are offered in this report as a means of improving final experimental results. To make the discussion more tractable, experimental measurements (dynamic data) are evaluated and analyzed, in Section 4, under three headings: Timing Signal, Input Measurements, and Output Measurements. In this section the main tools for analysis and evaluation are presented. First, a method for harmonic analysis that facilitates computation of higher harmonics and parameter error bounds is presented. This method effectively provides a test to detect nonlinear responses when nonzero high-order harmonics exist. Second, a conventional linear aerodynamic model representing a single degree of freedom forced-oscillation experiment is presented. Third, key metrics for assessing measurement accuracy are provided. Metric sensitivities to measurement errors and thresholds defining acceptable levels of error are presented in Section 4.

Measurement error, e, is generally assumed to be a zero mean, normally distributed, stochastic process with variance, σ^2. Measurement, z, true value, y, and error, e are related as

$$z = y + e \,. \tag{1}$$

In this case, $E[z] = y$ and $E[(z-y)^2] = \sigma^2$. Since the true value, y, is unknown and unknowable, a

model is usually identified that provides estimates of the responses as $\hat{y}$. Using the model estimates of response, the measurement equation becomes

$$z = \hat{y} + \varepsilon .$$

In this case, $E[\varepsilon^2]$ does not equal σ^2, since the model estimate $\hat{y}$ may contain error contributions from several sources. In addition to measurement error the model may be inadequate to predict the responses. For example, if the inputs produce nonlinear responses a linear model will be inadequate and predict responses with additional errors. The analysis method suggested in this report offers an approach that can detect this problem.

3.1 Harmonic Analysis

It is assumed that a periodic function $f(t) = f(t + 2\pi)$ with the period 2π is specified by a time series of measured data points $z(0), z(1), ..., z(N-1)$ at $t_i = \frac{2\pi}{N} i$ for $i = 0,1,...,(N-1)$.

Further, the postulated model for $y(i)$ is assumed in the form

$$y(i) = a_0 + \sum_{k=1}^{m} a_k \cos(k\omega_0 i) + \sum_{k=1}^{m} b_k \sin(k\omega_0 i) \tag{2}$$

where $\omega_0 = \frac{2\pi}{N}$ and $i = 1,2,...,N$ for $k = 1,2,...,m$.

The parameters a_0, a_k, and b_k are the Fourier coefficients obtained from the measured data by applying the least squares principle

$$Min \sum_{i=1}^{N} [z(i) - y(i)]^2 . \tag{3}$$

The resulting estimates of the parameters are the solution to the equation

$$\hat{\theta} = M^{-1} g \tag{4}$$

where

$$\hat{\theta} = \left[\hat{a}_0 \quad \hat{a}_1 \quad \hat{a}_2 \ \ldots\ \hat{a}_m \quad \hat{b}_1 \quad \hat{b}_2 \quad \hat{b}_3 \ \ldots\ \hat{b}_m\right]^T$$

$$g = \left[\sum_i z(i) \quad \sum_i z(i)\cos(\omega_0 i) \ \ldots\ \sum_i z(i)\cos(m\omega_0 i) \quad \sum_i z(i)\sin(\omega_0 i) \ \ldots\ \sum_i z(i)\sin(m\omega_0 i)\right]^T$$

$$M = diag\left[N \quad \frac{N}{2} \quad \frac{N}{2} \ \ldots\ \frac{N}{2}\right].$$

Then the parameter estimates are obtained as

$$\hat{a}_0 = \frac{1}{N}\sum_i z(i)$$
$$\hat{a}_k = \frac{2}{N}\sum_i z(i)\cos(kw_0 i) \quad . \tag{5}$$
$$\hat{b}_k = \frac{2}{N}\sum_i z(i)\sin(kw_0 i)$$

If the measurement errors $e(i) = z(i) - y(i)$ form a zero mean random sequence with the variance σ^2, then the parameter covariance matrix is

$$Cov(\hat{\theta}) = \sigma^2 M^{-1} . \tag{6}$$

The estimation for the variance σ^2 can be found as

$$s^2 = \frac{1}{N}\sum_i \left[z(i) - \hat{y}(i)\right]^2 \tag{7}$$

where

$$\hat{y}(i) = \hat{a}_0 + \sum_k \hat{a}_k \cos(k\omega_0 i) + \sum_k \hat{b}_k \sin(k\omega_0 i) . \tag{8}$$

From Eqs. (6) and (7), the estimates of parameter variance are

$$s^2(\hat{a}_0) = \frac{s^2}{N}$$
$$s^2(\hat{a}_k) = s^2(\hat{b}_k) = \frac{2s^2}{N} \tag{9}$$

for all *k*.

The model adequacy can be assessed by the Multiple Correlation Coefficient defined as

$$R^2 = 1 - \frac{\sum_i \left[z(i) - \hat{y}(i)\right]^2}{\sum_i \left[z(i) - \bar{z}\right]^2} \ , \ 0 < R^2 < 1 \tag{10}$$

where

$$\bar{z} = \frac{1}{N}\sum_i z(i) .$$

3.2 Conventional Forced Oscillation Analysis

During conventional forced-oscillation tests the model is assumed to undergo periodic motion. In this study only small amplitude motions are considered so linear responses are expected. For analysis

of this conventional oscillatory data it is assumed that the aerodynamic coefficients are linear functions of angle of attack, pitching velocity and their rates. Then the increment in the lift coefficient with respect to its mean value can be formulated as

$$\Delta C_L = C_{L_\alpha}\Delta\alpha + \frac{\ell}{V}C_{L_{\dot\alpha}}\dot\alpha + \frac{\ell}{V}C_{L_q}q + \left(\frac{\ell}{V}\right)^2 C_{L_{\dot q}}\dot q \tag{11}$$

where for the harmonic motion

$$\begin{aligned}\Delta\alpha &= \alpha_A \sin\omega t\\ \dot\alpha = q &= \omega\alpha_A \cos\omega t\\ \ddot\alpha = \dot q &= -\omega^2\alpha_A \sin\omega t\end{aligned} \quad . \tag{12}$$

Substitution of Eq. (12) into Eq. (11) yields

$$\begin{aligned}\Delta C_L &= \alpha_A\left(C_{L_\alpha} - k^2 C_{L_{\dot q}}\right)\sin\omega t + \alpha_A k\left(C_{L_{\dot\alpha}} + C_{L_q}\right)\cos\omega t\\ &= \alpha_A\left(\overline{C}_{L_\alpha}\sin\omega t + k\overline{C}_{L_q}\cos\omega t\right)\end{aligned} \tag{13}$$

where

$$k = \omega\ell / V \tag{14}$$

and

$$\alpha_A\overline{C}_{L_\alpha} = \alpha_A\left(C_{L_\alpha} - k^2 C_{L_{\dot q}}\right) \tag{15}$$

$$\alpha_A k\overline{C}_{L_q} = \alpha_A k\left(C_{L_{\dot\alpha}} + C_{L_q}\right) \tag{16}$$

represent the Fourier coefficients. The in-phase and out-of-phase components of C_L ($\overline{C}_{L_\alpha}$ and $\overline{C}_{L_q}$) can be obtained by integrating the time histories of ΔC_L over n_c cycles as

$$\begin{aligned}\overline{C}_{L_\alpha} &= \frac{2}{\alpha_A n_c T}\int_o^{n_c T}\Delta C_L(t)\sin\omega t\, dt\\ \overline{C}_{L_q} &= \frac{2}{\alpha_A k n_c T}\int_o^{n_c T}\Delta C_L(t)\cos\omega t\, dt\end{aligned} \tag{17}$$

where $T = 2\pi/\omega$. Using the results from harmonic analysis, the integrals in Eq. (17) represent continuous-time versions of Eq. (5). Therefore, the in-phase and out-of-phase components can be also expressed as

$$\begin{aligned}\overline{C}_{L_\alpha} &= \frac{\hat b_1}{\alpha_A}\\ \overline{C}_{L_q} &= \frac{\hat a_1}{k\alpha_A}\end{aligned} \tag{18}$$

and their variance as

$$s^2(\overline{C}_{L_\alpha}) = \frac{2}{N}\frac{s^2}{\alpha_A{}^2}$$
$$s^2(\overline{C}_{L_q}) = \frac{2}{N}\frac{s^2}{(k\alpha_A)^2} \quad . \tag{19}$$

3.3 Evaluation Metrics and Outlier Rejection Rules

The Multiple Correlation Coefficient (R^2), expressed in Eq. (10), may be computed as part of the parameter estimation process. This metric varies between 0 and 1 and provides a measure of model adequacy. As the output signal fails to be represented by the model, the R^2 term will be reduced from 1.

Mean square error (s^2) defined in Eq. (7) characterizes the fit error of the model. A check to determine how well this metric reflects measurement accuracy can be made if repeated measurements are available. Calculation of the variance from repeated measurements provides a direct estimate of measurement accuracy. The variance can be computed from repeated measurements at each point in time as

$$s_i^2(C_a(t_i)) = \frac{1}{N_r - 1}\sum_{r=1}^{N_r}\left([C_a(t_i)]_r - \overline{C}_a(t_i)\right)^2 \tag{20}$$

where N_r is the number of repeated runs, $C_a\,(t_i)$ is a measured value of an aerodynamic coefficient at time t_i, and $\overline{C}_a$ is the mean value of C_a for the repeated runs. From these results an equivalent fit error, comparable to Eq. (7), can be computed as

$$s^2 = \frac{1}{N}\sum_i s_i^2 \tag{21}$$

Comparison of s^2, computed from harmonic analysis in Eq. (7), with the variance computed from repeated measurements in Eqs. (20)-(21) provides an indication of the level of measurement accuracy and an indication of good model adequacy if the two metrics are close in value.

During execution of an experiment, occasionally data points are obtained that appear to be outliers. If the experimentalist can determine verifiable problems with those points then clearly these points should be removed. However, in some cases the results are not clearly wrong and no obvious problem can be found. Points at the edge of the 2σ bound might be good candidates for checking and certainly points outside the 2σ bound should be checked for problems. Statistical methods to check results can be easily automated so these tests can be used frequently. Among the various methods, two methods to statistically determine whether to reject outliers are Grubb's Test and Chauvenet's Criterion. These are summarized in Appendix A and Appendix B, respectively. Grubb's Test assumes a student's *t*-distribution to allow hypothesis testing. Chauvenet's Criterion uses a distribution defined

by the number of samples, *N*, such that points should be retained that fall within a region around the mean with probability *(1-1/(2N$_r$))*. Since Chauvenet's Criterion has achieved relatively wide acceptance[4], this criterion is used in this report.

4 Data Evaluation and Analysis

Evaluation and analysis methods proposed in this study are suggested as a method to assess measurement accuracy. In this report, the methodology has been applied as part of a data post-processing procedure; however, some calculations may be done during the experiment for a faster online assessment. This section demonstrates application of the analysis methods to sample data from the 2000 experiment.

4.1 Static Data

For static analysis, five longitudinal aerodynamic coefficients (C_N, C_A, C_m, C_L and C_D) are evaluated. C_N, C_A, and C_m are directly measured and C_L and C_D are computed from Eq. (22).

$$\begin{bmatrix} C_D \\ C_L \end{bmatrix} = \begin{bmatrix} \cos\alpha & \sin\alpha \\ -\sin\alpha & \cos\alpha \end{bmatrix} \begin{bmatrix} C_A \\ C_N \end{bmatrix}. \tag{22}$$

In the 2000 experiment, static measurements were made at two different sets of angle of attack settings. The first set was measured at 18 different values of angle of attack, (α = -2, 0, 5, 10, 15, 20, 25, 28, 30, 32, 34, 36, 38, 40, 45, 50, 60, and 70 degrees) and these measurements were repeated 3 times. The second set was measured at 38 angles of attack to determine if any aerodynamic critical points existed. Angles of attack for this set were at α = -2, 0, 5, 10, 11, 12, 13, 14, 15, 16, 17, 18, 19, 20, 21, 22, 23, 24, 25, 26, 27, 28, 29, 30, 31, 32, 33, 34, 35, 36, 37, 38, 39, 40, 45, 50, 60, and 70 degrees. Measurements at the second α-set were made only once. At each time before taking any measurement, instruments were calibrated with respect to each static test point. With this calibration, the bias error associated with angle of attack for each static point is less than ±0.05°.

A co-plot of the three data sets showing repeatability of the measurements is given in Figure 2. Repeated measurements allow an assessment of the output dispersion; in this example the repeated measurement of C_A begins to highlight an instrument problem. A plot of the aerodynamic coefficient mean values and their 2σ bounds for the three data sets is shown in Figure 3. These plots show the measurements are very repeatable with only the C_A coefficient showing significant dispersion at low angle of attack. For α <20°, the 2σ error bounds are somewhat large and inconsistent with values at other angles of attack. These error bounds are also inconsistent with that found for the other force and moment measurements. Although mean values for C_A are very small in this region, less dispersion

was computed at smaller mean values of C_A at other angles of attack. With this information, the test engineer is prompted to determine the source of the larger dispersions. One possible source was found to be measurement noise due to the dynamic range of the C_A data channel being scaled too large. This issue will be further addressed in Section 4.2.

Mean values and standard deviations of 5 aerodynamic coefficients are summarized in Table 1. Further verification of repeatability is shown by plotting the first α -set mean values against the second α -set measurements in Figure 4 and against the available 1996 static data in Figure 5. Measurements of the five longitudinal aerodynamic coefficients for the second α -set are summarized in Table 2. Figure 5 indicates static measurements, except the C_A coefficient, made during the 1996 and 2000 experiments were consistent and without any significant difference.

4.2 Dynamic Data

During dynamic tests, data from single-frequency forced oscillation in pitch were obtained at 5 different frequencies (0.5, 0.9, 1.1, 1.5, and 2.0 Hz) and 13 different mean angles of attack (α_0 = 2, 5, 10, 15, 20, 25, 30, 35, 40, 45, 50, 55, and 60 degrees) with amplitude of ±5°. Time histories of the aerodynamic coefficients were measured for 10 repeated runs at the same amplitude and frequency. The following table shows the corresponding angular velocities and reduced frequencies for each single frequency used in forced oscillation test.

Frequency (Hz)	W (rad/sec)	*k*
0.5	3.14	0.068
0.9	5.65	0.122
1.1	6.91	0.149
1.5	9.42	0.203
2.0	12.57	0.270

From Eq. (14), the corresponding reduced frequencies are given by

$$k = \frac{l}{V}\omega = \frac{\bar{c}}{2V}(2\pi f) = 0.1350 f$$

where $\bar{c} = 0.753$ meter and V=17.52 m/sec.

For the dynamic tests, instruments were not calibrated with respect to each initial angle of attack. The measured mean values of α_0 were 2.4, 5.4, 10.5, 15.6, 20.7, 25.8, 30.9, 36.0, 41.2, 46.6, 51.9, 57.6 and 63.4 degrees. The bias error for pitch angle varied from 0.4 to 3.4 degrees for this test range. During the repeated runs, the maximum deviation of α_0 was less than 0.1°.

A co-plot of 10 repeated runs is shown in Figure 6 and Figure 7 depicts the time history of the

corresponding ensemble average run. Here the oscillations are about $\alpha_0 = 20°$ and at a frequency of 1.1 Hz. The C_N measurement shows a good repeatability, while a degraded repeatability is depicted in C_m measurement. This degradation is addressed in Ref. [1] and the cause is still unknown. A significant anomaly is found in C_A measurement. It shows a large inconsistency over 10 repeated runs and the measurement was dominated by noise.

Before a detailed assessment of the experimental data, two questions need to be answered: how many repeats (both cycles and runs) are required to achieve stable estimates and how many harmonics in harmonic analysis are adequate for detailed analysis.

Number of Repeats

Each oscillatory time history was comprised of more than 5 cycles and the actual number of cycles generated at each test frequency is shown in the table below.

Test Frequency (Hz)	0.5	0.9	1.1	1.5	2
Number of Cycles	6	7	8	10	12

Theoretically one can estimate the unknown parameters with just one cycle of oscillation. However, by using both ensemble averaging and estimating over a number of cycles the effects of measurement noise can be effectively reduced. As an example, Table 3 shows in-phase and out-of-phase components of C_N and C_m estimated using only one run and an increasing number of cycles from 1 to 10. This case is for oscillations about $\alpha_0 = 10°$ and at a frequency of 1.5 Hz. In Figure 8, the values from Table 3 are plotted as circles against the mean values and standard deviations (solid and dashed lines) that are computed from, effectively, 100 cycles of data, i.e., an ensemble average of 10 repeated runs each containing 10 cycles. When the number of cycles used in a single run is 10, all 4 estimates are convergent to those mean values with very small errors. For the ensemble-averaged data analysis in this study, at each test frequency and test angle, the number of cycles used is effectively more than 60 since the analysis is done on an ensemble average run of 10 repeated runs with at least 6 cycles.

Number of Harmonics

Before using harmonic analysis described in Section 3.1, the required number of harmonics for an adequate model was investigated. For a linear system, only the primary harmonic is required. For this analysis, a single run, s726, is used where oscillations are about $\alpha_0 = 10°$ and the frequency is 1.5 Hz. Time histories of angle of attack, C_N, C_A, and C_m are shown in Figure 9. Figure 10 depicts co-plots of measured and estimated values of angle of attack, C_N, and C_m. Estimated values using only the first

harmonic are shown in the figure. The models with first harmonic for angle of attack and C_N are very close to measured data. The computed coefficients of the first harmonic in Eq. (2) are dominant, while the other coefficients for second and higher harmonics are negligible. Also, from Eq. (10), the computed value of R^2 using only the first harmonic is very close to 1 and there is almost no change when R^2 is computed with higher harmonics. For the pitching moment coefficient (C_m), the model using the first harmonic is also close to measured data and there is very little gained by adding the additional harmonics.

Figure 11 shows that the model for the axial force coefficient (C_A) with the first harmonic is insufficient to explain the measured data. Note that the model including the forth harmonic is reasonably close to the measurement. Also, computed coefficients of the forth harmonic are dominant and the corresponding R^2 value is close to 1. Since the test frequency was 1.5 Hz, the forth harmonic is 6 Hz, which is the same frequency as the digital low pass filter. This is very likely related to a low signal-to-noise ratio (SNR) issue instead of any non-linearity in the dynamics.

In general, models for all coefficients, except C_A, with just the first harmonic explain the measurements well, so analyses with the first harmonic are adequate for further investigation in this report.

4.2.1 Timing Signal

The first data check for dynamic tests should be to determine the accuracy of the time stamp and then the sample time fidelity. Accuracy of the time stamp may be an important issue when a large number of signals are measured. Time stamp accuracy was not an issue for this study. Checking the fidelity of the sample time during each duty cycle is a key test for dynamic experiments, especially when the analysis involves mathematical transforms. Commonly used transform algorithms require the sample time to be in equal time intervals. If a personal computer (PC) or workstation is used to run the real-time experiment, it is not uncommon for the operating system to introduce delays (from multitasking) in the duty cycle and thus produce uneven sample time intervals. If this type of error exists, it may require the data to be re-sampled or the experiment re-run depending on the degree of error. Re-sampling the data assumes that in spite of the duty cycle error, the measurements and the associated time stamp are still correct. If large delays or variable delays exist between the time stamp and measurement, then clearly no analysis would be possible. Fidelity of the sample time and accuracy of the time stamp must be ensured before any analysis is done. In some cases, if appropriate, analysis using time-domain least squares may be an option that might resolve the problem since the analysis would then be time independent.

A simple test metric to assess the degree of this problem is to compute the time difference, δt_a, between samples n and $n+1$. δt_a is defined as

$$\delta t_a = t_{n+1}^a - t_n^a \tag{23}$$

where "*a*" indicates actual sample times. For 100 Hz sample rate, a graph of δt_a vs. sample number index should always equal 0.01 seconds for perfect sample timing. Another helpful sample-time metric is defined as the time difference between actual measured time and expected clock time or simulated time, both at sample *n*. δt_s is defined as

$$\delta t_s = t_n^a - t_n^s \tag{24}$$

where "*s*" indicates expected clock time or simulated time. This metric reflects the cumulative delay experienced during the run. Consequently, as delays occur this metric will grow in magnitude and indicate the total delay for the whole run at the last index value. These two metrics in Eqs. (23) and (24) could be easily added to testing software to ensure high-fidelity sample times.

An example highlights some of the issues associated with checking sample time fidelity. Analysis of the 2000 data revealed some cases where sampling was not occurring at 100 Hz as expected. As desktop computers and workstations have become very fast it has become popular to use these machines to run experiments and real-time simulations. Although the operating system was required to give the highest priority to the experimental task, duty cycle slips likely occurred due to multi-user, multi-tasking, or system level service. Figure 12 (a) depicts the proper timing signal and duty cycle and Figure 12 (b) depicts the timing problem when a duty cycle slip or frame overrun occurs. Figure 12 (b) also shows another anomaly, unique to this experiment, i.e., sampling could be done faster than 100 Hz to compensate for any delay caused by duty cycle slips. This occurred because the data acquisition logic required the number of samples to be consistent with the desired sample rate and length of run where no sampling delays occur. Also the timing logic comparing actual time with desired time was not a controlling factor after a duty cycle slip.

Data, typical of 75% of all cases in this study, are shown in Figure 13. In the figure, the pitch angle position measurement in the wind tunnel (equivalent to angle of attack) is analyzed and found to have numerous cases where the sample time is not stepping in increments of 0.01 seconds as expected. In this example, the δt_a error is occasionally in the 20% to 30% range or 0.002 to 0.003 seconds. Note that no visible error appears in the angle of attack time history. Figure 13 also shows another timing metric, δt_s. In this particular experiment, the timing logic requiring a faster sample rate to make up missed samples and logic requiring the system to "catch up" has the effect of canceling any delays that occur. Consequently only for this particular experiment does this metric return to zero after a delay period.

Figures 13-17 provide a sequence showing the effect of increasing timing error. In Figure 14, a test case is shown with a timing error up to approximately 2.5 samples. This produced a time difference between 2 samples of 0.025 seconds at sample number 360. In this case, deviation of the

angle of attack time history from a sinusoid is becoming visible (at approximately 4.1 seconds). An offset in time exists between the sample numbers where delay occurs and the actual time associated with the distorted angle of attack signal. 25% of all test cases were found to have timing delay greater than 0.01 seconds or duty cycle slips greater than one cycle. Figure 15 shows a test case with timing slips greater than 6 samples. The angle-of-attack time history reflects this delay and shows significant distortion from the expected sinusoidal shape. 10% of all test runs contained timing delay greater than 0.05 seconds (5 cycle slips). A worst-case example is shown in Figure 16 where timing slips greater than 9 samples occurred more than 10 times in the specific single run. Figure 17 shows the corresponding time history data for the worst-case along with the rest of the ten ensemble runs. In this case, the abnormal run is clearly visible and easily detected and removed with only visual inspection.

To investigate the impact of duty cycle slip on experimental results a fictitious time delay followed by catch-up sequence was added to good data to create a second data set and allow comparison of final estimates of in-phase and out-of phase coefficients from the two different data sets. The test case used 1.5 Hz forced oscillation data at α_0=10°. Using ensemble-averaged data, estimates of mean values and standard deviations for this case, based on 100 combined cycles, are given in the table below.

	Mean	Standard Error
$\overline{C}_{N_\alpha}$	2.7273	0.0200
$\overline{C}_{N_q}$	4.5606	0.0582

Using a single run from the ensemble of runs, fictitious data were created with varying time delay injected at the 501st sample (= 5.5 sec). Test case data with 5, 10, 20 sample delays are shown in Figures 18-21. Distortion in the fictitious angle of attack is aggravated as more delays are added. The simulated results demonstrate similar distortion seen in measured data, shown in Figures 13-16. Results from the simulated cases, shown in the table below, provide mean values for a varying number of sample delays. The first column shows the mean value for the case without any delay.

Number of Slips	0	5	10	20	30	40
Delay (sec)	0.00	0.05	0.10	0.20	0.30	0.40
$\overline{C}_{N_\alpha}$	2.7349	2.7314	2.7252	2.7347	2.7441	2.6481
$\overline{C}_{N_q}$	4.5087	4.4944	4.4862	4.4391	4.0176	3.5128

Based on these results, estimated coefficients were within $\pm 2\sigma$ of their correct mean values

when delays were less than 10 samples. Since 90% of all test runs contained delays less than 0.05 seconds or 5 cycle slips, it is likely both in-phase and out-of phase coefficients for the 2000 experiment are computed within an error bound less than $\pm 2\sigma$. This is consistent with the intended purpose of the 2000 experiment but may not be satisfactory for investigations where nonlinear dynamics play a significant role.

4.2.2 Input Measurements

Input tests involve calculation of test metric values that should bring attention to faulty input signals and errors that may not be immediately visible in a graphic representation or in a large data set generated in an automated fashion. Graphical tests are always included, however, to catch relatively large or obvious errors. The numerical values of the test metrics are generally very large for cases where the errors become visible in a graph.

The primary input signal for this study was angle of attack, $\alpha(t)$, and it is the only input signal tested in this report. Secondary inputs are temperature and tunnel dynamic pressure. Tunnel dynamic pressure was manually monitored and adjusted to maintain a constant value prior to each run. Temperature was regularly recorded whenever calibration zeroes were recorded. Secondary inputs had very slow variation and are assumed to be constant for these dynamic tests.

In this section, three issues associated with the primary input measurement are addressed and then harmonic analysis, described in Section 3.1, is applied to check the impact of those anomalies in input measurement.

4.2.2.1 Effect of Timing Signal

Time delay, discussed in Section 4.2.1, impacts the angle of attack time history by causing a deviation from a single-frequency pure sinusoidal waveform (see Figures 14-16). Harmonic analysis of the input for the same set of data shown in Figures 13-16 is done to further investigate the timing issue. A model with the first harmonic is estimated and used to compute R^2 and s^2 from Eqs. (10) and (7). Computed values are shown in the below table.

Test Case	R^2	s^2
s726	0.9986	0.0043
s738	0.9978	0.0143
s768	0.9954	0.0454
s815	0.9615	0.4478

With bigger delays in time, R^2 decreases and s^2 increases. Though the trend makes sense, it is quite less sensitive than expected for this analysis. This result brought attention to the difference in using actual measured time vs. a timing index for analysis. A co-plot of the measured α (solid line)

and estimated α (dashed line) for test case s768 is shown in Figure 22 (top graph). A plot of measure α (solid line) used for harmonic analysis is suspicious between 6.2 sec and 6.7 sec. It is less distorted compared to Figure 15. This is because the actual measured time is not used for analysis. Instead, the timing index (sampling point) is used with a significant assumption that test data is equally spaced in time. When timing delay is present in the data an option might be to re-sample to create data that is equally spaced in time. Re-sampling is shown in Figure 23 for test case s768. The first two plots shows measured α with respect to measured time and measured α with respect to index (n0). The second plot shows less distortion compared to the first plot. After re-sampling the data, the re-sampled α with respect to the re-sampled index (n1) is shown in the next plot. The last plot is a co-plot of first and third plots and shows a good match. In this case re-sampling is a legitimate option to obtain evenly spaced data. Computed values with re-sampled data are shown in the below table. Also, a co-plot of re-sampled measured α (solid line) and estimated α (dashed line) for a test case s768 is shown in Figure 22 (bottom graph).

Test Case	R^2	s^2
s726	0.9986	0.0043
s738	0.9973	0.0203
s768	0.9850	0.1729
s815	0.1160	13.6544

Due to a significant distortion in test case s815 (Figures 16 and 17), R^2 is far less than 1 with a large error (s^2) and implies that the model with the first harmonic is inadequate. For other test cases, the values of R^2 and s^2, with respect to increasing timing delay, are meaningful though the sensitivity is not as large as expected. Using 10 repeated cycles for analysis caused the lack of sensitivity and reduced the impact of the small time delay. Analysis with one cycle could show the sensitivity in R^2 value but the analysis with one cycle is not recommended for this study. So, except few extreme cases, analysis indicates the estimated models were adequate to explain the data ($R^2 \approx 1, s^2 \ll 1$) and that the test data is reasonably well represented by linear models since a single-frequency harmonic was the dominant feature.

4.2.2.2 Calibration

A second test is a comparison of the commanded and measured input signals without the hardware in the loop, i.e., without including the test rig dynamics. This is intended to check software implementation.

A simplified block diagram of test setup is shown below and the output of the first conversion (from degree to voltage) is directly fed to the input of the second conversion (from voltage to degree)

as depicted with a dashed line. With a proper conversion, commanded and measured input values should be the same.

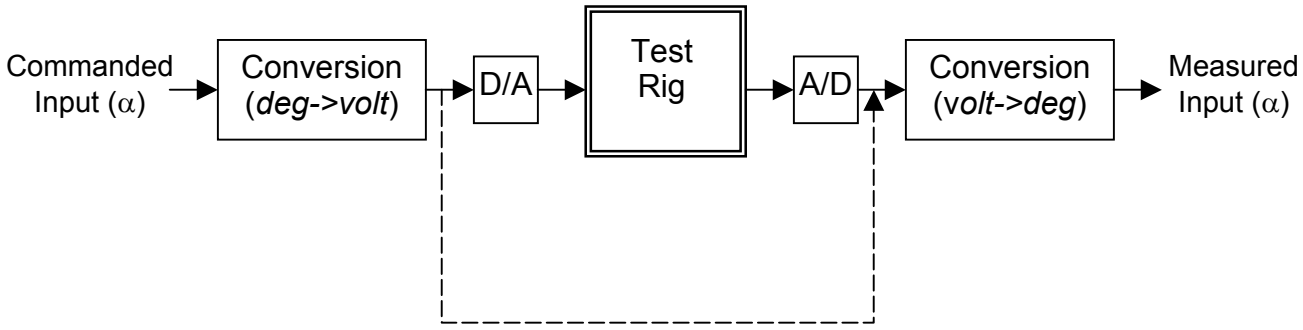

A test case is considered using 1.0 Hz forced oscillation data at α_0=70°. The top graph in Figure 24 shows an example of commanded and measured angle of attack versus sample number index. The second plot shows the difference or residuals between these two graphs. Besides relatively large residual values, a bias error of 4.7° exists and the amplitudes are different between the top and bottom of the oscillation (6.2459° vs. 6.5102°). This is shown in the bottom two graphs by subtracting out the mean angle of attack from the top two graphs. This also removes the bias between the two plots. These new large residuals brought attention to a calibration technique used for this experiment. In this case, instead of an exact point-to-point table look up to convert degree to voltage and visa-versa, a 3rd order polynomial approximation was used. This approach was intended to save test time but the cost was some distortion in the harmonic input signal. Deviation from a pure sinusoid introduced additional harmonics and biases into the experiment.

With the same test data, harmonic analysis with the first harmonic is used to compute R^2 and s^2. Computed values are presented in the below table.

Mean(α)	***Amplitude(α)***	R^2	s^2
74.7230°	6.3626°	0.9959	0.0023

A co-plot of measured α and estimated α, with the corresponding residuals, are shown in Figure 25. From Figure 25 and the computed values, the model with the first harmonic is close to measured angle of attack except for bias and scaling errors.

So, with the proper consideration of bias error (74.7230-70) and amplitude scaling error (6.3626/5), the test data presents reasonably linear dynamics, in the sense of having a single-frequency harmonic characteristic, and an adequate linear model where R^2 is almost 1 and s^2 is very small.

4.2.2.3 Mechanical Issues

The next test considers the mechanical system, Test Rig, in the above figure. A large "jump" distortion was found in several runs. As an example, Figures 26 and 27 shows the α signal plotted against time in the top graph and then the same plot with a zoomed view of the distortion in the lower graph. In cases where this problem occurred the large jump in α was always followed by a large timing error. Jump errors were sometimes large enough to observe visually during the test. This seems likely to be caused by a mechanical system anomaly.

Another input anomaly that may be caused by the mechanical system is input saturation. Since input saturation can defeat the planned input spectrum used to excite a dynamic system, it can be an issue for the test engineer. Figure 28 depicts this issue for the single-frequency forced oscillation experiment at 0.5 Hz and $\alpha_0 = 5°$. The effect of saturation is shown in the plots of α, C_L, and C_N. Figure 29 shows other input waveforms for different frequencies and different offset angles. Saturation is observed in the low frequency experiments and does not appear to be affected by offset angle variation. This may imply a mechanical limitation of the test rig, however, the exact source of this error has not been identified. Calibration error does not appear to be source of this error.

To investigate the impact of mechanical issues on inputs, the same test data (s789: $\alpha_0 = 45°$ and $f = 1.5$ Hz), shown in Figure 27, is used for harmonic analysis. With only the first harmonic, computed values of R^2 and s^2 fare shown in the below table. Since the jump anomaly was followed by a time delay, computed values with re-sampled data are also presented.

Test Case	R^2	s^2	Note
s789	0.9926	0.0873	with measured data
	0.9484	0.6949	with re-sampled data

Figure 30 depicts co-plots of measured α (solid line) and estimated α (dashed line). A top graph shows the test data used for analysis and a co-plot of re-sampled measured α (solid line) and estimated α (dashed line) is shown at the bottom. In the top graph, the data between 6 sec and 7 sec is suspicious compared to Figure 27, as already addressed in Section 4.2.2.1.

For the analysis of input saturation, computed values of R^2 and s^2 for a test case s217 ($\alpha_0 = 5°$ and $f = 0.5$ Hz) are shown in the below table. Similar to the last case, the model appears to be adequate.

Mean(α)	*Amplitude(α)*	R^2	s^2
5.3657°	5.3591°	0.9974	0.0110

In this section, three issues were addressed and harmonic analysis has been applied to assess the

impact by those issues. In general, the contribution from a large number of repeated cycles in each test case allows production of test data that is reasonably acceptable. However, these kinds of issues would need to be resolved for investigations into nonlinear regimes.

4.2.3 Output Measurements

After conversion to non-dimensional engineering units, aerodynamic total force and moment coefficients are direct output measurements. Substantial efforts have been made to develop methodology for ensuring data accuracy using various statistical measures. For this report, analysis is done with the assumption that the test facility has followed recommended procedure[6-7] and worked to obtain the accurate data. Even with this assumption, it is prudent for the investigator to evaluate experimental results. Fairly simple calculations can often be used to prevent a variety of errors and minimize data uncertainty.

In this section, a conventional linear aerodynamic model is assumed and harmonic analysis is performed on angle of attack and force and moment measurements to estimate the in-phase and out-of-phase model coefficients. Analysis of repeatability or dispersion of the time histories and the in-phase and out-of-phase components is investigated using the variance expressions given by Eqs. (19) and (21).

4.2.3.1 Aerodynamic Force and Moment Coefficients

For the total force and moment outputs, mean and standard deviation of total aerodynamic loads are computed from the 10 repeated single runs. The variance at each time instant is used to compute overall variance. Then, harmonic analysis is applied to the ensemble average run to estimate aerodynamic force coefficients with the parameter covariance matrix for the estimated coefficients.

A co-plot of 10 repeated runs and the ensemble average run (1.1 Hz and $\alpha_0 = 20°$), shown in Figures 6 and 7, are used as a first test case. With the first cycle of C_N, a co-plot of 10 single runs and the corresponding plot of computed mean values with 2σ bounds at each time instant are depicted in Figure 31. The overall variance, s_E^2, computed from Eq. (21) is 0.9939×10^{-4}.

After using only the first harmonic for harmonic analysis in Eq. (2) to compute an estimate of C_N, a co-plot of measured C_N and estimated C_N are also shown in Figure 31(bottom plot). This figure illustrates that the model with the first harmonic matches the measured data fairly well. The computed values of the parameter covariance, s_M^2, from Eq. (7) for the estimated coefficients is 0.4224×10^{-4}.

In order to investigate other cases, variances, s_E^2 and s_M^2, are computed for measurements shown in Figures 32, 34, and 35. In Figures 32, 34, and 35, a co-plot of 10 single runs, the corresponding plot of computed mean values with 2σ bounds at each time instant, and a co-plot of measured and estimated coefficients are presented respectively. Figures 34 and 35 show degraded test repeatability

as well as a distortion in the time histories. The computed variances, s_E^2 and s_M^2, and their corresponding standard errors, s_E and s_M, are shown in the below table. In Figures 33 and 36, time histories of s_i with s_E and s_M are depicted for these four cases.

	1.1 Hz & $\alpha_0 = 20°$		1.1 Hz & $\alpha_0 = 60°$	
	C_N	C_m	C_N	C_m
s_E^2	0.9939×10^{-4}	0.2462×10^{-4}	0.5859×10^{-3}	0.7201×10^{-4}
s_E	0.0100	0.0050	0.0242	0.0085
s_M^2	0.4224×10^{-4}	0.4487×10^{-5}	0.1376×10^{-3}	0.1628×10^{-4}
s_M	0.0065	0.0021	0.0117	0.0040

Theoretically, the two variances, s_E^2 and s_M^2, are the same if there were no errors in modeling with the first harmonic and if accurate data with good repeatability were acquired during experiments. In these test cases, with s_E^2 greater than s_M^2, a larger error in test repeatability is implied with a smaller error in modeling. An example of poor repeatability is shown in Figures 32, 34, and 35.

4.2.3.2 In-phase and out-of-phase components

Ensemble Average Runs

The conventional procedure to obtain a model in forced-oscillation testing is to form an ensemble average of repeated runs. Harmonic analysis is then used to obtain the parameters in model equation Eq. (13). From Eqs. (18) and (19), in-phase and out-of-phase components with the corresponding standard errors are computed. Results are presented in Tables 4-6 and plotted against the angle of attack in Figures 37-39. Figures 37-39 show the strong effect of frequency especially on the out-of-phase components.

Ten Repeated Single Runs

Harmonic analysis is also applied to individual runs (before averaging). Figure 40 depicts in-phase and out-of-phase components of the lift coefficient, C_L, for each of the 10 single runs against angle of attack**.** Dispersion is visually apparent and it is readily seen that more scatter occurs with the damping term estimates. Figure 41 offers less cluttered view by plotting the mean values and 2σ bounds. Figure 42 co-plots the individual estimates from Figure 40 with the 2σ bounds. This figure provides repeatability and error bound information as a variation with angle of attack. In Figures 43-46, results for other frequencies are presented. While Figure 43 shows a good repeatability, fairly larger deviations are shown in Figures 44-46. From these plots, a test engineer can quickly assess progress of the experiment and the presence of any outlier results.

4.2.3.3 Outlier Rejection Rules

From Table B-1 in Appendix B, when the number of repeats, N_r, is 10, the ratio of maximum acceptable deviation to precision index, τ, is 1.96 with a corresponding probability of 0.95. Applying Chauvenet's criterion to the test case shown in Figure 17 and Figure 45 (f = 1.5 Hz and α_0 = 55°), the outlier screening metric, 1.96*σ, requires the single run, s815, to be rejected. In-phase and out-of phase coefficients for all 10 runs and for selected runs (9 runs in this case) are computed and shown in the table below. Figure 47 depicts each value of coefficients with 2σ confidence range.

	All 10 Runs		Selected Runs	
	Mean	σ	Mean	σ
$\overline{C}_{N_\alpha}$	1.2603	0.0830	1.2406	0.0582
$\overline{C}_{N_q}$	4.8351	0.5424	4.9933	0.2224

The data from the above table and Figure 47 demonstrates that Chauvenet's criterion successfully removed the questionable test data and improved data consistency by reducing standard deviations. This methodology provides a straightforward method for post-data analysis to improve test data accuracy, however, the approach requires sufficient numbers of repeated tests be performed.

5 Concluding Remarks

NASA Langley Research Center has been conducting a series of wind tunnel tests to develop and test mathematical models and system identification methodology for aircraft rigid-body aerodynamics in nonlinear unsteady flight regimes. Analysis of measurement accuracy, especially for nonlinear dynamic systems that may exhibit complicated behaviors, is an essential component of this ongoing effort. In this report, tools for harmonic analysis of dynamic data and assessing measurement accuracy have been presented. A linear aerodynamic model is assumed that is appropriate for conventional forced-oscillation experiments, although more general models can be used with these tools. Application of the tools to experimental data is demonstrated and results indicate the levels of uncertainty in output measurements that can arise from experimental setup, calibration procedures, mechanical limitations, and input errors. During the evaluation, several issues have been highlighted: 1) duty-cycle slips in real-time experiments, 2) signal-to-noise ratio (SNR), 3) calibration, and 4) input design. Suggestions that could address these issues have been proposed for ensuring high measurement accuracy of future experiments.

Extension of this work may support implementation of closed-loop automated testing where feedback measurements are analyzed, in real-time, with the appropriate metrics to produce the highest

data quality possible during dynamic testing. This would provide efficient experimental systems that can reduce experimental time and increase measurement accuracy.

Appendix A: Outlier Rejection Rule – Grubb's Test

For the rejection of extreme values (outliers) in repeated observations under the same conditions, the Grubb's test of extreme deviation can be used. The related hypotheses for testing of significant difference between the ensemble mean and an observation are

$$H_0: \; x_n - \bar{x} = 0 \text{ or } x_1 - \bar{x} = 0$$

$$H_1: \; x_n - \bar{x} \neq 0 \text{ or } x_1 - \bar{x} \neq 0 .$$

The testing criterion is

$$T_n = \frac{x_n - \bar{x}}{s} \text{ or } T_1 = \frac{x_1 - \bar{x}}{s} \qquad \text{(A-1)}$$

depending on testing the smallest or largest value in the observed data. Variables in Eq. (A-1) mean the first and the last value in the ordered sequence $x_1 \leq x_2 \leq ..... \leq x_n$. The terms $\bar{x}$ and s are the ensemble mean and ensemble standard error respectively.

The critical values $T_{1;\alpha}$ and $T_{n;\alpha}$ for $\alpha = 0.05$ and 0.01 are given in Table A-1. If $T_n > T_{n;\alpha}$ (or $T_1 > T_{1;\alpha}$), the null hypothesis rejected on the significance level $(1-\alpha)$. It means that the data point x_n (or x_1) should be removed from the ensemble and the ensemble mean and standard error recomputed.

Table A-1. Critical Values of Grubb's Test.

n	α		N	α	
	0.05	**0.01**		**0.05**	**0.01**
3	1.412	1.414	**15**	2.493	2.800
4	1.689	1.723	**16**	2.523	2.837
5	1.869	1.955	**17**	2.551	2.871
6	1.996	2.130	**18**	2.557	2.903
7	2.093	2.265	**19**	2.600	2.932
8	2.172	2.374	**20**	2.623	2.959
9	2.237	2.464	**21**	2.644	2.984
10	2.294	2.540	**22**	2.664	3.008
11	2.343	2.606	**23**	2.683	3.030
12	2.387	2.663	**24**	2.701	3.051
13	2.426	2.714	**25**	2.717	3.071
14	2.461	2.759			

Appendix B: Outlier Rejection Rule – Chauvenet's Criterion

Chauvenet's criterion specifies that all measured data points should be retained that are within a region around the mean value that corresponds to a probability $P = 1 - \frac{1}{2N_r}$. It means that a measured data point can be rejected if the probability of its deviation from the mean value is less than $\frac{1}{2N_r}$. Chauvenet's criterion is based on Gaussian probability distribution and is shown in the sketch below.

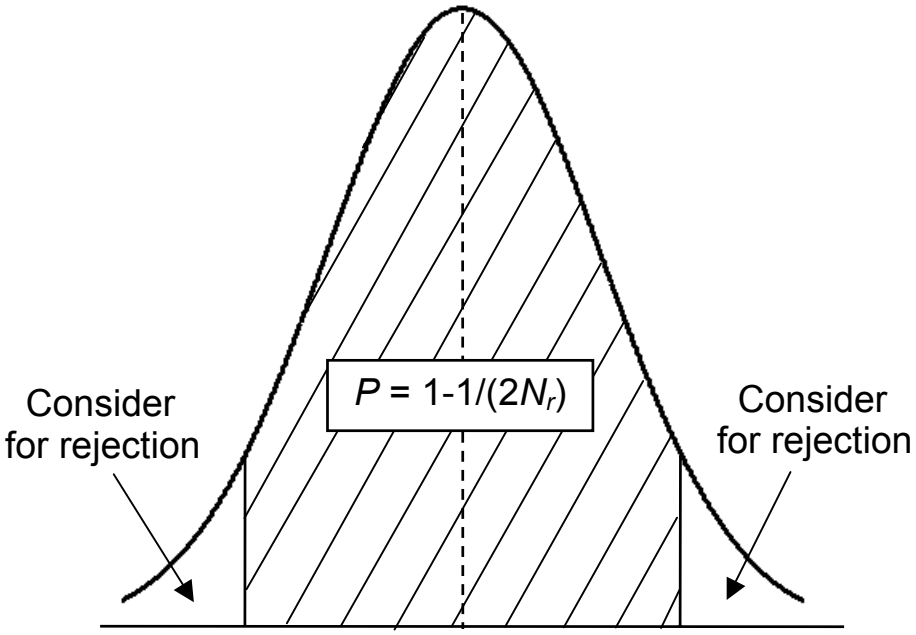

In order to apply this criterion, the mean value, $\bar{x}$, and the standard deviation, *s(x)*, must be estimated from measured data points x_i, i = 1, 2, …., N_r. Then, the non-dimensional random variable is defined as

$$\tau = \frac{x_i - \bar{x}}{s(x)} \tag{B-1}$$

The measured data point is rejected if

$$x_i > \bar{x} + \tau s(x) \quad \text{or} \quad x_i < \bar{x} - \tau s(x) \tag{B-2}$$

where τ can be found from a table of standard nominal distribution. Some values for various N_r's are shown in the below table.

Table B-1. Chauvenet's Criterion: Values of τ for various N_r's.

N_r	τ	N_r	τ
3	1.380	**15**	2.130
4	1.540	**20**	2.240
5	1.650	**25**	2.330
6	1.730	**50**	2.570
7	1.800	**100**	2.810
8	1.870	**300**	3.140
9	1.910	**500**	3.290
10	1.960	**1000**	3.480

Example: An experiment with 10 repeated measurements

According to Chauvenet's criterion, all of the measured data points that fall inside a probability range around the mean of $1 - \frac{1}{2 \times 10} = 0.95$ must be retained. From the above table, $\tau(P=0.95) = 1.96$. Therefore, all measurements that deviate from the mean by more than $1.96 \times s(x)$ can be rejected. Then, a new mean and a new standard deviation are recomputed from the measurements that remain. No further application of the criterion to the measurements is allowed. Chauvenet's criterion can be applied only once for a given set of measurements.

Acknowledgements

Wind tunnel tests were carried out with the assistance of NASA researcher Jay M. Brandon and George Washington University student Leslie Gould.

References

1. Vladislav Klein, Patrick C. Murphy, Timothy J. Curry and Jay M. Brandon, "Analysis of Wind Tunnel Longitudinal Static and Oscillatory Data of the F-16XL Aircraft," NASA/TM-97-206276, December 1997.
2. Vladislav Klein and Patrick C. Murphy, "Estimation of Aircraft Nonlinear Unsteady Parameters From Wind Tunnel Data," NASA/TM-1998-208969, December 1998.
3. Patrick C. Murphy and Vladislav Klein, "Estimation of Aircraft Unsteady Aerodynamic Parameters From Dynamic Wind Tunnel Testing," AIAA Atmospheric Flight Mechanics Conference, Aug. 2001.
4. H. W. Coleman and W. Glenn Steele, Jr.: Experimentation and Uncertainty Analysis For Engineers, 1989.
5. J. M. Brandon: Dynamic Stall Effects and Application to High Performance Aircraft. Special Course on Aircraft Dynamics at High Angles of Attack: Experiment and Modeling. AGARD Report No. 776, April 1991, pp. 2-1 to 2-15.
6. Michael J. Hemsch, "Development and Status of Data Quality Assurance Program at NASA Langley Research Center – Toward National Standards," AIAA Advanced Measurement and Ground Testing Technology Conference, June 1996.
7. Michael J. Hemsch et al, "Langley Wind Tunnel Data Quality Assurance – Check Standard Results," AIAA Advanced Measurement and Ground Testing Technology Conference, Jun. 2000.

Table 1. Mean values and standard errors of aerodynamic coefficients.

Angle of Attack (degree)	C_N		C_A		C_m		C_L		C_D	
	$\hat{C}_N$	$s(\hat{C}_N)$	$\hat{C}_A$	$s(\hat{C}_A)$	$\hat{C}_m$	$s(\hat{C}_m)$	$\hat{C}_L$	$s(\hat{C}_L)$	$\hat{C}_D$	$s(\hat{C}_D)$
-2.0	0.0204	0.0040	0.0280	0.0027	0.0129	0.0018	0.0214	0.0040	0.0272	0.0027
0.0	0.0927	0.0021	0.0261	0.0025	0.0189	0.0016	0.0927	0.0021	0.0261	0.0025
5.0	0.2884	0.0045	0.0172	0.0022	0.0400	0.0010	0.2858	0.0047	0.0422	0.0019
10.0	0.5198	0.0071	0.0081	0.0023	0.0699	0.0004	0.5105	0.0071	0.0982	0.0020
15.0	0.7698	0.0037	0.0015	0.0023	0.1054	0.0010	0.7432	0.0038	0.2006	0.0022
20.0	1.0340	0.0111	-0.0037	0.0017	0.1482	0.0007	0.9729	0.0107	0.3501	0.0034
25.0	1.2935	0.0115	-0.0109	0.0014	0.1901	0.0004	1.1769	0.0108	0.5367	0.0043
28.0	1.3907	0.0113	-0.0117	0.0013	0.2104	0.0012	1.2334	0.0102	0.6425	0.0049
30.0	1.4420	0.0142	-0.0106	0.0002	0.2170	0.0012	1.2541	0.0122	0.7117	0.0072
32.0	1.4703	0.0078	-0.0088	0.0008	0.2158	0.0024	1.2516	0.0067	0.7717	0.0040
34.0	1.4848	0.0153	-0.0072	0.0008	0.2116	0.0010	1.2350	0.0130	0.8243	0.0082
36.0	1.4706	0.0219	-0.0048	0.0005	0.2041	0.0013	1.1926	0.0180	0.8604	0.0125
38.0	1.4446	0.0232	-0.0030	0.0015	0.1978	0.0017	1.1402	0.0192	0.8870	0.0132
40.0	1.3429	0.0174	0.0022	0.0007	0.1759	0.0020	1.0273	0.0136	0.8648	0.0108
45.0	1.2659	0.0099	0.0029	0.0010	0.1764	0.0022	0.8931	0.0072	0.8971	0.0068
50.0	1.2590	0.0098	-0.0037	0.0009	0.1658	0.0007	0.8122	0.0058	0.9621	0.0080
60.0	1.3420	0.0050	-0.0143	0.0010	0.1388	0.0024	0.6835	0.0016	1.1550	0.0049
70.0	1.4099	0.0167	-0.0199	0.0022	0.1050	0.0021	0.5010	0.0069	1.3180	0.0154

Table 2. Measured values of aerodynamic coefficients at different angles of attack.

Angle of Attack (degree)	C_N	C_A	C_m	C_L	C_D
-2.0	-0.0047	0.0262	0.0146	-0.0037	0.0264
0.0	0.0673	0.0248	0.0186	0.0673	0.0248
5.0	0.2614	0.0156	0.0371	0.2590	0.0383
10.0	0.4957	0.0061	0.0654	0.4871	0.0921
11.0	0.5455	0.0046	0.0727	0.5346	0.1086
12.0	0.5926	0.0030	0.0799	0.5790	0.1261
13.0	0.6433	0.0014	0.0864	0.6265	0.1461
14.0	0.6952	0.0001	0.0931	0.6745	0.1683
15.0	0.7500	-0.0011	0.1008	0.7247	0.1930
16.0	0.7980	-0.0016	0.1078	0.7675	0.2184
17.0	0.8464	-0.0022	0.1160	0.8101	0.2453
18.0	0.9068	-0.0034	0.1258	0.8635	0.2769
19.0	0.9556	-0.0043	0.1336	0.9050	0.3071
20.0	1.0025	-0.0054	0.1412	0.9439	0.3378
21.0	1.0713	-0.0073	0.1512	1.0028	0.3771
22.0	1.1197	-0.0082	0.1590	1.0412	0.4118
23.0	1.1731	-0.0096	0.1673	1.0836	0.4495
24.0	1.2321	-0.0111	0.1757	1.1301	0.4910
25.0	1.2878	-0.0123	0.1843	1.1723	0.5330
26.0	1.3326	-0.0138	0.1926	1.2038	0.5717
27.0	1.3715	-0.0143	0.2001	1.2285	0.6099
28.0	1.3864	-0.0137	0.2042	1.2306	0.6387
29.0	1.4215	-0.0129	0.2107	1.2496	0.6778
30.0	1.4275	-0.0125	0.2123	1.2425	0.7029
31.0	1.4650	-0.0114	0.2154	1.2617	0.7447
32.0	1.4762	-0.0108	0.2153	1.2576	0.7730
33.0	1.4866	-0.0098	0.2129	1.2521	0.8014
34.0	1.4990	-0.0087	0.2109	1.2476	0.8309
35.0	1.4928	-0.0078	0.2074	1.2274	0.8498
36.0	1.4883	-0.0066	0.2056	1.2080	0.8694
37.0	1.4902	-0.0058	0.2044	1.1937	0.8921
38.0	1.4890	-0.0052	0.2019	1.1766	0.9126
39.0	1.4538	-0.0037	0.1950	1.1322	0.9120
40.0	1.3801	0.0002	0.1776	1.0571	0.8872
45.0	1.2549	0.0022	0.1725	0.8859	0.8888
50.0	1.2550	-0.0039	0.1653	0.8097	0.9588
60.0	1.3402	-0.0131	0.1377	0.6815	1.1541
70.0	1.4159	-0.0212	0.1091	0.5043	1.3232

Table 3. Number of cycles required for stable parameter estimates (1.5 Hz and $\alpha_0 = 10°$).

Number of Cycles	C_N		C_m	
	$\overline{C}_{N_\alpha}$	$\overline{C}_{N_q}$	$\overline{C}_{m_\alpha}$	$\overline{C}_{m_q}$
1	2.8579	1.6492	0.3854	-0.6892
2	2.7747	2.3233	0.3799	-0.6141
3	2.8046	2.1016	0.3833	-0.6586
4	2.7686	3.2429	0.3907	-0.4935
5	2.7790	3.0120	0.3874	-0.5113
6	2.7962	2.7900	0.3860	-0.5439
7	2.7559	3.9233	0.3968	-0.3868
8	2.7661	3.7093	0.3957	-0.4144
9	2.7866	3.4677	0.3964	-0.4613
10	2.7321	4.5528	0.4032	-0.3050

Table 4. In-phase and out-of-phase components of lift coefficient.

Angle of Attack (degree)	k=0.067		k=0.121		k=0.148		k=0.201		k=0.270	
	$\overline{C}_{L_\alpha}$	$s(\overline{C}_{L_\alpha})$	$\overline{C}_{L_\alpha}$	$s(\overline{C}_{L_\alpha})$	$\overline{C}_{L_\alpha}$	$s(\overline{C}_{L_\alpha})$	$\overline{C}_{L_\alpha}$	$s(\overline{C}_{L_\alpha})$	$\overline{C}_{L_\alpha}$	$s(\overline{C}_{L_\alpha})$
2.4036	2.2881	0.0041	2.3030	0.0052	2.3210	0.0057	2.3433	0.0068	2.3463	0.0062
5.3857	2.5148	0.0040	2.5090	0.0050	2.5325	0.0053	2.3980	0.0102	2.5449	0.0059
10.4589	2.7470	0.0030	2.7336	0.0042	2.7313	0.0042	2.5958	0.0103	2.6910	0.0064
15.5519	2.6748	0.0025	2.6760	0.0038	2.6684	0.0034	2.5286	0.0099	2.6213	0.0055
20.6637	2.5247	0.0029	2.6009	0.0035	2.5914	0.0029	2.4570	0.0095	2.5710	0.0045
25.7697	1.7634	0.0085	2.0877	0.0066	2.1671	0.0059	2.0906	0.0089	2.3118	0.0062
30.9134	0.7759	0.0050	1.3441	0.0066	1.4897	0.0060	1.4251	0.0095	1.7995	0.0069
36.0349	0.1099	0.0043	0.8162	0.0067	0.9222	0.0065	0.8520	0.0095	1.1978	0.0077
41.2319	-0.1065	0.0063	0.5046	0.0059	0.5717	0.0052	0.4797	0.0083	0.7677	0.0071
46.5557	-0.2918	0.0033	0.1270	0.0053	0.2160	0.0067	0.2166	0.0080	0.4159	0.0086
51.9286	-0.4678	0.0037	-0.1216	0.0058	-0.1026	0.0050	-0.0907	0.0053	0.0928	0.0064
57.5852	-0.6639	0.0035	-0.4829	0.0041	-0.4470	0.0054	-0.4256	0.0053	-0.2302	0.0101
63.3500	-0.8740	0.0029	-0.7701	0.0047	-0.7255	0.0042	-0.6736	0.0061	-0.5804	0.0087

(a) In-phase component

Angle of Attack (degree)	k=0.067		k=0.121		k=0.148		k=0.201		k=0.270	
	$\overline{C}_{L_q}$	$s(\overline{C}_{L_q})$	$\overline{C}_{L_q}$	$s(\overline{C}_{L_q})$	$\overline{C}_{L_q}$	$s(\overline{C}_{L_q})$	$\overline{C}_{L_q}$	$s(\overline{C}_{L_q})$	$\overline{C}_{L_q}$	$s(\overline{C}_{L_q})$
2.4036	1.7427	0.0612	2.0859	0.0437	2.3760	0.0389	2.3567	0.0254	2.3382	0.0231
5.3857	1.6308	0.0606	1.9621	0.0419	2.2165	0.0362	4.2849	0.0513	2.2356	0.0223
10.4589	1.6713	0.0447	0.5033	0.0350	2.0911	0.0285	4.4304	0.0521	2.3109	0.0241
15.5519	1.6069	0.0379	0.3931	0.0317	1.9385	0.0232	4.1763	0.0498	2.0104	0.0208
20.6637	3.1797	0.0435	1.2980	0.0290	2.5196	0.0198	4.2626	0.0474	2.0299	0.0168
25.7697	8.1950	0.1271	5.3493	0.0551	5.2165	0.0403	5.6548	0.0446	3.0095	0.0233
30.9134	15.4230	0.0739	9.5717	0.0550	8.1963	0.0408	6.9031	0.0477	4.1225	0.0259
36.0349	21.6164	0.0649	11.2670	0.0560	8.9447	0.0441	6.8256	0.0477	4.4713	0.0286
41.2319	21.8885	0.0944	9.6921	0.0487	7.6542	0.0352	5.4757	0.0413	3.8182	0.0266
46.5557	11.9459	0.0494	7.1025	0.0442	5.6574	0.0453	4.0031	0.0399	2.8693	0.0321
51.9286	7.0711	0.0552	4.2326	0.0481	3.4562	0.0338	2.5054	0.0263	1.9930	0.0237
57.5852	4.6937	0.0528	3.3718	0.0340	2.6704	0.0369	1.7342	0.0262	1.5447	0.0376
63.3500	3.2883	0.0431	2.0036	0.0391	1.6396	0.0286	0.6858	0.0303	1.0099	0.0321

(b) Out-of-phase component

Table 5. In-phase and out-of-phase components of normal-force coefficient.

Angle of Attack (degree)	k=0.067		k=0.121		k=0.148		k=0.201		k=0.270	
	$\overline{C}_{N_\alpha}$	$s(\overline{C}_{N_\alpha})$	$\overline{C}_{N_\alpha}$	$s(\overline{C}_{N_\alpha})$	$\overline{C}_{N_\alpha}$	$s(\overline{C}_{N_\alpha})$	$\overline{C}_{N_\alpha}$	$s(\overline{C}_{N_\alpha})$	$\overline{C}_{N_\alpha}$	$s(\overline{C}_{N_\alpha})$
2.4036	2.3199	0.0042	2.3351	0.0053	2.3521	0.0058	2.3743	0.0069	2.3768	0.0063
5.3857	2.5680	0.0043	2.5630	0.0054	2.5855	0.0057	2.4502	0.0106	2.5970	0.0063
10.4589	2.8939	0.0034	2.8813	0.0046	2.8793	0.0046	2.7414	0.0109	2.8390	0.0053
15.5519	2.9882	0.0027	2.9951	0.0041	2.9901	0.0037	2.8480	0.0110	2.9419	0.0049
20.6637	3.0786	0.0036	3.1710	0.0051	3.1610	0.0045	3.0169	0.0118	3.1481	0.0059
25.7697	2.5615	0.0083	2.9269	0.0073	3.0011	0.0070	2.9306	0.0120	3.1932	0.0079
30.9134	1.7827	0.0047	2.4183	0.0061	2.5944	0.0057	2.5054	0.0126	2.9703	0.0086
36.0349	1.2164	0.0055	2.0587	0.0074	2.1890	0.0071	2.0899	0.0127	2.5702	0.0080
41.2319	0.9984	0.0066	1.7922	0.0063	1.8965	0.0053	1.7667	0.0123	2.2048	0.0076
46.5557	0.8601	0.0035	1.4735	0.0052	1.5914	0.0066	1.5944	0.0102	1.9640	0.0082
51.9286	0.7992	0.0042	1.3476	0.0068	1.3833	0.0056	1.4103	0.0076	1.7766	0.0086
57.5852	0.7717	0.0046	1.1460	0.0056	1.2135	0.0060	1.2647	0.0099	1.6611	0.0161
63.3500	0.7154	0.0044	0.9467	0.0077	1.0435	0.0060	1.0808	0.0102	1.4151	0.0238

(a) In-phase component

Angle of Attack (degree)	k=0.067		k=0.121		k=0.148		k=0.201		k=0.270	
	$\overline{C}_{N_q}$	$s(\overline{C}_{N_q})$	$\overline{C}_{N_q}$	$s(\overline{C}_{N_q})$	$\overline{C}_{N_q}$	$s(\overline{C}_{N_q})$	$\overline{C}_{N_q}$	$s(\overline{C}_{N_q})$	$\overline{C}_{N_q}$	$s(\overline{C}_{N_q})$
2.4036	1.7387	0.0627	2.0880	0.0447	2.3781	0.0399	2.3538	0.0260	2.3350	0.0236
5.3857	1.6281	0.0650	1.9666	0.0450	2.2248	0.0390	4.3379	0.0533	2.2346	0.0236
10.4589	1.6864	0.0510	0.4504	0.0383	2.1189	0.0314	4.5862	0.0553	2.3263	0.0198
15.5519	1.6453	0.0412	0.2889	0.0344	2.0122	0.0255	4.5097	0.0556	2.0436	0.0185
20.6637	3.3762	0.0546	1.2110	0.0420	2.7101	0.0308	4.8908	0.0591	2.1162	0.0222
25.7697	8.6048	0.1242	5.5646	0.0606	5.7554	0.0480	6.7531	0.0601	3.2500	0.0296
30.9134	17.2872	0.0696	10.4790	0.0505	9.3472	0.0389	8.6484	0.0628	4.6634	0.0321
36.0349	25.8476	0.0824	13.2146	0.0613	10.9842	0.0480	9.3080	0.0635	5.5106	0.0297
41.2319	28.3970	0.0979	12.2830	0.0525	10.2518	0.0358	8.3375	0.0618	5.1176	0.0285
46.5557	17.3199	0.0516	9.8932	0.0431	8.4460	0.0447	7.1076	0.0511	4.2987	0.0306
51.9286	11.5517	0.0622	6.3754	0.0565	5.9877	0.0380	5.6257	0.0378	3.4465	0.0320
57.5852	7.7360	0.0688	5.4186	0.0460	5.1658	0.0405	4.8819	0.0493	2.8488	0.0597
63.3500	7.3488	0.0648	4.6496	0.0631	3.9334	0.0406	3.9036	0.0509	2.1453	0.0881

(b) Out-of-phase component

Table 6. In-phase and out-of-phase components of pitching-moment coefficient.

Angle of Attack (degree)	k=0.067		k=0.121		k=0.148		k=0.201		k=0.270	
	$\overline{C}_{m_\alpha}$	$s(\overline{C}_{m_\alpha})$	$\overline{C}_{m_\alpha}$	$s(\overline{C}_{m_\alpha})$	$\overline{C}_{m_\alpha}$	$s(\overline{C}_{m_\alpha})$	$\overline{C}_{m_\alpha}$	$s(\overline{C}_{m_\alpha})$	$\overline{C}_{m_\alpha}$	$s(\overline{C}_{m_\alpha})$
2.4036	0.2372	0.0008	0.2410	0.0012	0.2367	0.0014	0.2254	0.0040	0.2245	0.0038
5.3857	0.2972	0.0011	0.2976	0.0016	0.2935	0.0016	0.3052	0.0024	0.2876	0.0049
10.4589	0.3974	0.0010	0.3923	0.0018	0.3949	0.0018	0.4034	0.0031	0.3755	0.0064
15.5519	0.4571	0.0010	0.4616	0.0015	0.4593	0.0017	0.4824	0.0029	0.4582	0.0059
20.6637	0.4934	0.0009	0.4949	0.0011	0.5055	0.0011	0.5244	0.0029	0.5111	0.0040
25.7697	0.4200	0.0017	0.4636	0.0018	0.4826	0.0022	0.5134	0.0029	0.5246	0.0072
30.9134	0.1020	0.0025	0.2675	0.0022	0.3047	0.0024	0.3333	0.0031	0.3706	0.0052
36.0349	-0.0610	0.0017	0.1914	0.0021	0.2137	0.0021	0.2318	0.0033	0.2307	0.0036
41.2319	0.0580	0.0027	0.1290	0.0020	0.1232	0.0019	0.1079	0.0027	0.0576	0.0030
46.5557	-0.0143	0.0014	0.0023	0.0019	0.0000	0.0023	0.0377	0.0030	0.0243	0.0039
51.9286	-0.0797	0.0015	-0.0344	0.0021	-0.0297	0.0022	-0.0112	0.0030	-0.0286	0.0035
57.5852	-0.1629	0.0018	-0.1542	0.0031	-0.1437	0.0027	-0.1203	0.0039	-0.0495	0.0038
63.3500	-0.1554	0.0015	-0.1545	0.0025	-0.1478	0.0025	-0.1299	0.0040	-0.1134	0.0072

(a) In-phase component

Angle of Attack (degree)	K=0.067		k=0.121		k=0.148		k=0.201		k=0.270	
	$\overline{C}_{m_q}$	$s(\overline{C}_{m_q})$	$\overline{C}_{m_q}$	$s(\overline{C}_{m_q})$	$\overline{C}_{m_q}$	$s(\overline{C}_{m_q})$	$\overline{C}_{m_q}$	$s(\overline{C}_{m_q})$	$\overline{C}_{m_q}$	$s(\overline{C}_{m_q})$
2.4036	-0.4569	0.0123	-0.4534	0.0104	-0.4297	0.0095	-0.4903	0.0149	-0.4924	0.0142
5.3857	-0.5923	0.0162	-0.5367	0.0137	-0.5340	0.0110	-0.3108	0.0123	-0.6206	0.0184
10.4589	-0.6989	0.0143	-0.8897	0.0148	-0.6804	0.0121	-0.3031	0.0156	-0.6450	0.0239
15.5519	-0.6537	0.0157	-0.8875	0.0126	-0.6485	0.0114	-0.2989	0.0146	-0.6841	0.0221
20.6637	-0.6069	0.0131	-0.9250	0.0091	-0.7075	0.0078	-0.3426	0.0146	-0.8799	0.0151
25.7697	-0.2071	0.0253	-0.5856	0.0152	-0.5479	0.0150	-0.2396	0.0144	-0.8335	0.0269
30.9134	2.2374	0.0369	0.6679	0.0186	0.4594	0.0166	0.2548	0.0153	-0.3014	0.0193
36.0349	4.0346	0.0254	0.7796	0.0174	0.2963	0.0145	-0.0298	0.0165	-0.4977	0.0133
41.2319	0.9936	0.0397	-0.4836	0.0163	-0.6544	0.0127	-0.7880	0.0135	-0.8458	0.0112
46.5557	0.1305	0.0203	-0.1236	0.0160	-0.2146	0.0158	-0.3462	0.0150	-0.5558	0.0146
51.9286	0.0487	0.0217	-0.0858	0.0178	-0.2665	0.0152	-0.4853	0.0147	-0.3703	0.0129
57.5852	0.4163	0.0265	0.1091	0.0257	0.0363	0.0182	-0.0629	0.0195	0.1634	0.0141
63.3500	-0.0998	0.0216	-0.2301	0.0207	-0.1775	0.0171	-0.2078	0.0200	-0.1408	0.0267

(b) Out-of-phase component

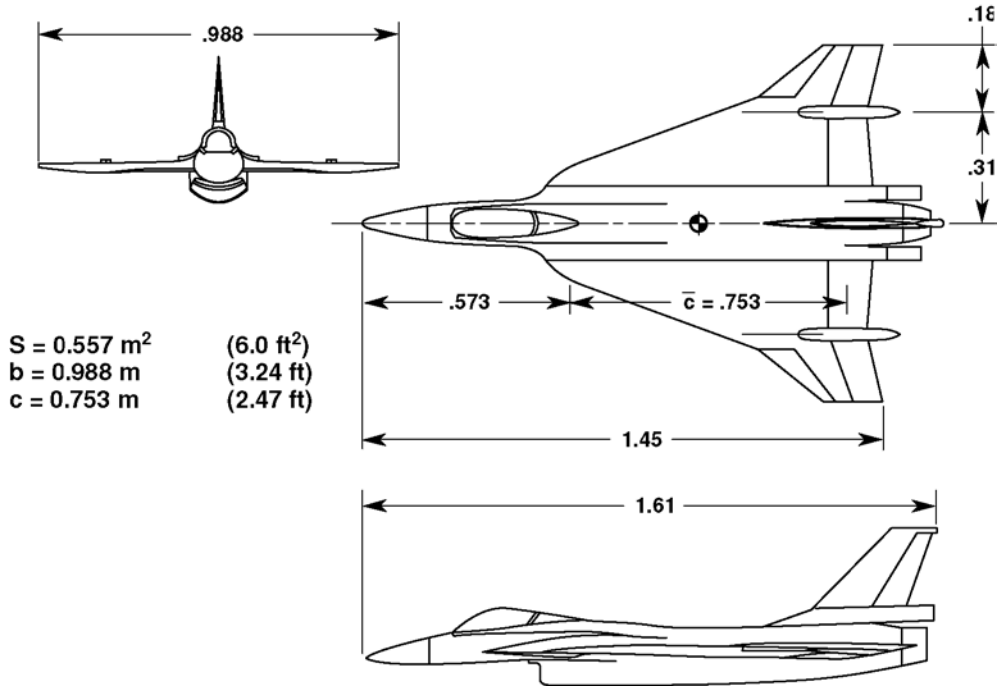

Figure 1. Three-dimensional view of 10% F-16 XL model.

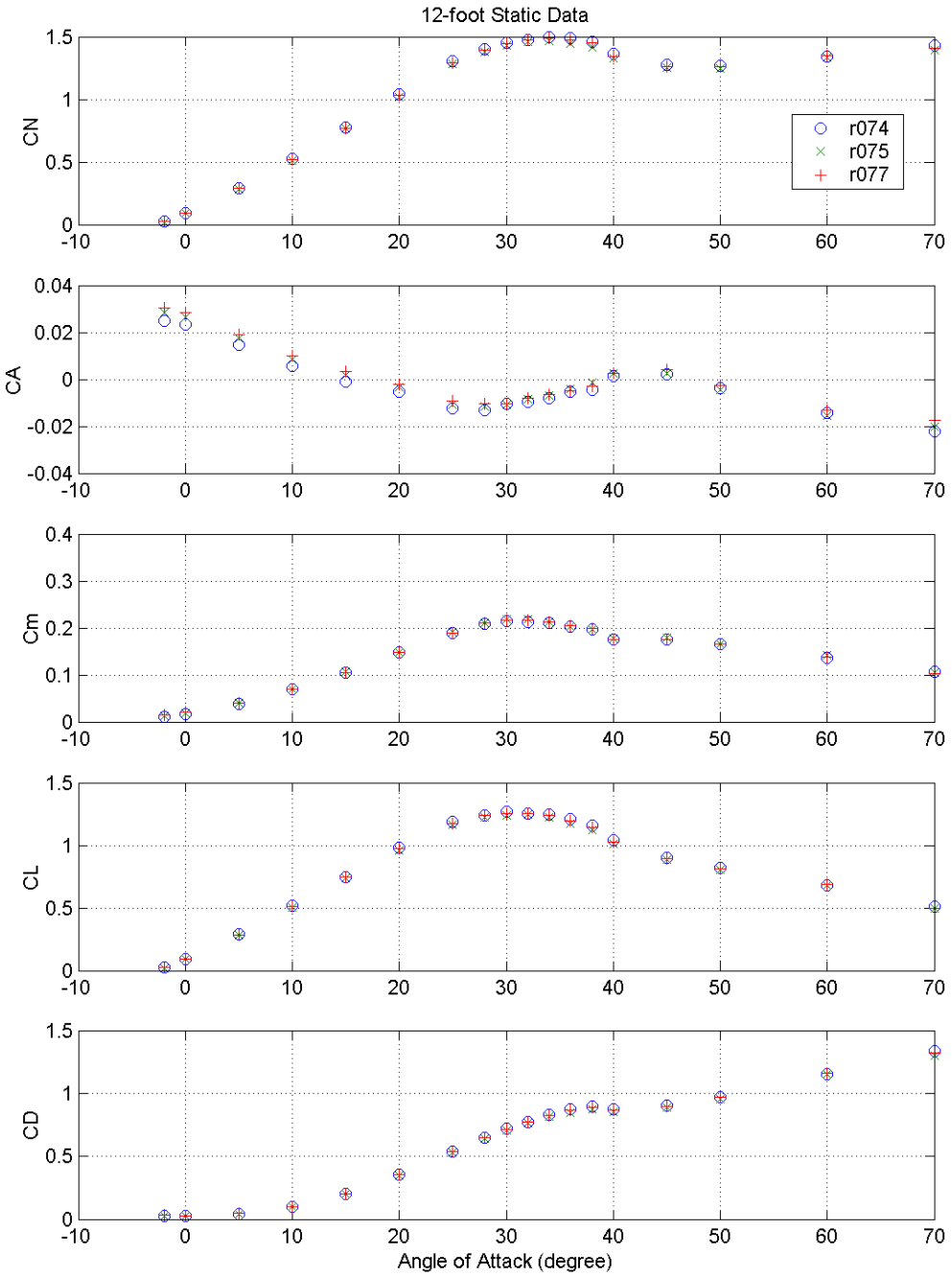

Figure 2. Variation of longitudinal coefficients with angle of attack (Three repeated measurements).

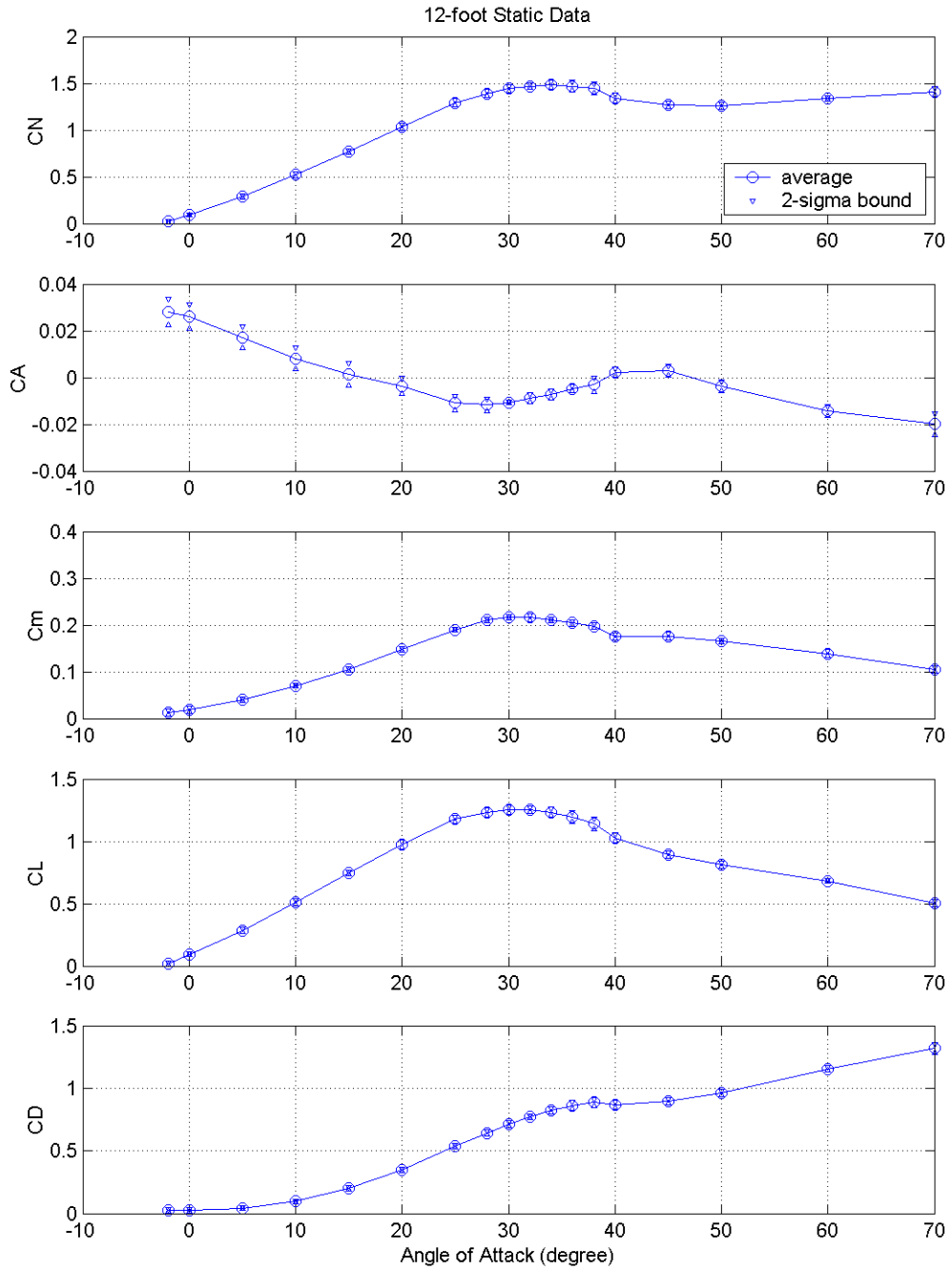

Figure 3. Variation of longitudinal coefficients with angle of attack (Mean values and 2σ bounds).

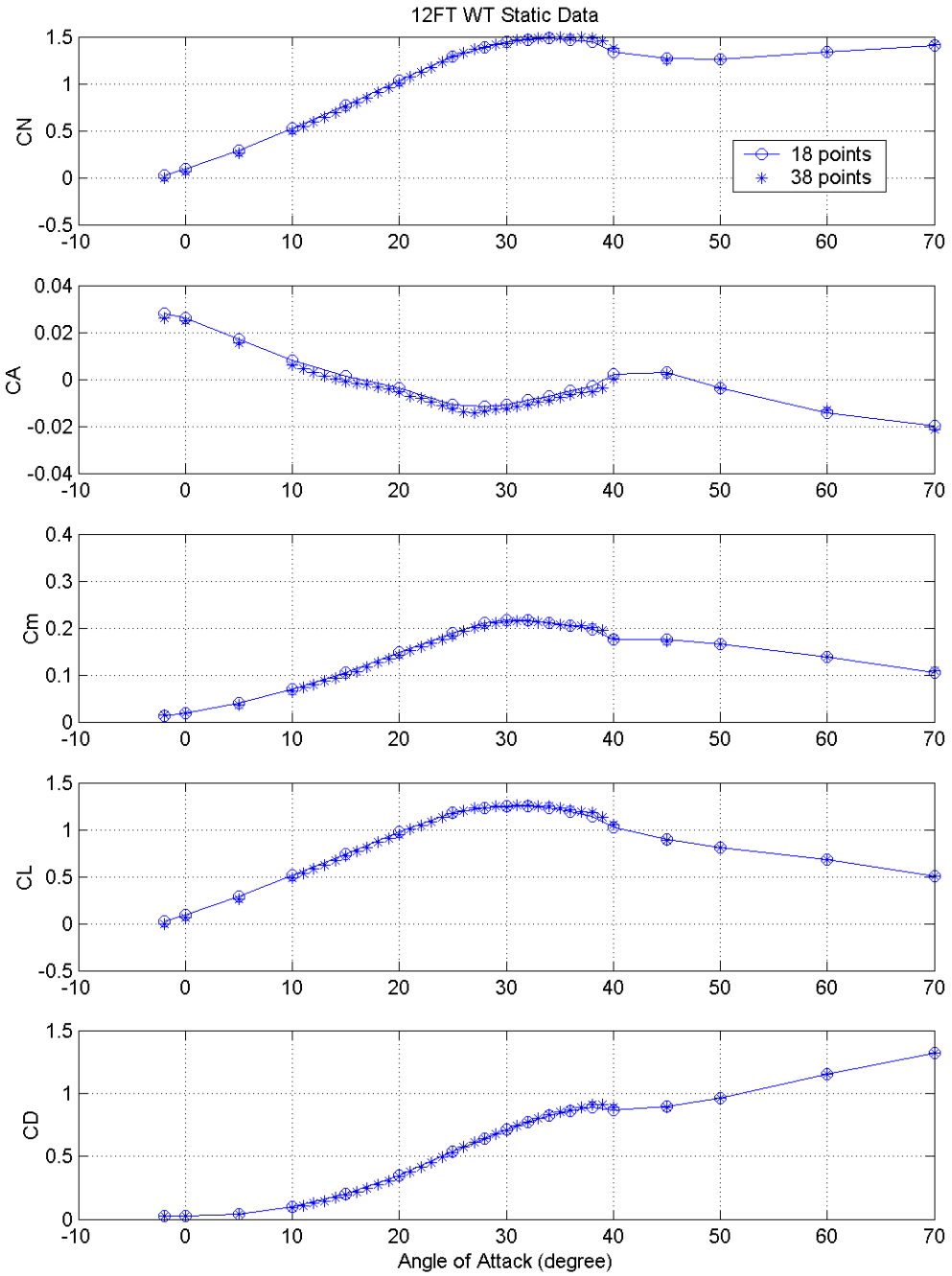

Figure 4. Variation of longitudinal coefficients with angle of attack (Repeated measurements).

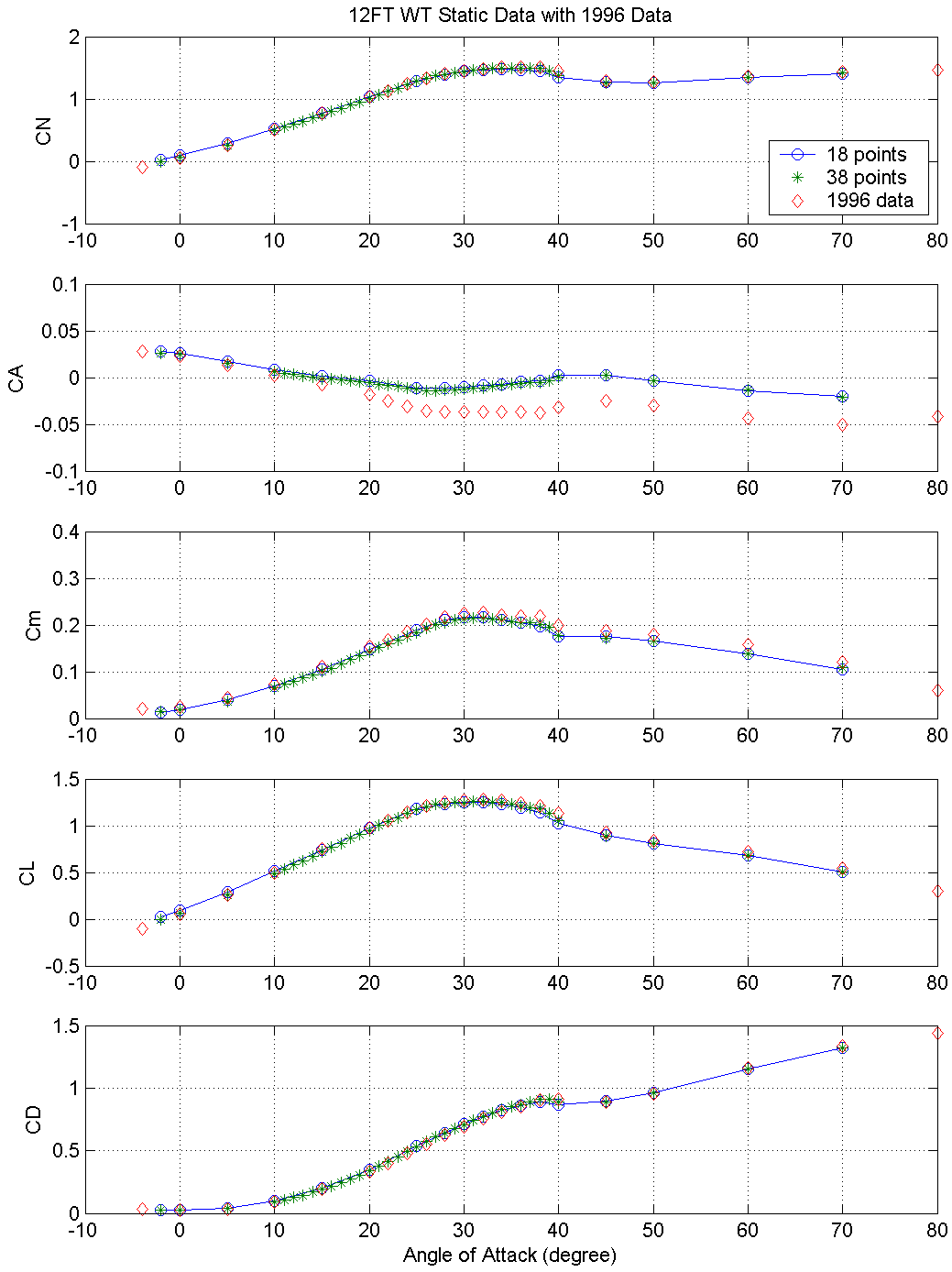

Figure 5. Static data comparison with 1996 data.

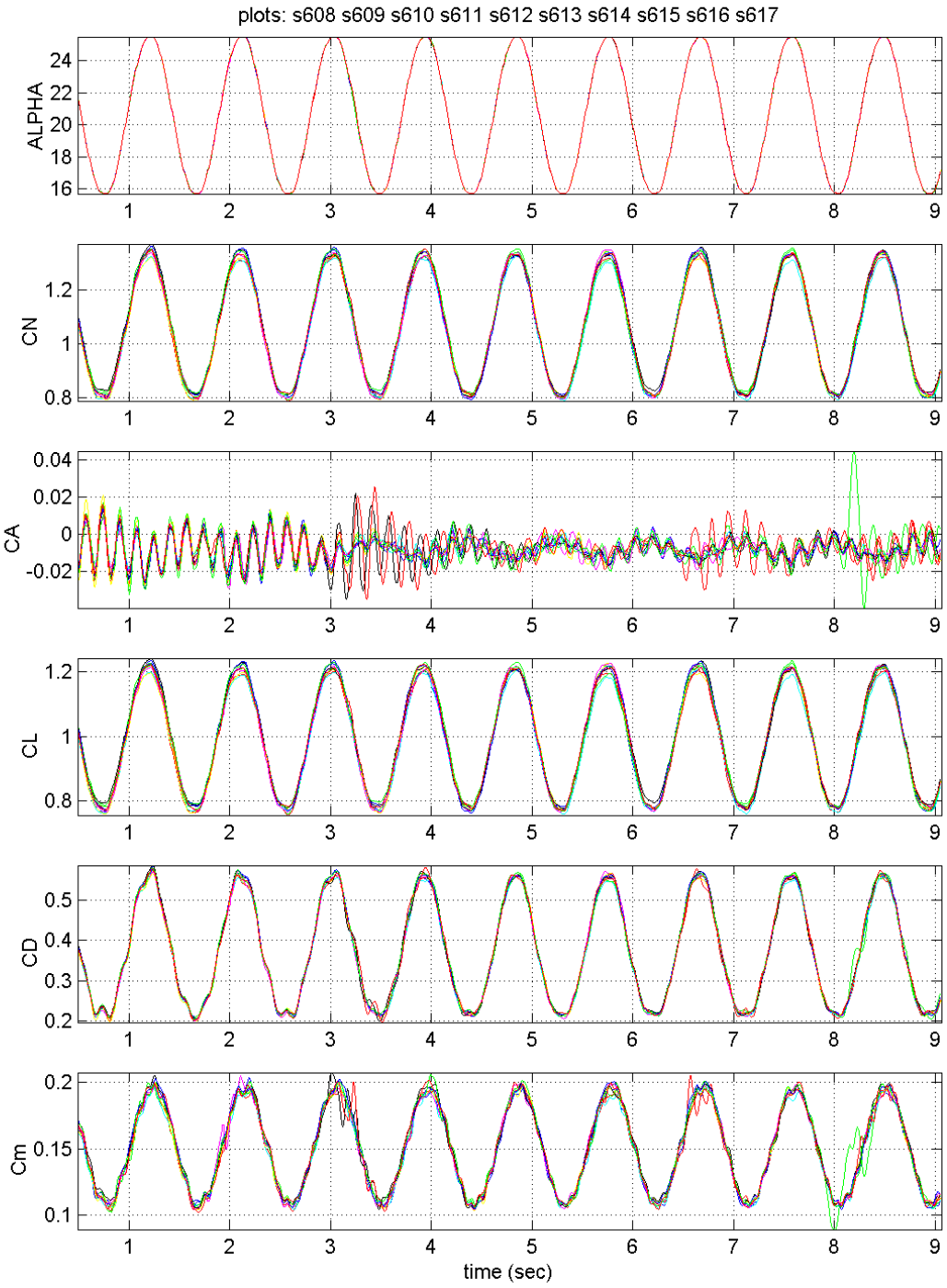

Figure 6. Typical dynamic test data (Ten repeated measurements): 1.1 Hz and α_0=20°.

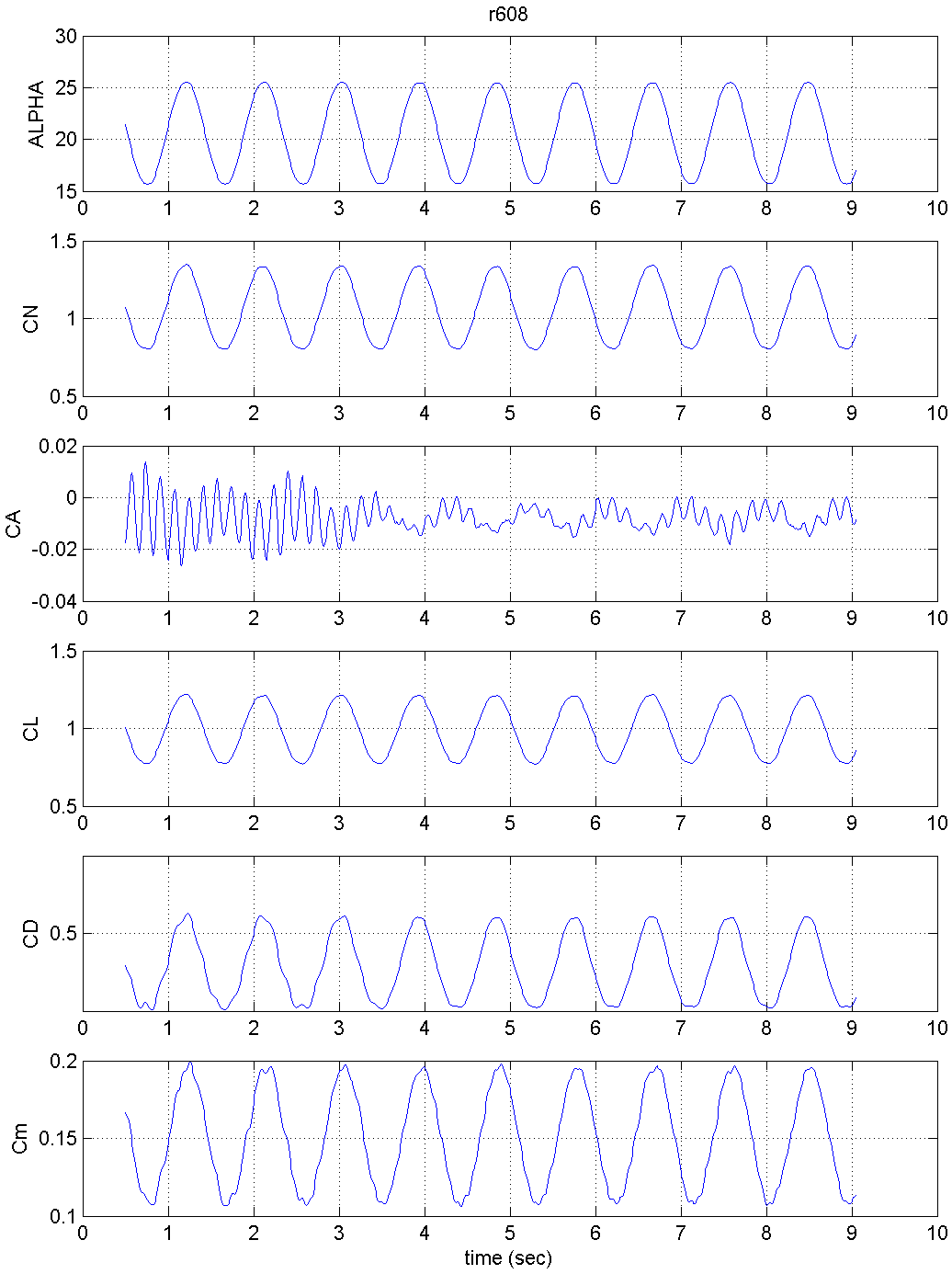

Figure 7. Typical dynamic test data (Ensemble average run): 1.1 Hz and α_0=20°.

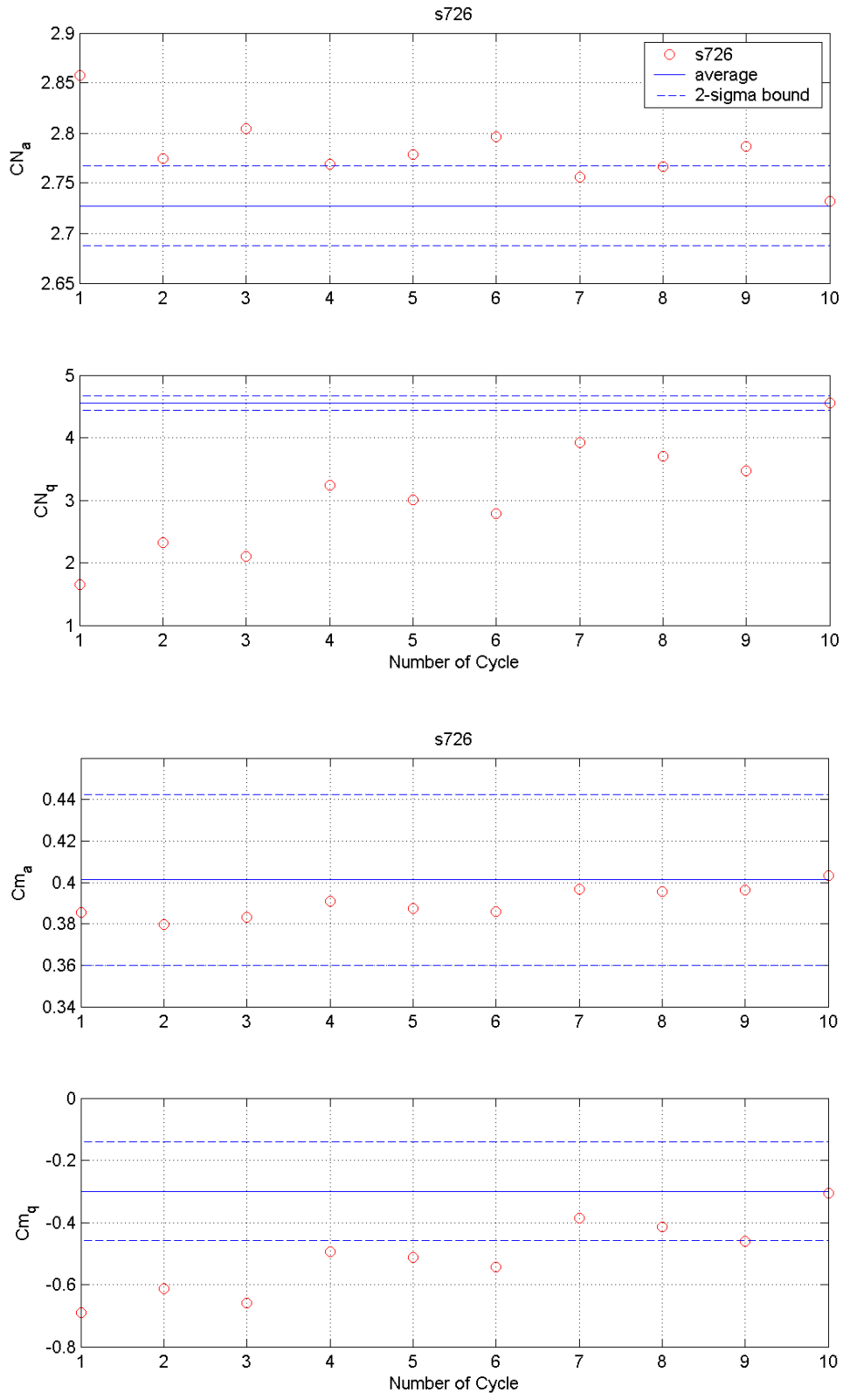

Figure 8. Number of cycles required for stable estimates.

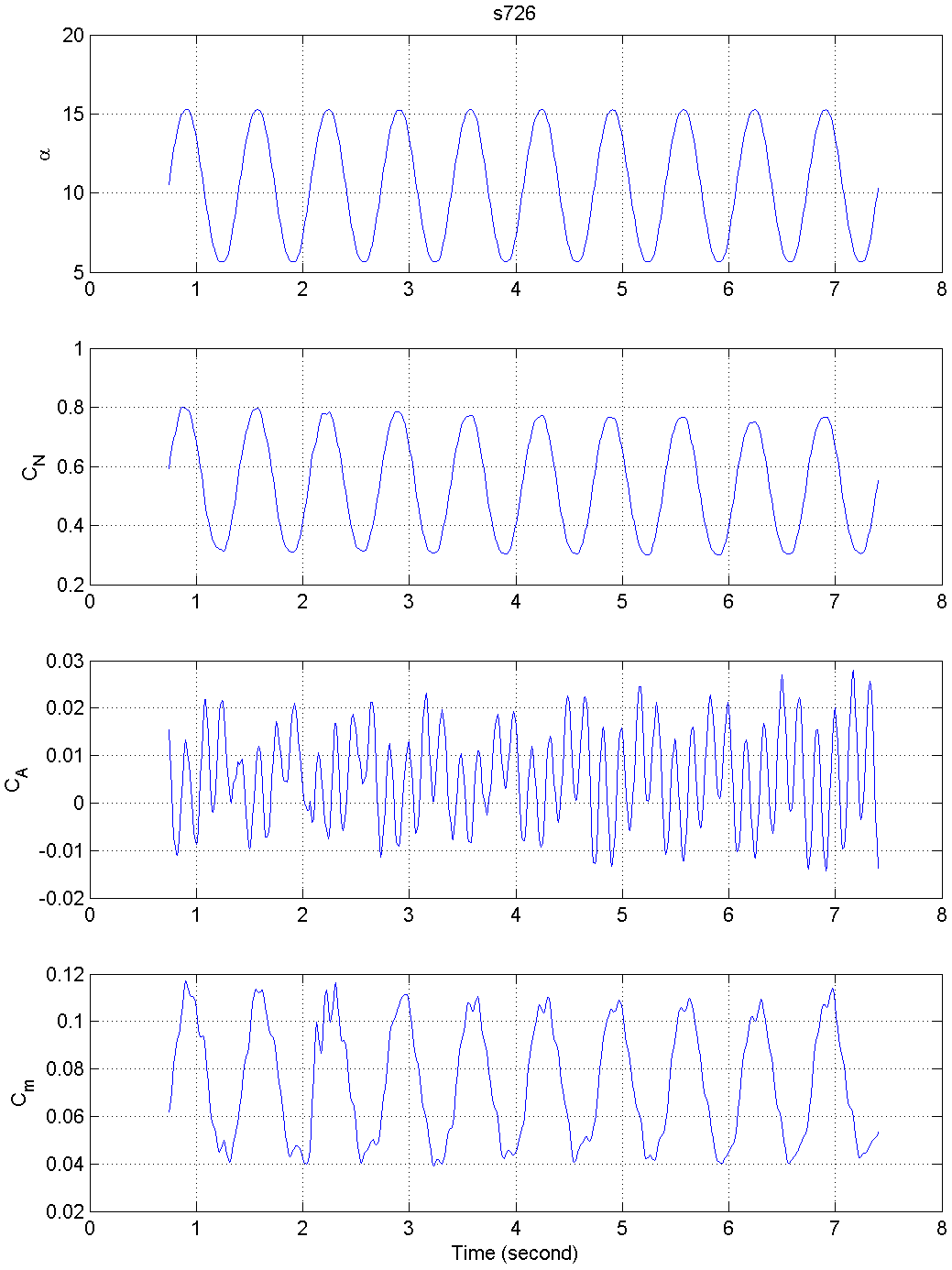

Figure 9. Test Case for Harmonic Analysis: 1.5 Hz and α_0 =10°.

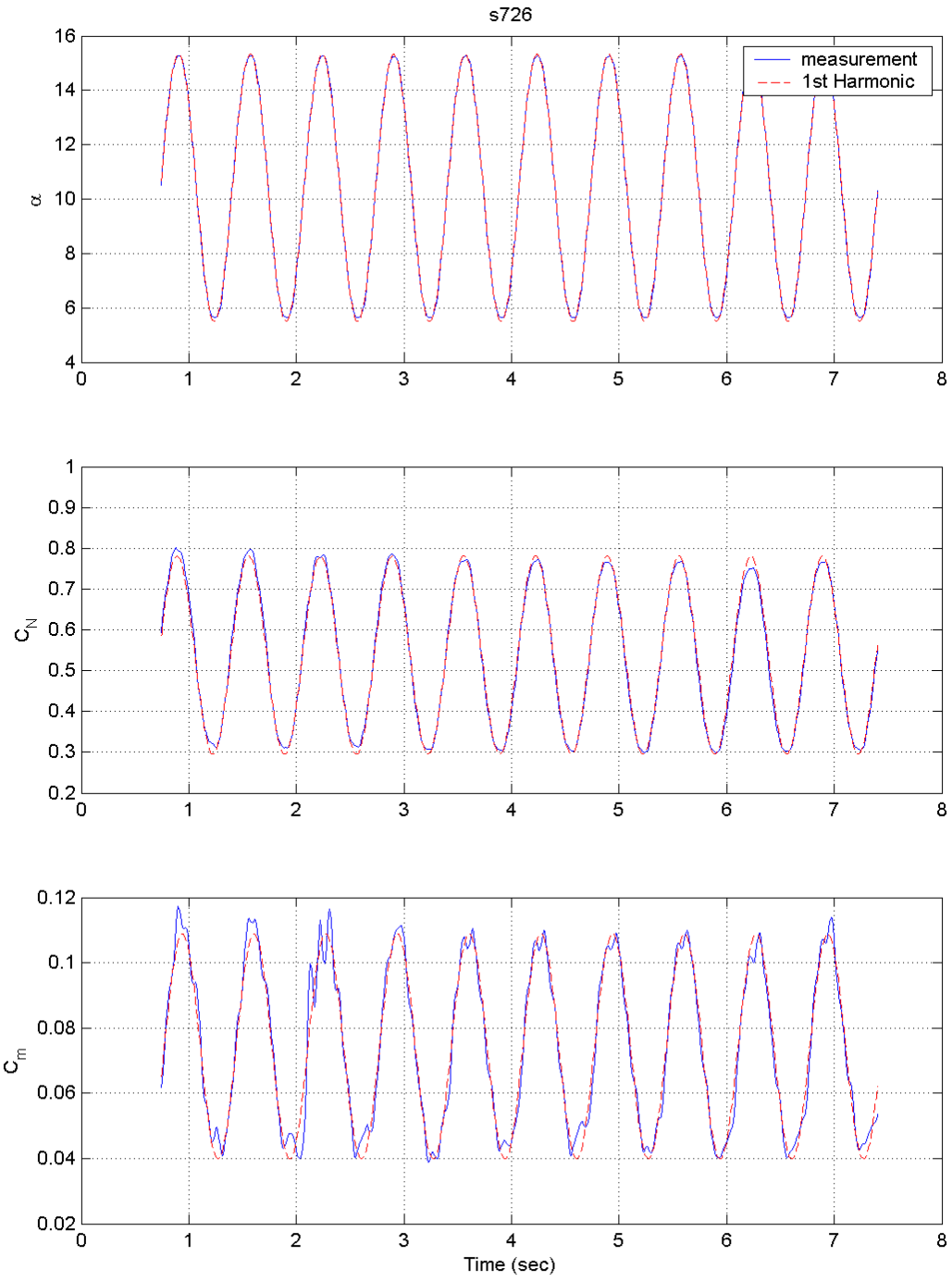

Figure 10. Harmonic Analysis - Angle of Attack, C_N, and C_m.

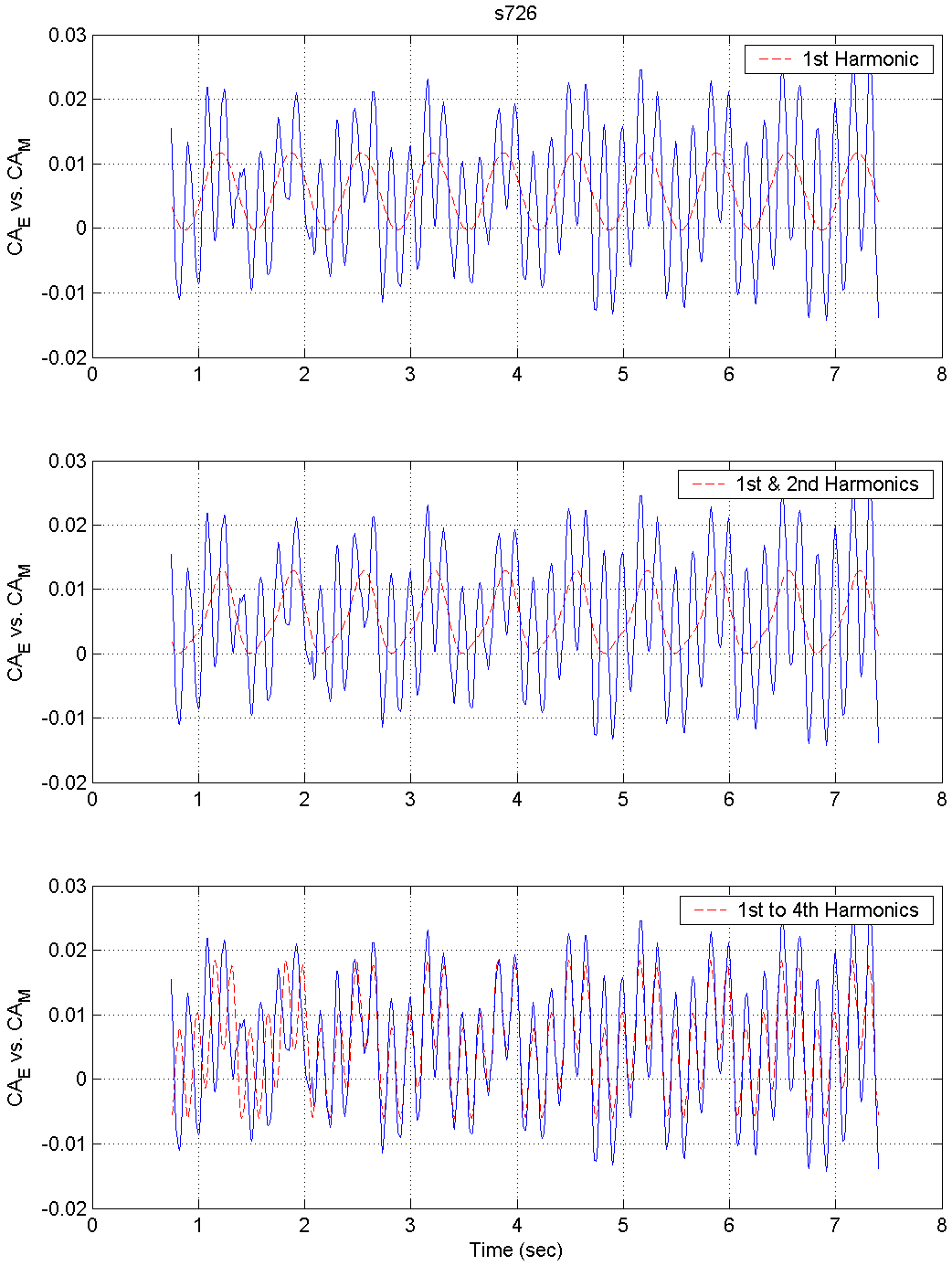

Figure 11. Harmonic Analysis - C_A.

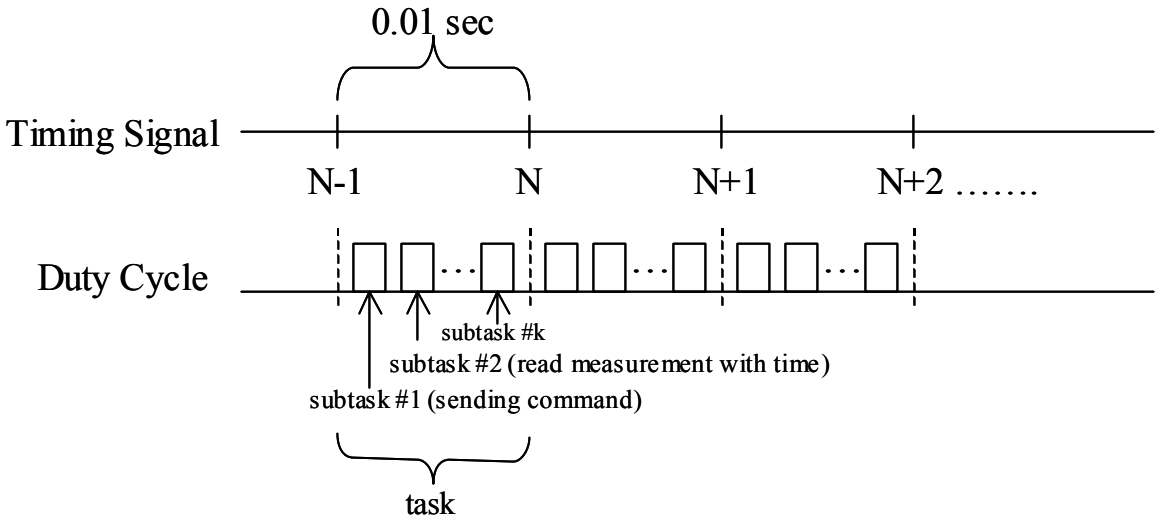

(a) proposed timing signal and task

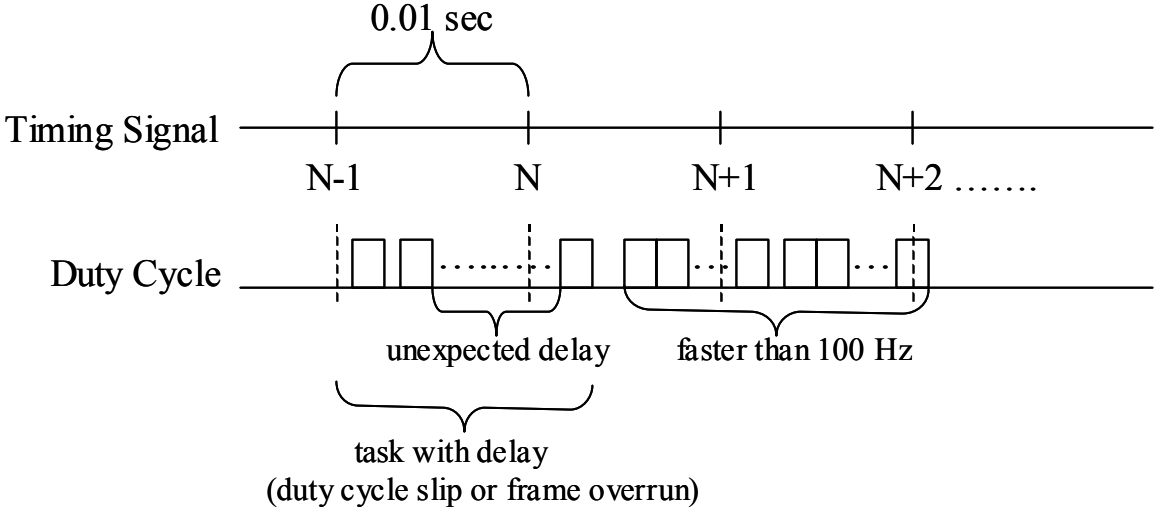

(b) timing signal and task with delay

Figure 12. Proposed timing signal and the signal with the timing issue.

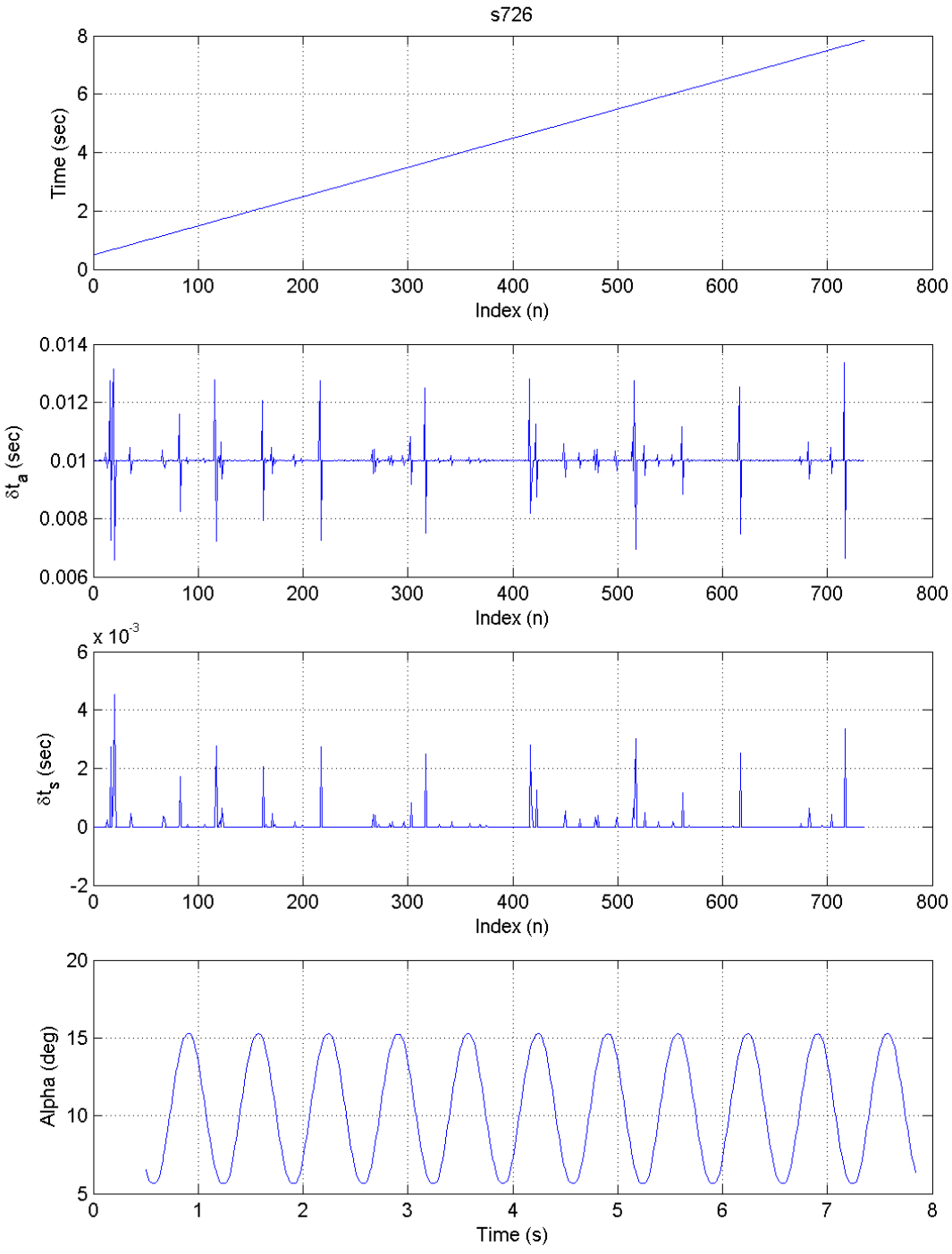

Figure 13. Typical timing signal of dynamic test data (1.5 Hz and α_0=10°).

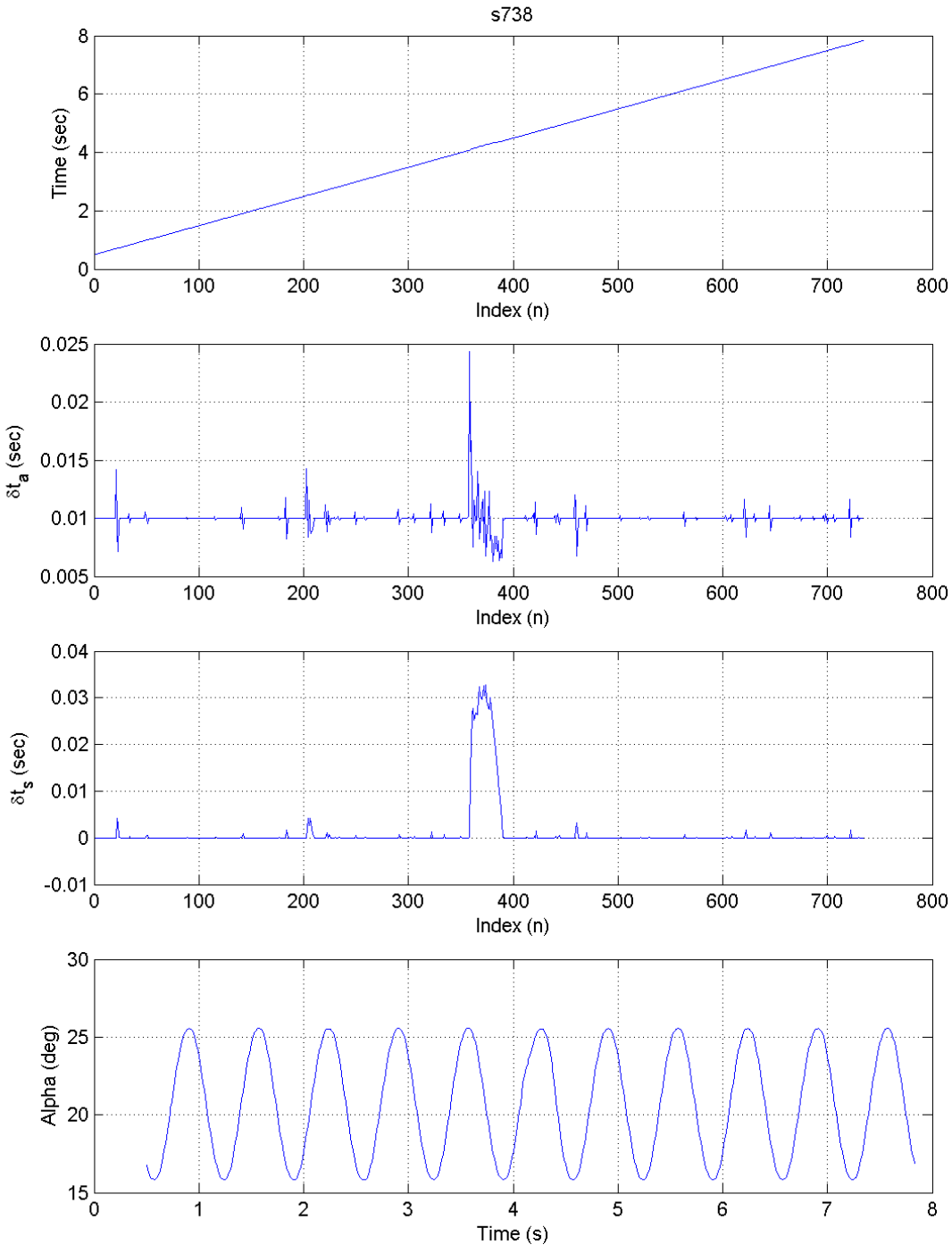

Figure 14. Dynamic test data with the slippage of duty cycles (1.5 Hz and α_0=20°).

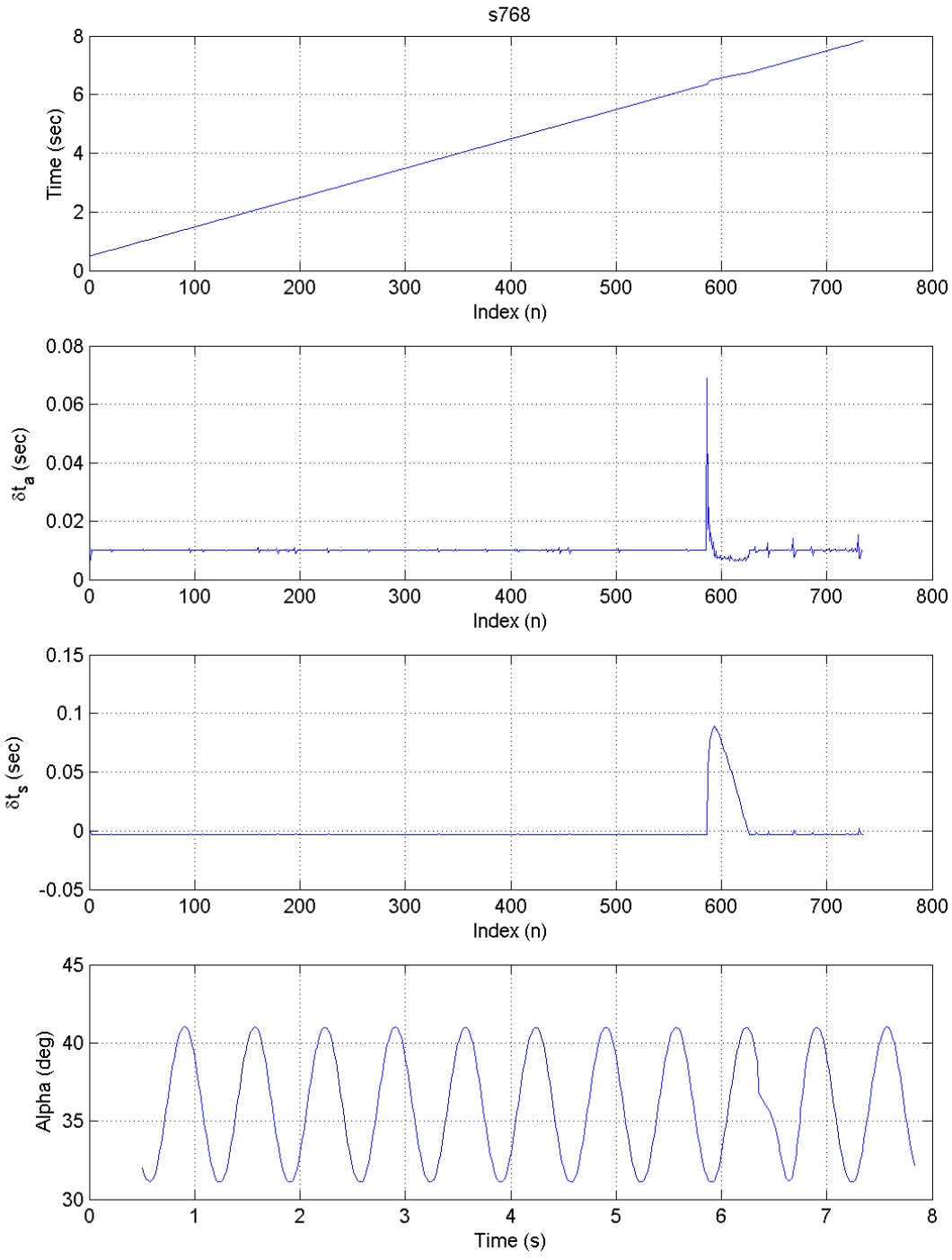

Figure 15. Dynamic test data with the slippage of duty cycles (1.5 Hz and α_0=35°).

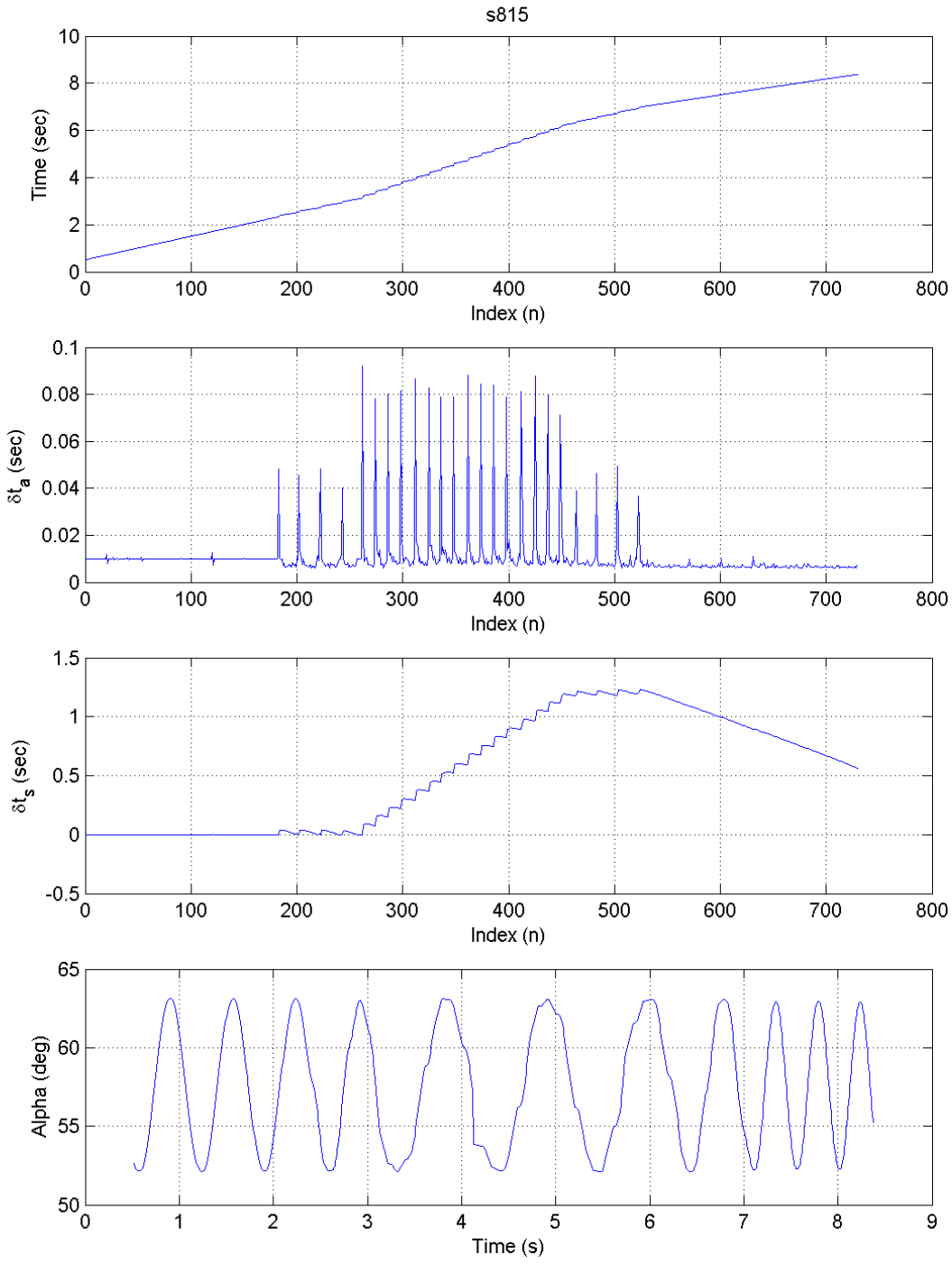

Figure 16. Dynamic test data with the slippage of duty cycles (1.5 Hz and α_0=55°).

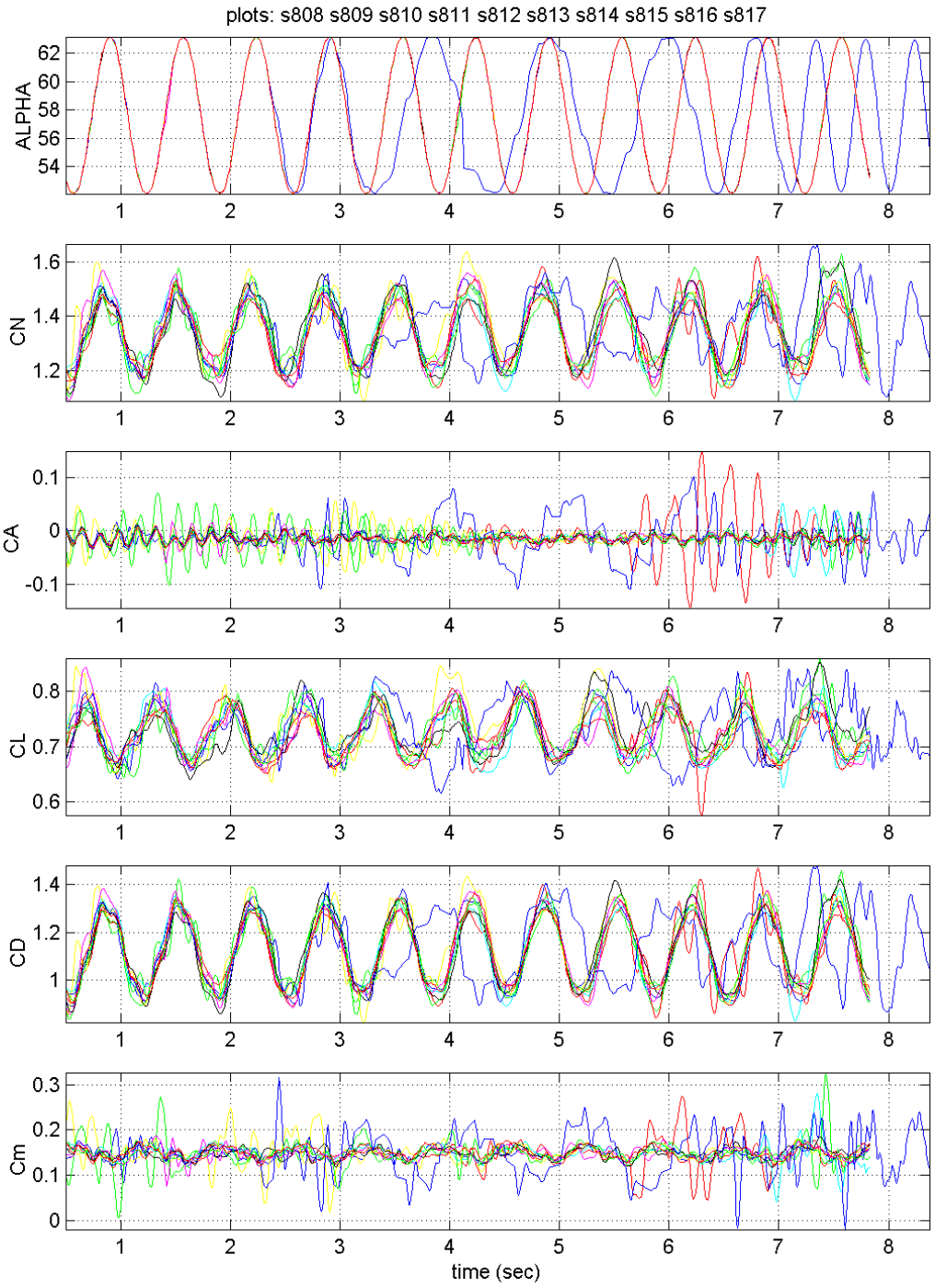

Figure 17. Corresponding co-plot of 10 single-runs (1.5 Hz and α_0=55°).

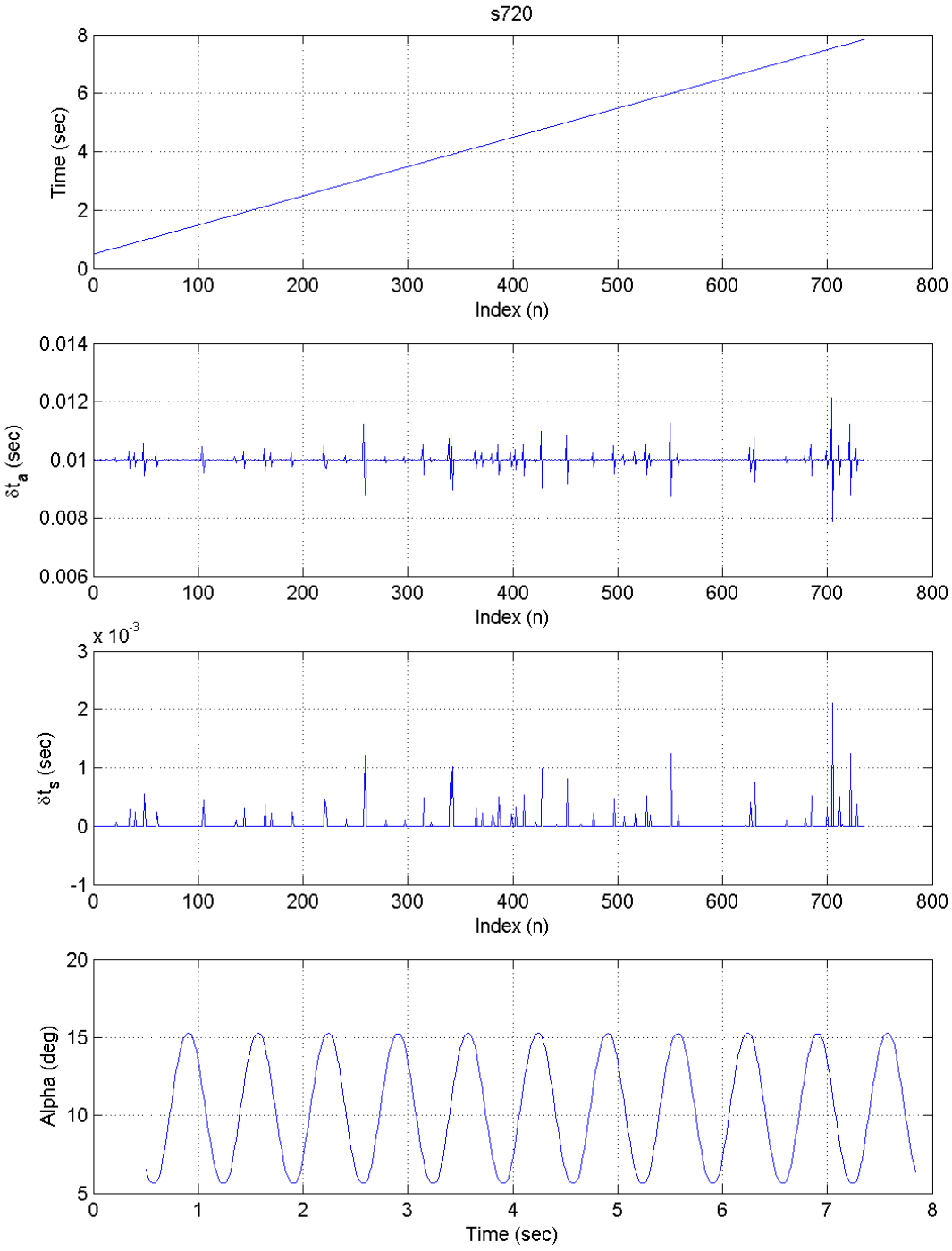

Figure 18. Test Case: 1.5 Hz and α_0=10°.

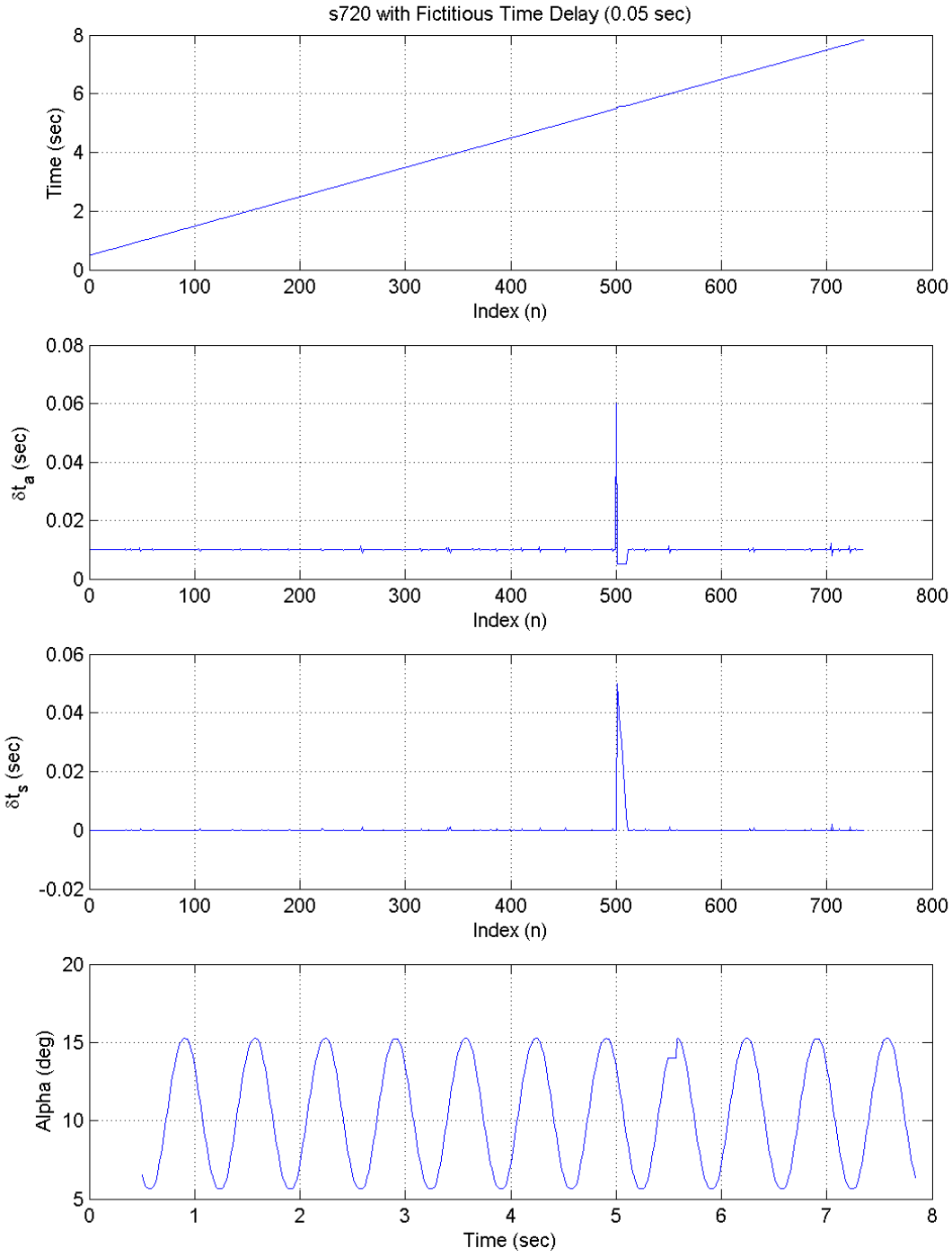

Figure 19. Test Case with 0.05 sec Delay (1.5 Hz and α_0=10°).

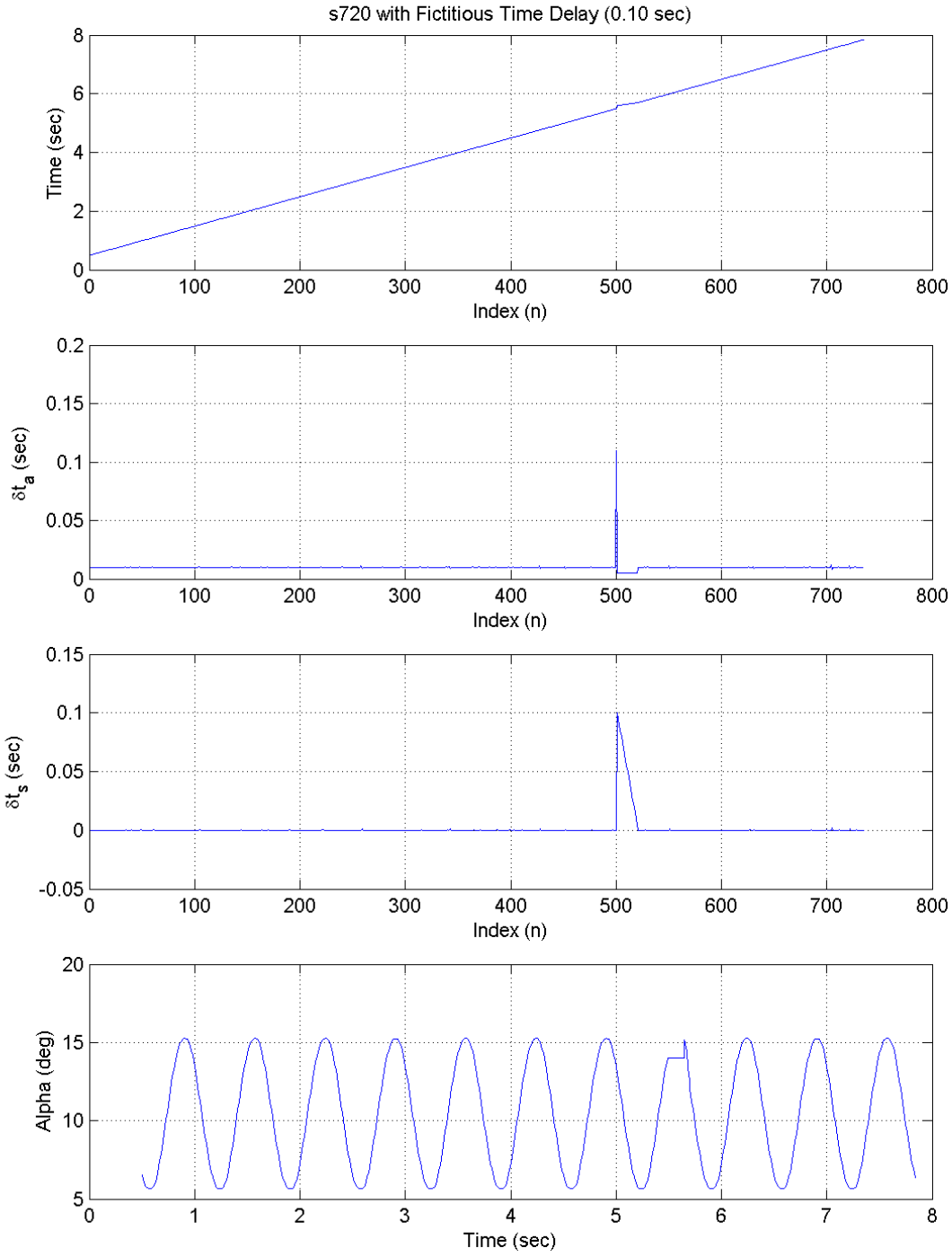

Figure 20. Test Case with 0.10 sec Delay (1.5 Hz and α_0=10°).

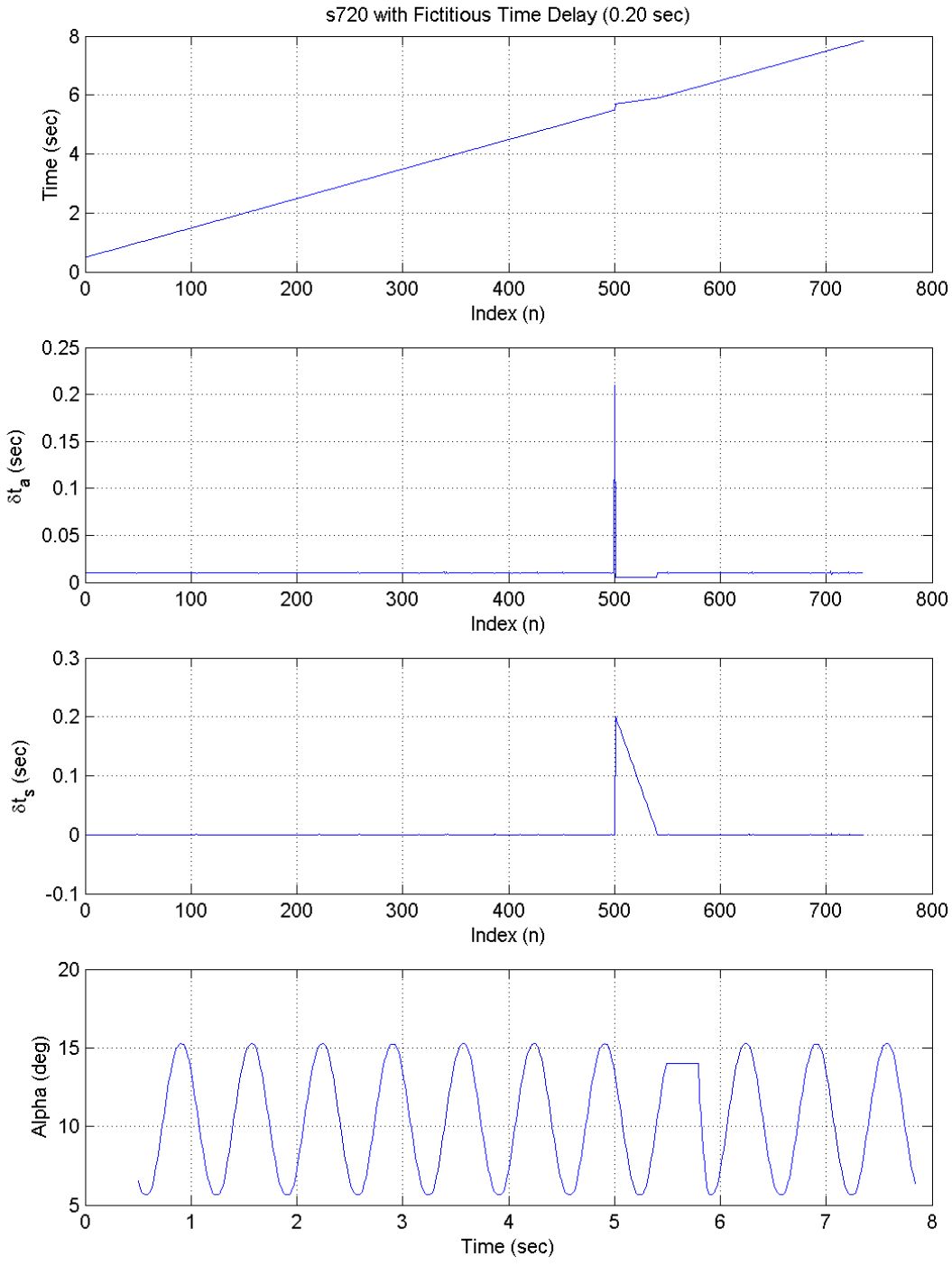

Figure 21. Test Case with 0.20 sec Delay (1.5 Hz and α_0=10°).

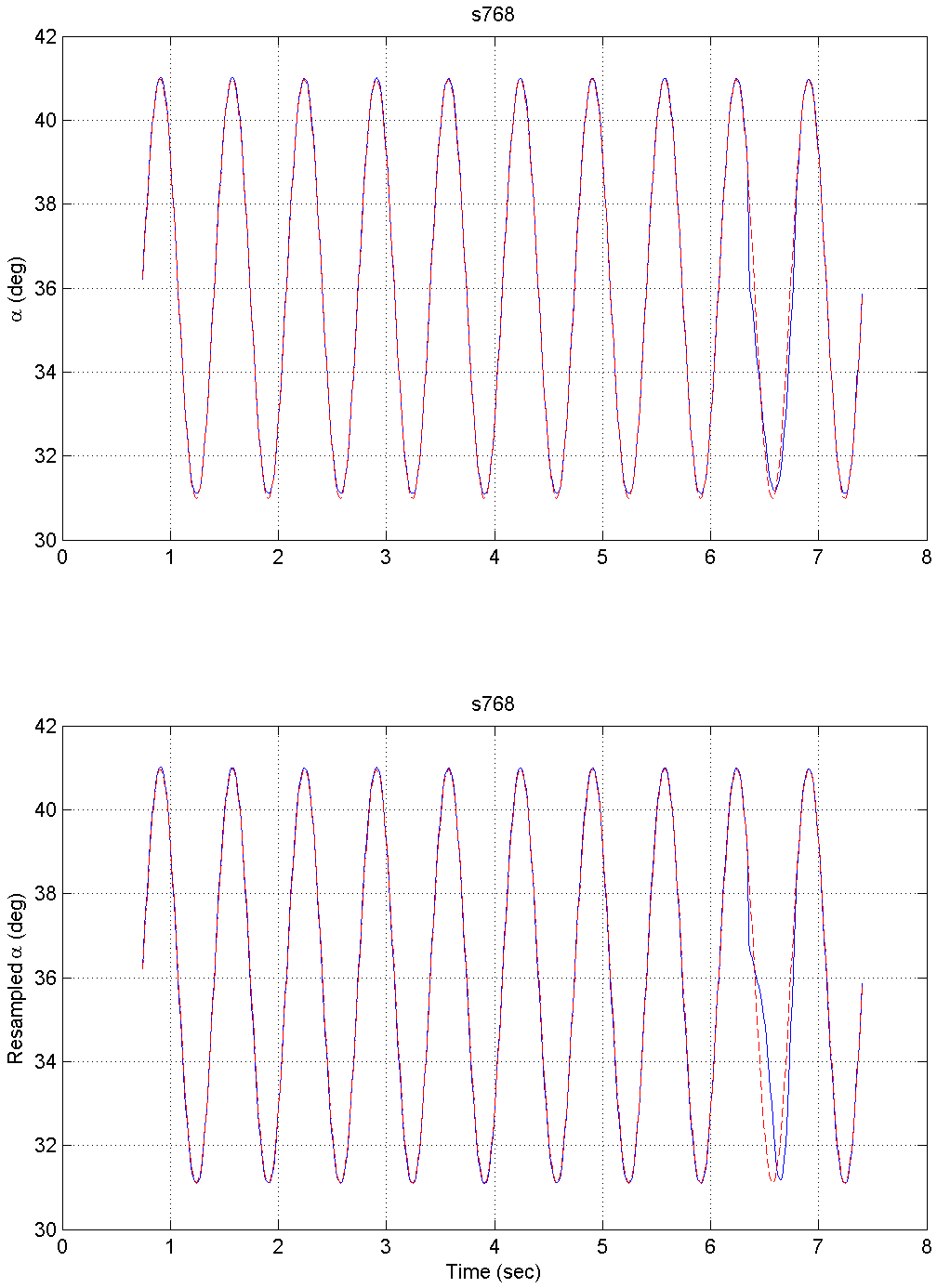

Figure 22. Co-plots of measured α (solid line) and estimated α (dashed line): Measured Test Data (Top) and Re-sampled Measured Data (Bottom).

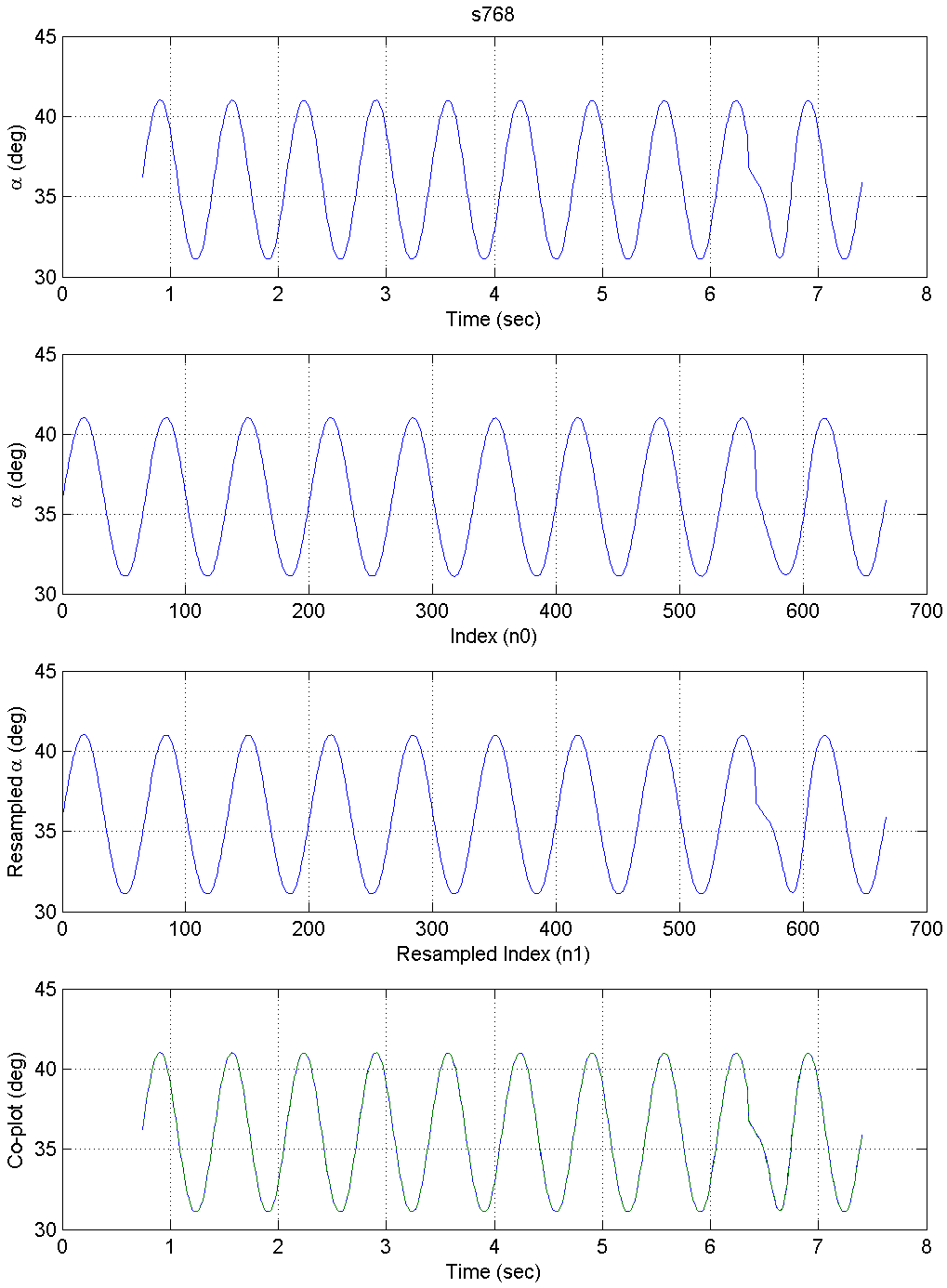

Figure 23. Input Measurement with a Timing Delay and Re-sampled Input.

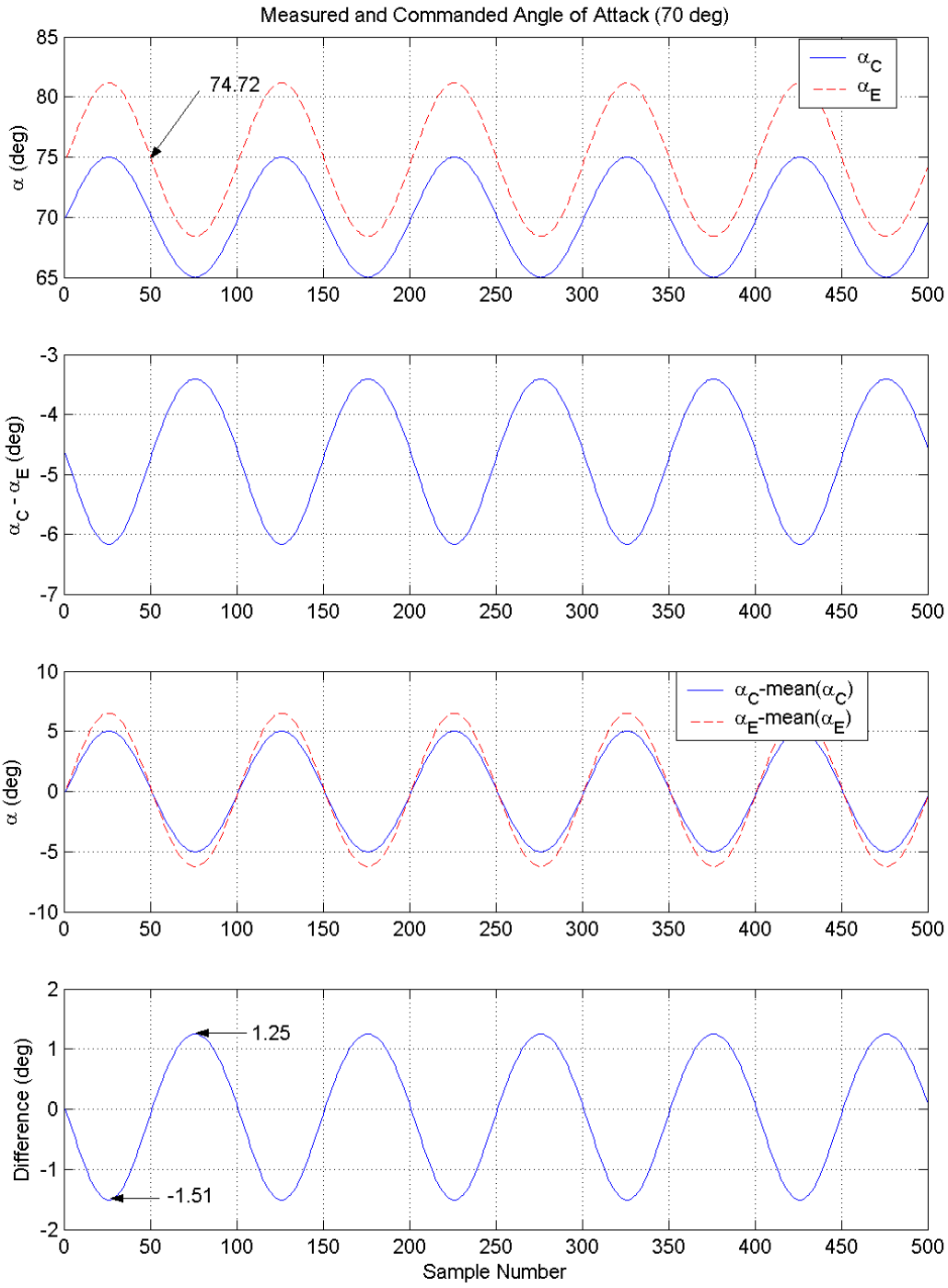

Figure 24. Measured and Commanded Angles of Attack: 1.0 Hz and α_0=70°.

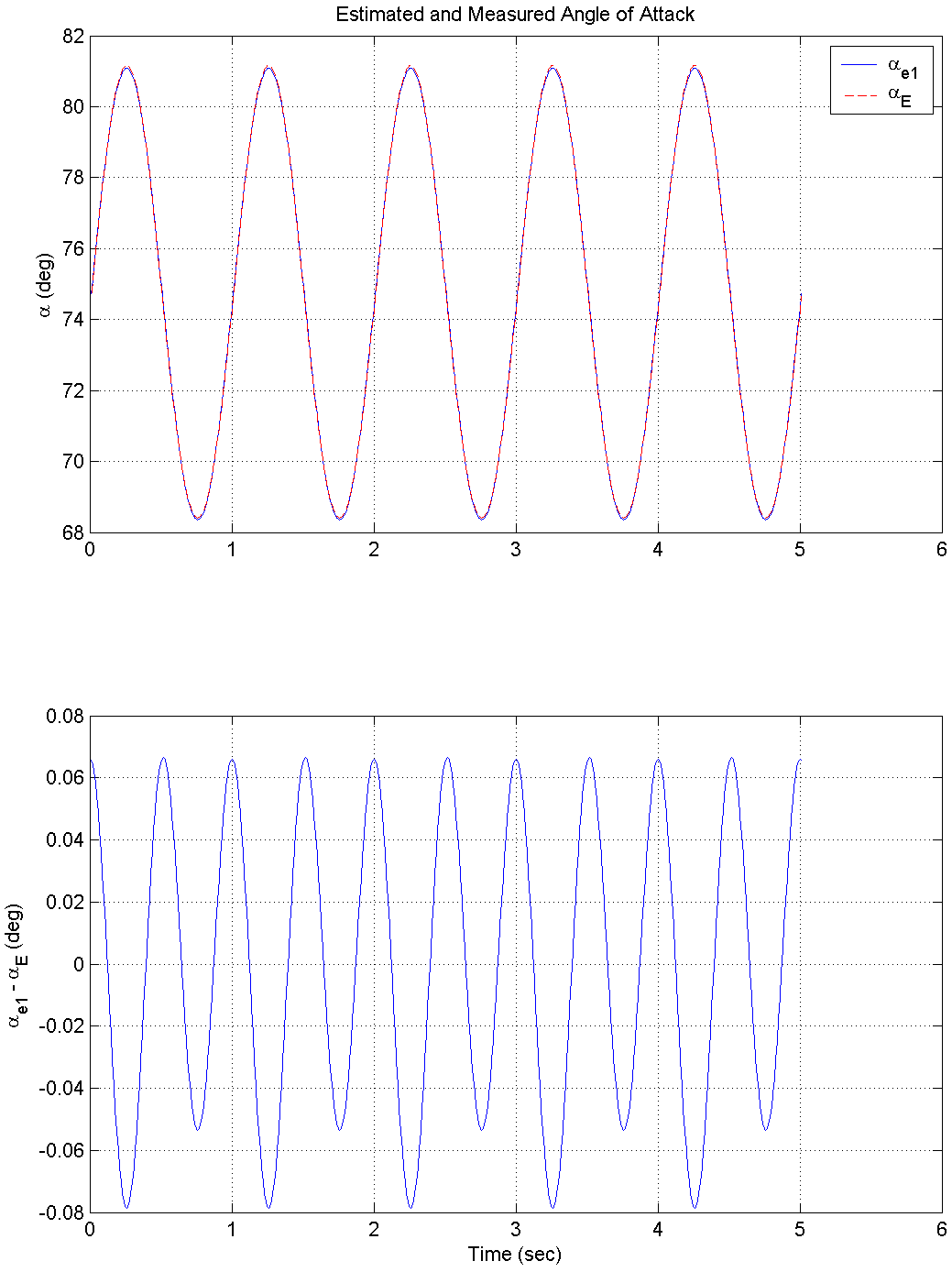

Figure 25. Estimated and Commanded Angles of Attack: 1.0 Hz and α_0=70°.

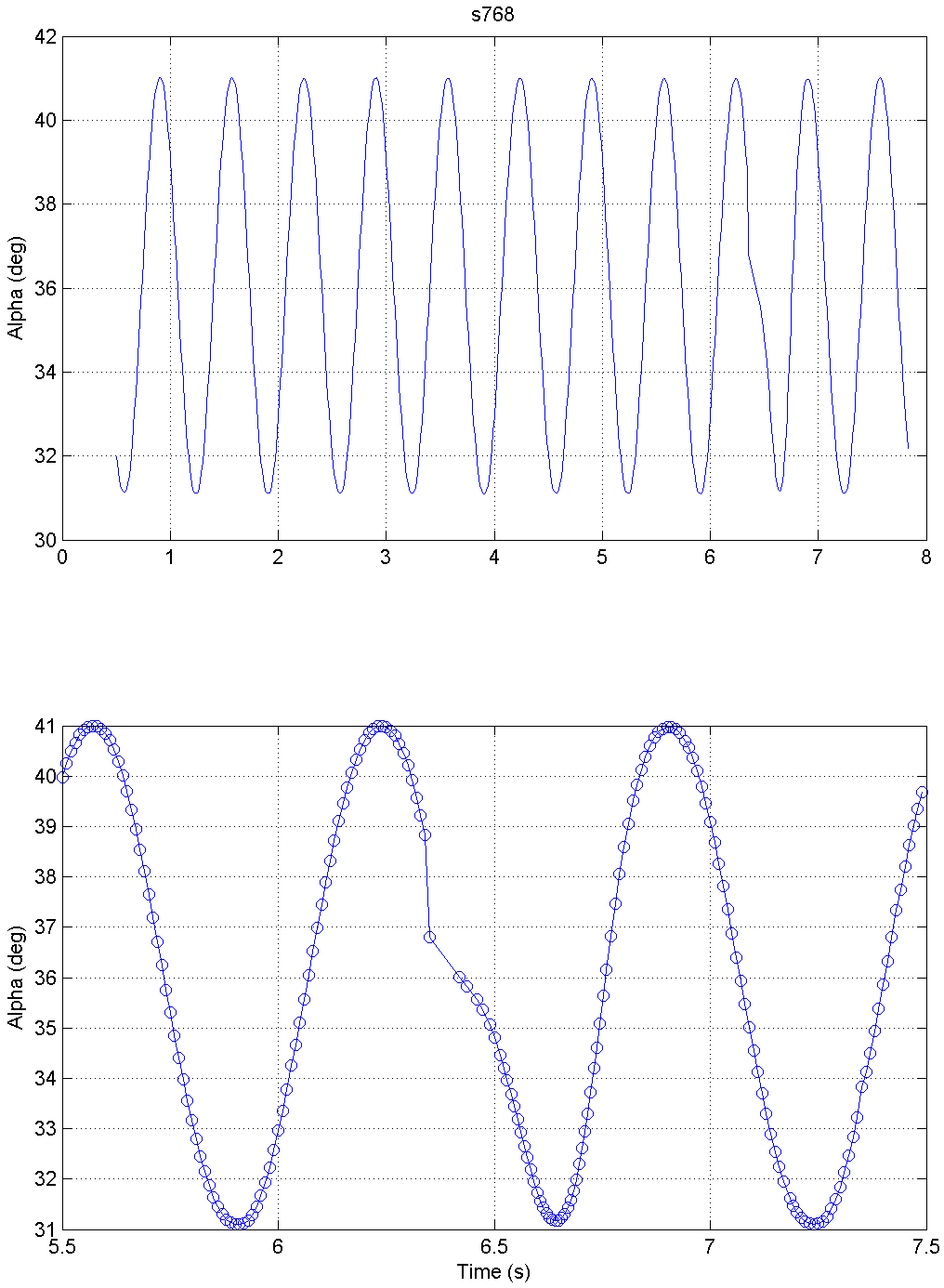

Figure 26. Jump in Angle of Attack Time History: 1.5 Hz and α_0=35°.

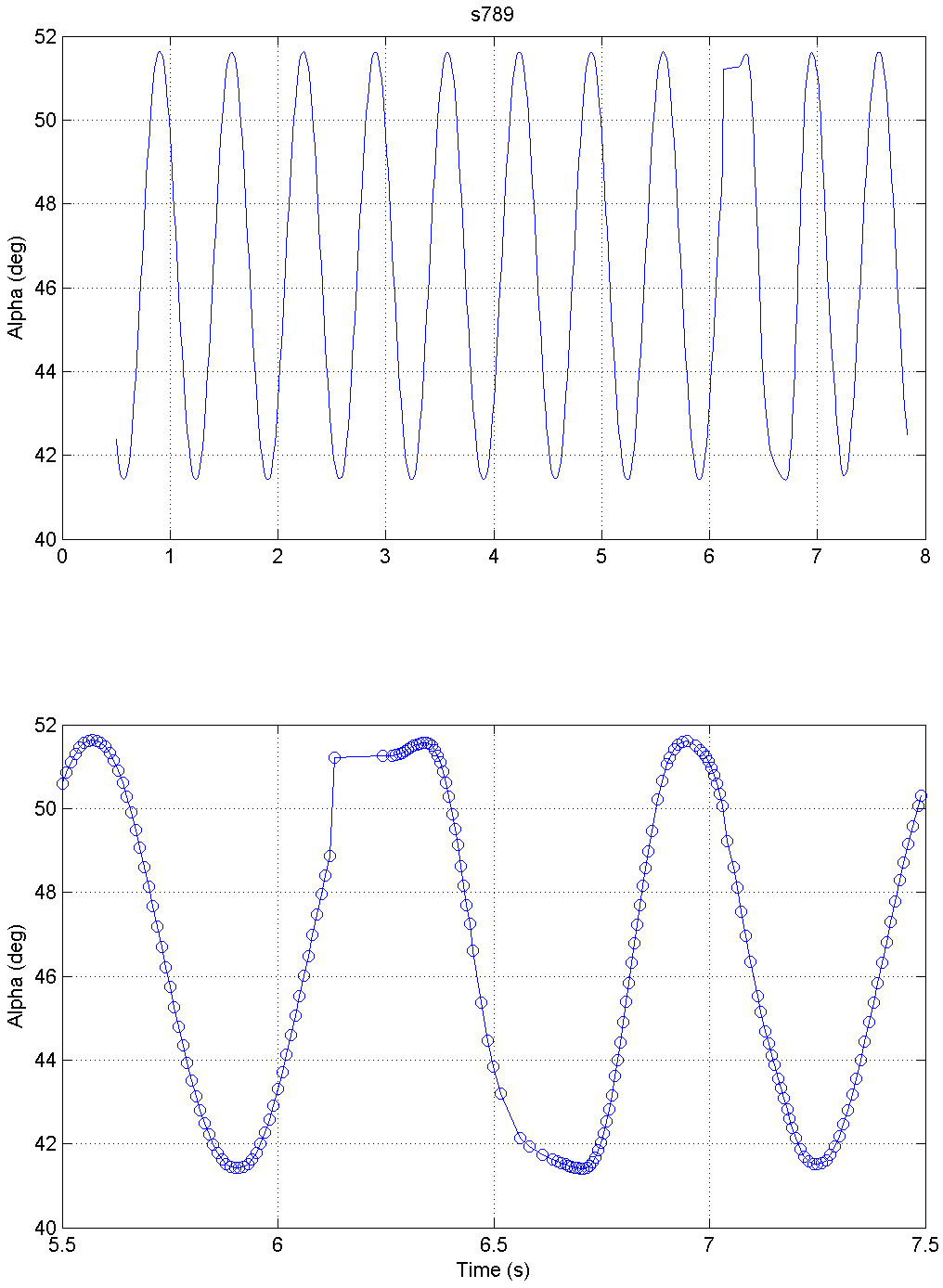

Figure 27. Jump in Angle of Attack Time History: 1.5 Hz and α_0=45°.

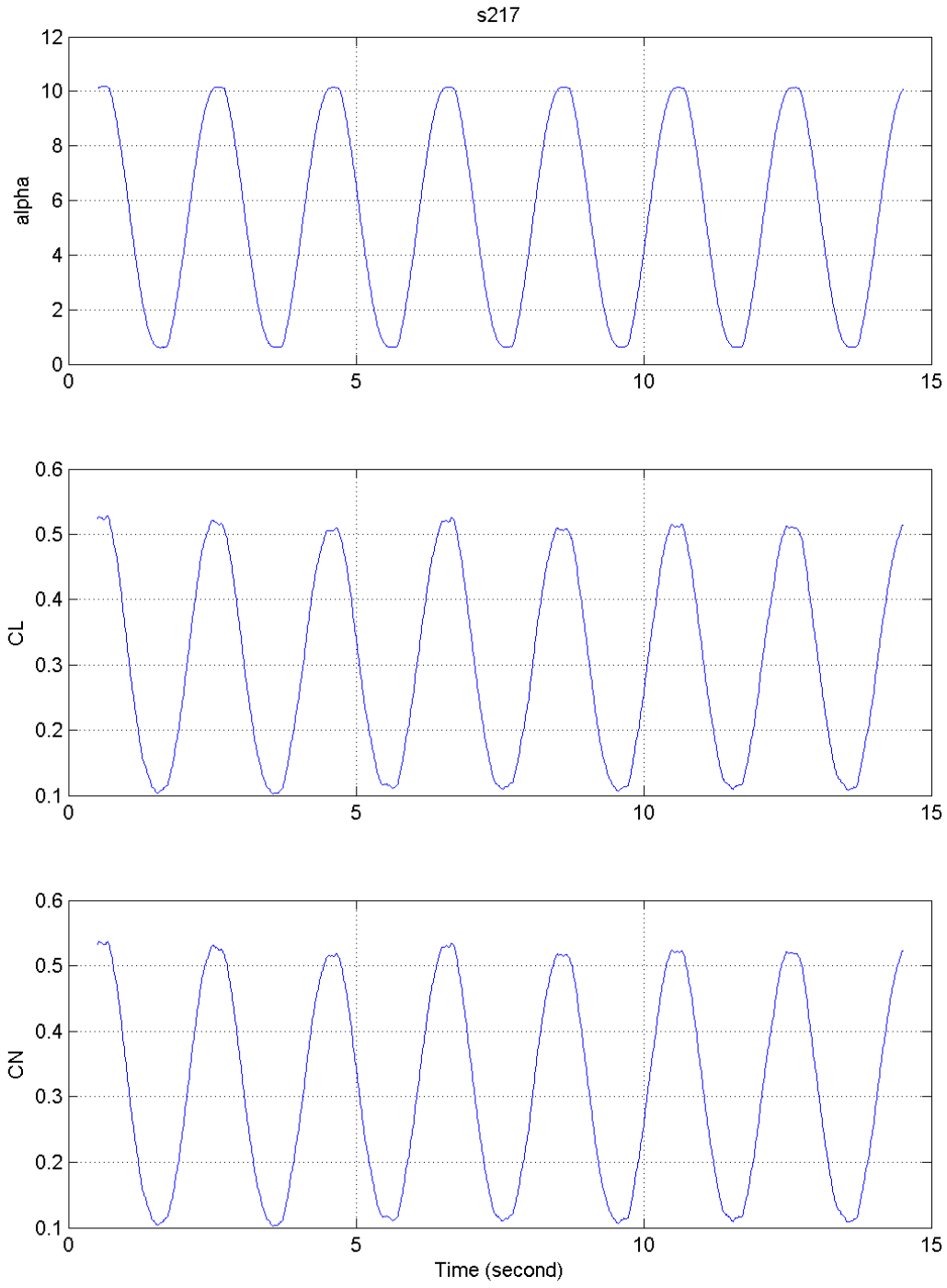

Figure 28. Saturated Input Command (Angle of Attack) and Corresponding C_L and C_N Time Histories: 0.5 Hz and α_0=5°.

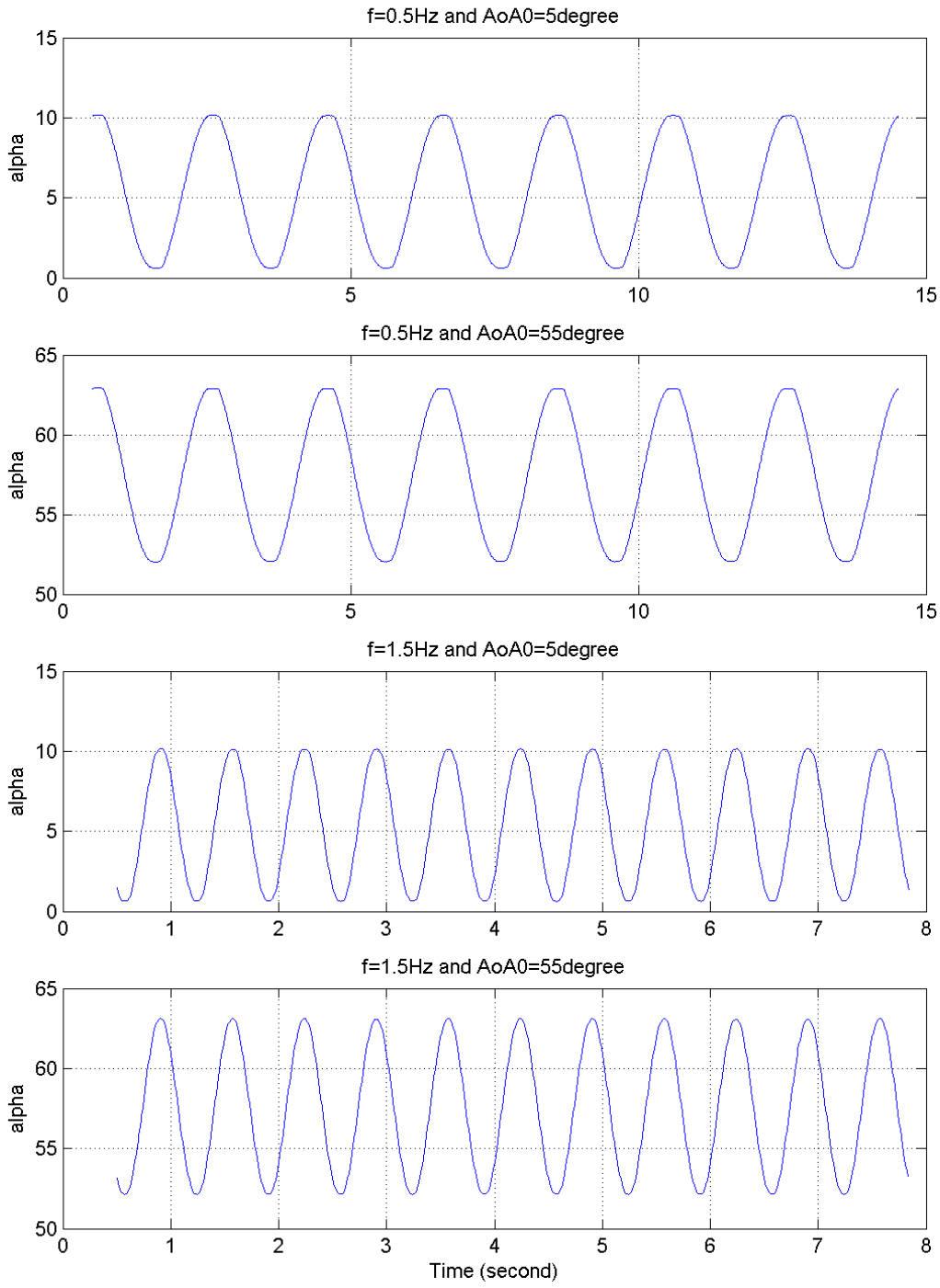

Figure 29 Input Command Waveforms with respect to Different Frequencies and Offset Angles.

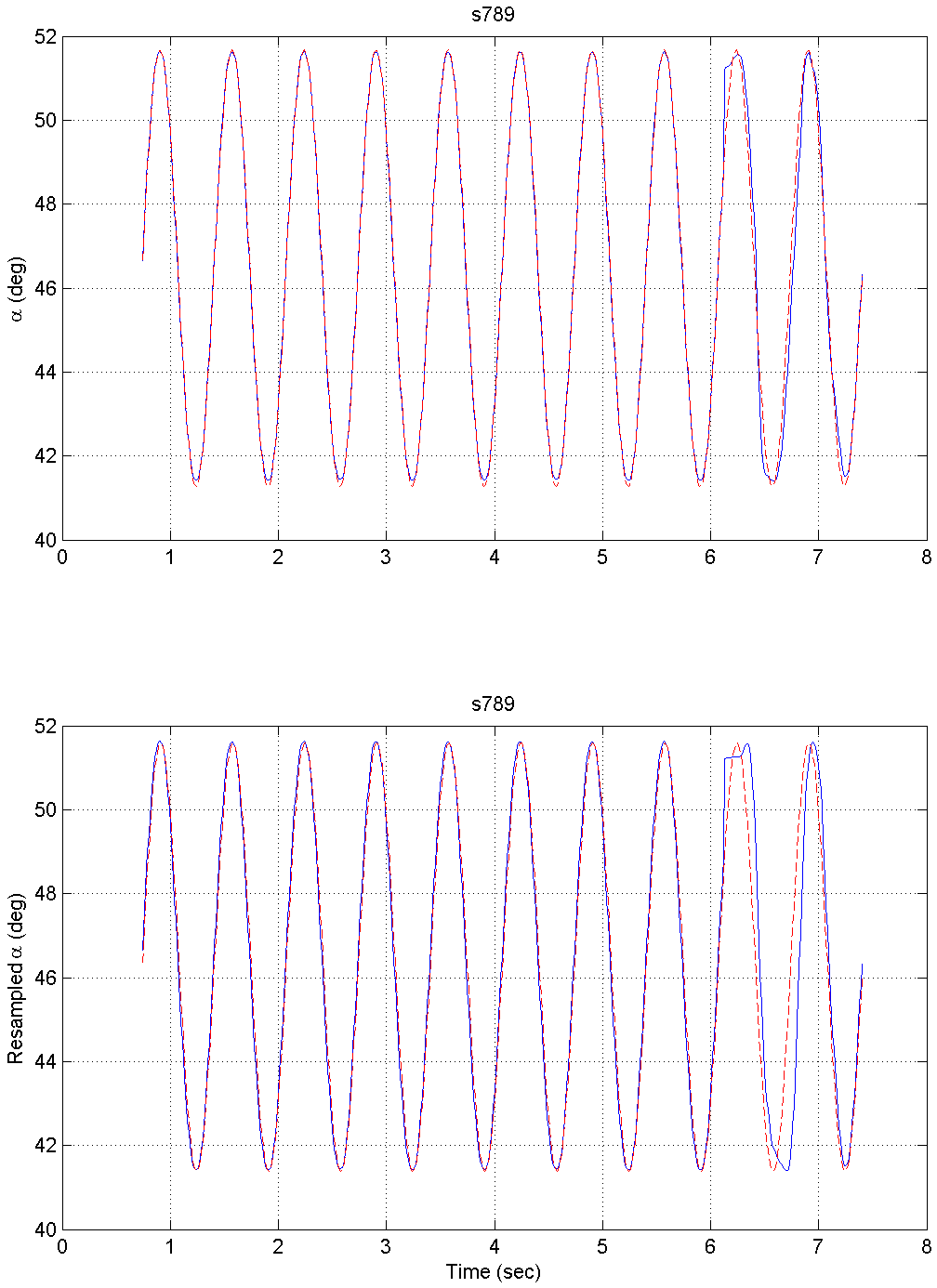

Figure 30. Co-plot of measured α (solid line) and estimated α (dashed line): Measured Test Data (Top) and Re-sampled Measured Data (Bottom).

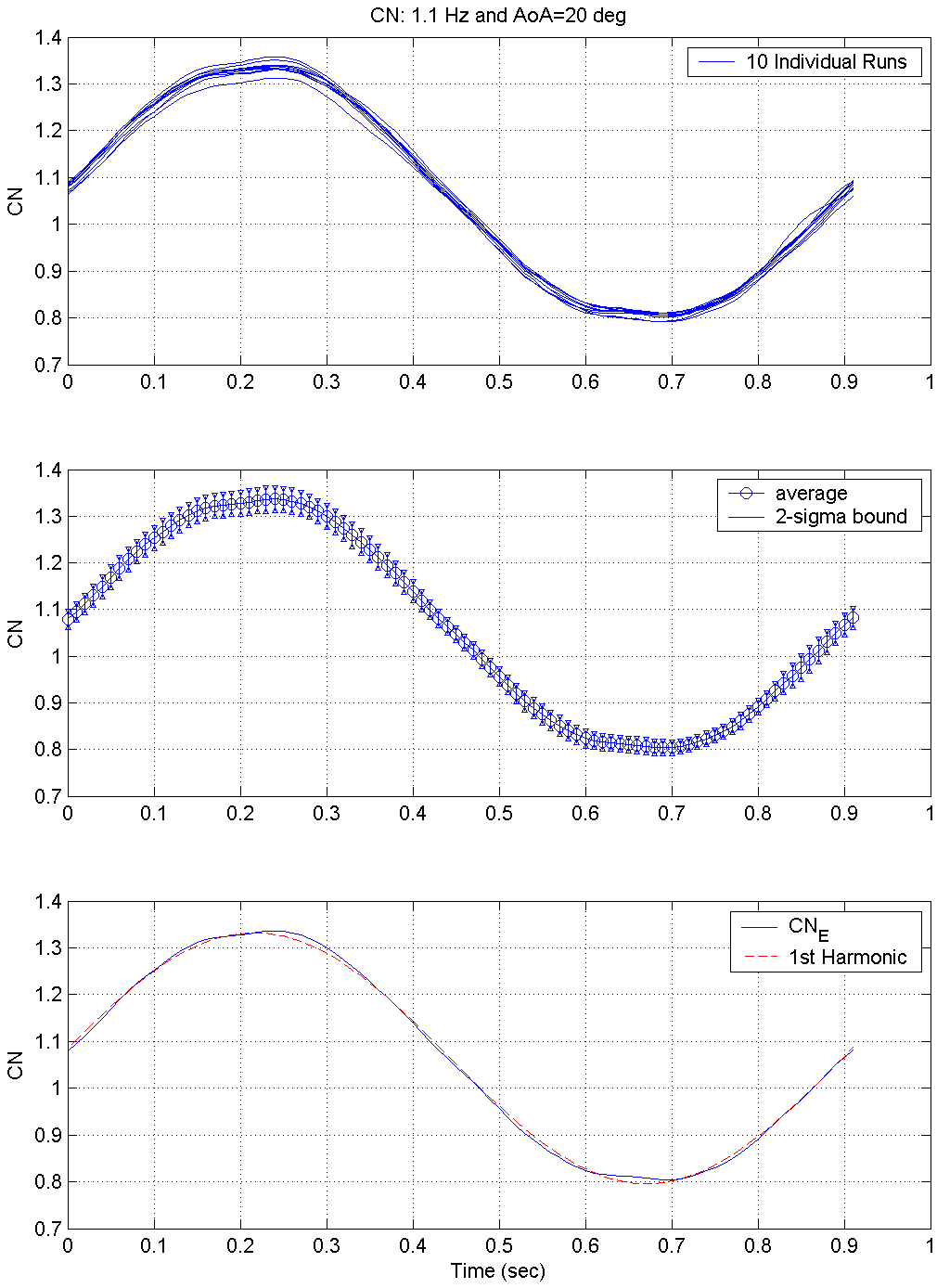

Figure 31. Co-plot of 10 Runs (Top), Mean Values with 2σ bound (Middle), and Co-plot of Measured C_N and Estimated C_N (Bottom).

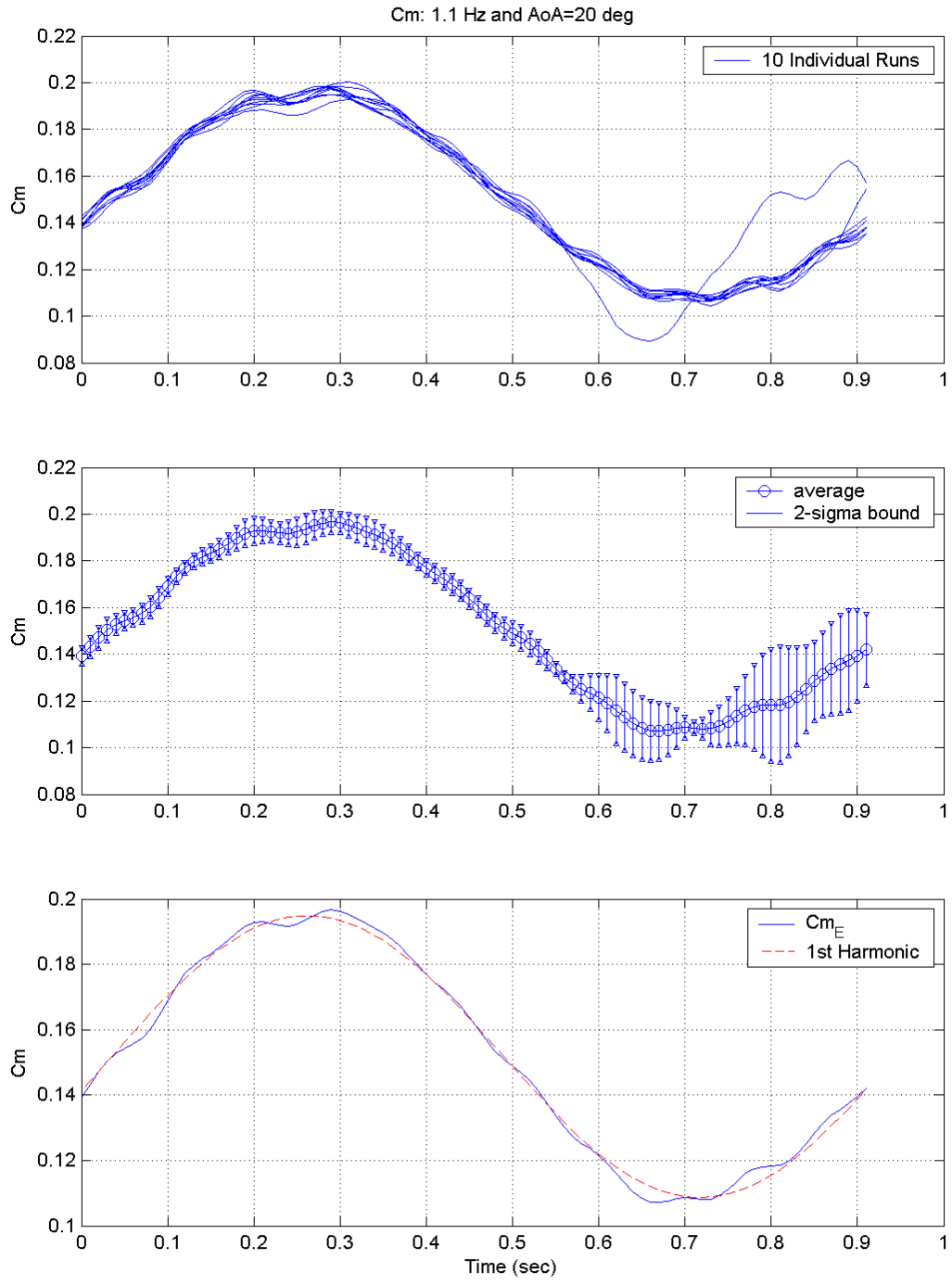

Figure 32. Co-plot of 10 Runs (Top), Mean Values with 2σ bound (Middle), and Co-plot of Measured C_m and Estimated C_m (Bottom).

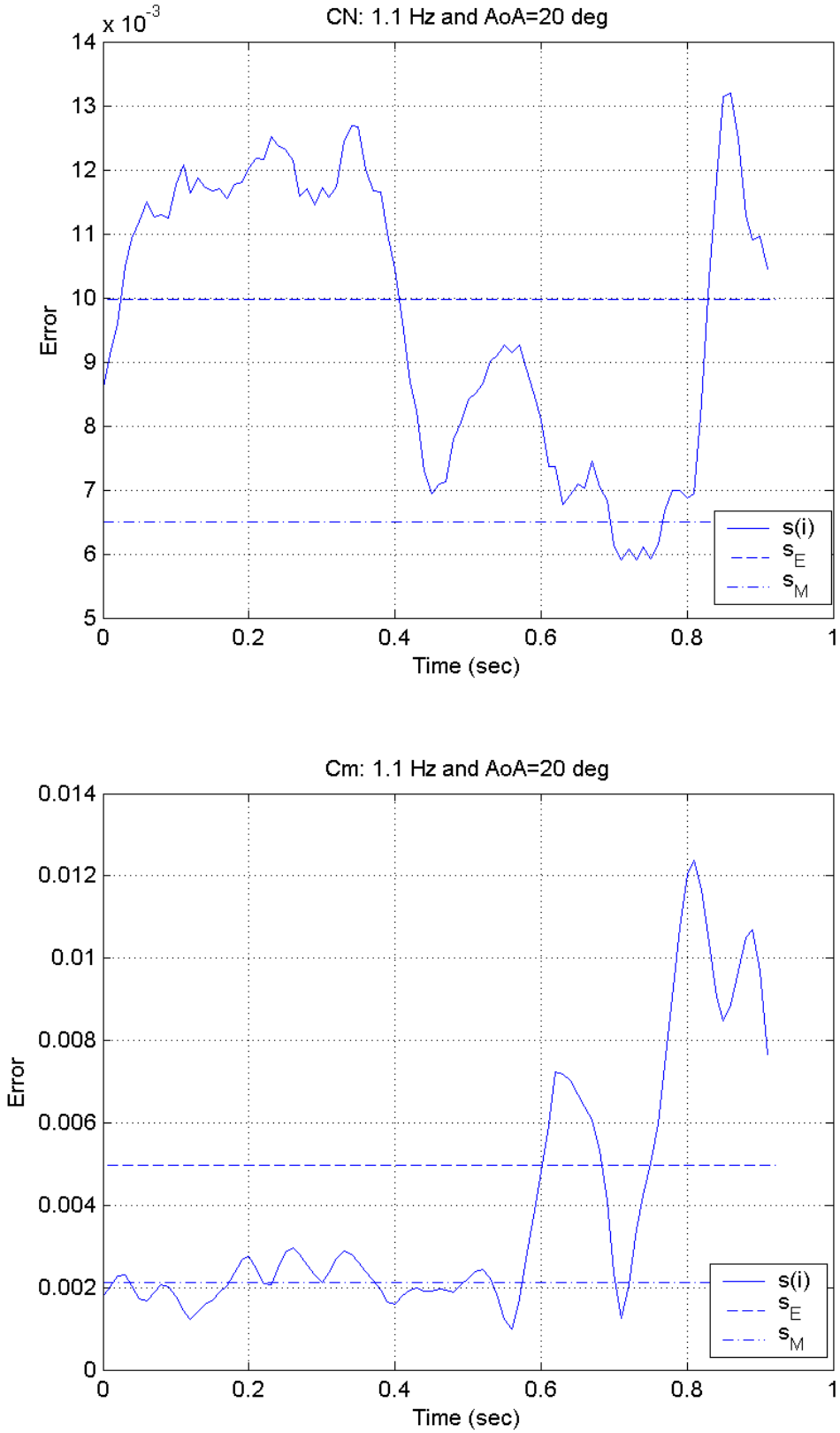

Figure 33. Error Plots for C_N and C_m.

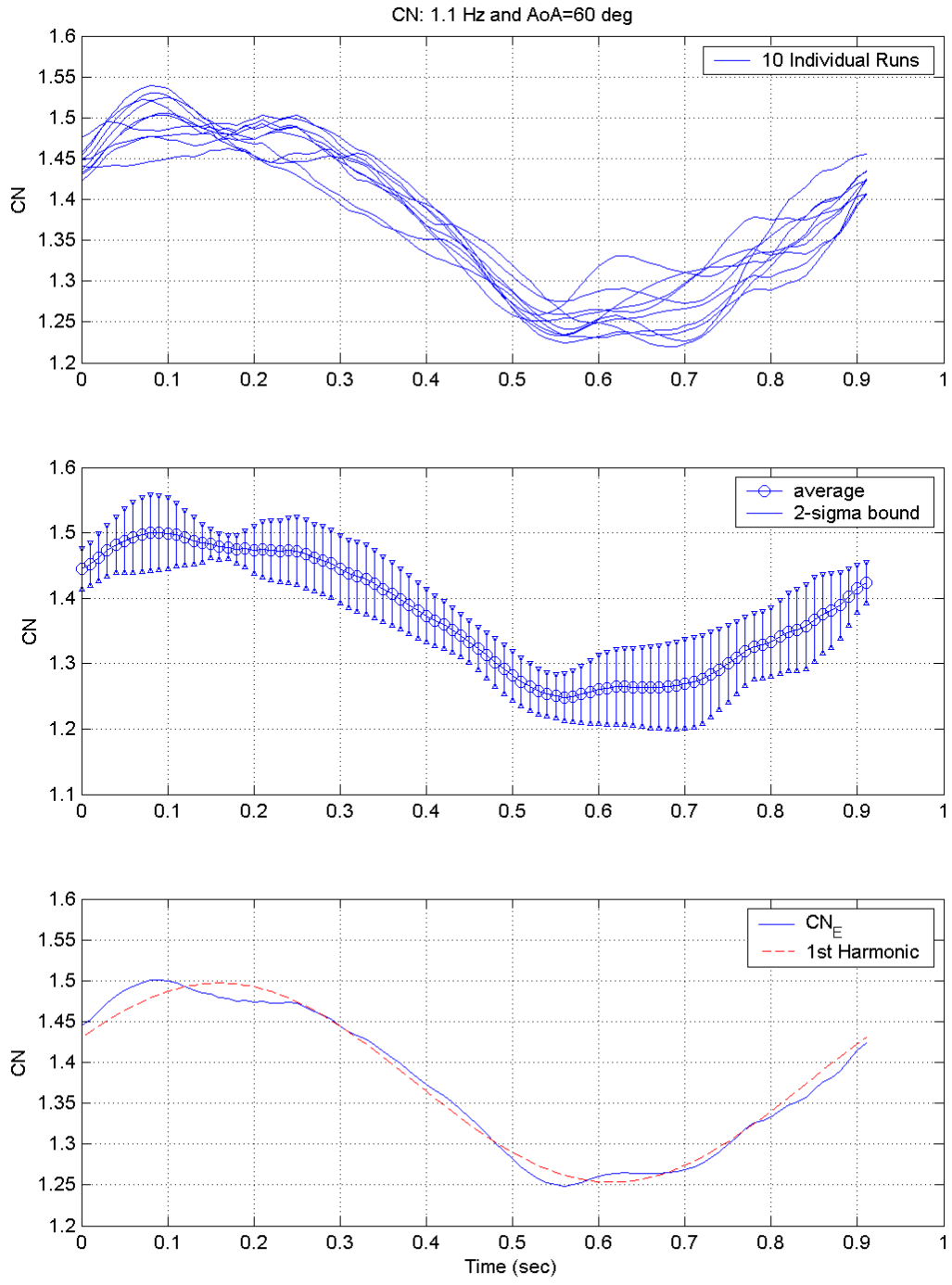

Figure 34. Co-plot of 10 Runs (Top), Mean Values with 2σ bound (Middle), and Co-plot of Measured C_N and Estimated C_N (Bottom).

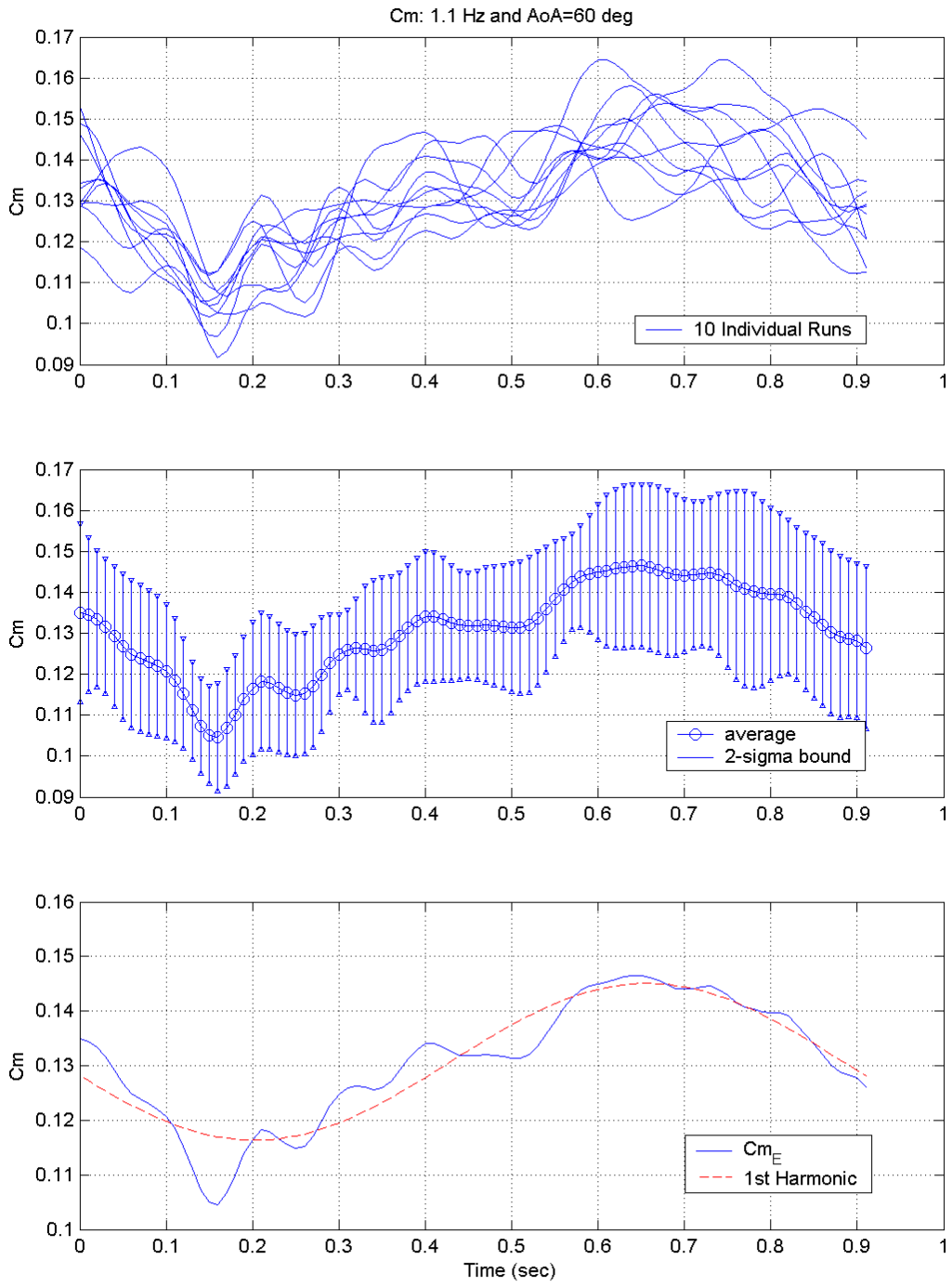

Figure 35. Co-plot of 10 Runs (Top), Mean Values with 2σ bound (Middle), and Co-plot of Measured C_m and Estimated C_m (Bottom).

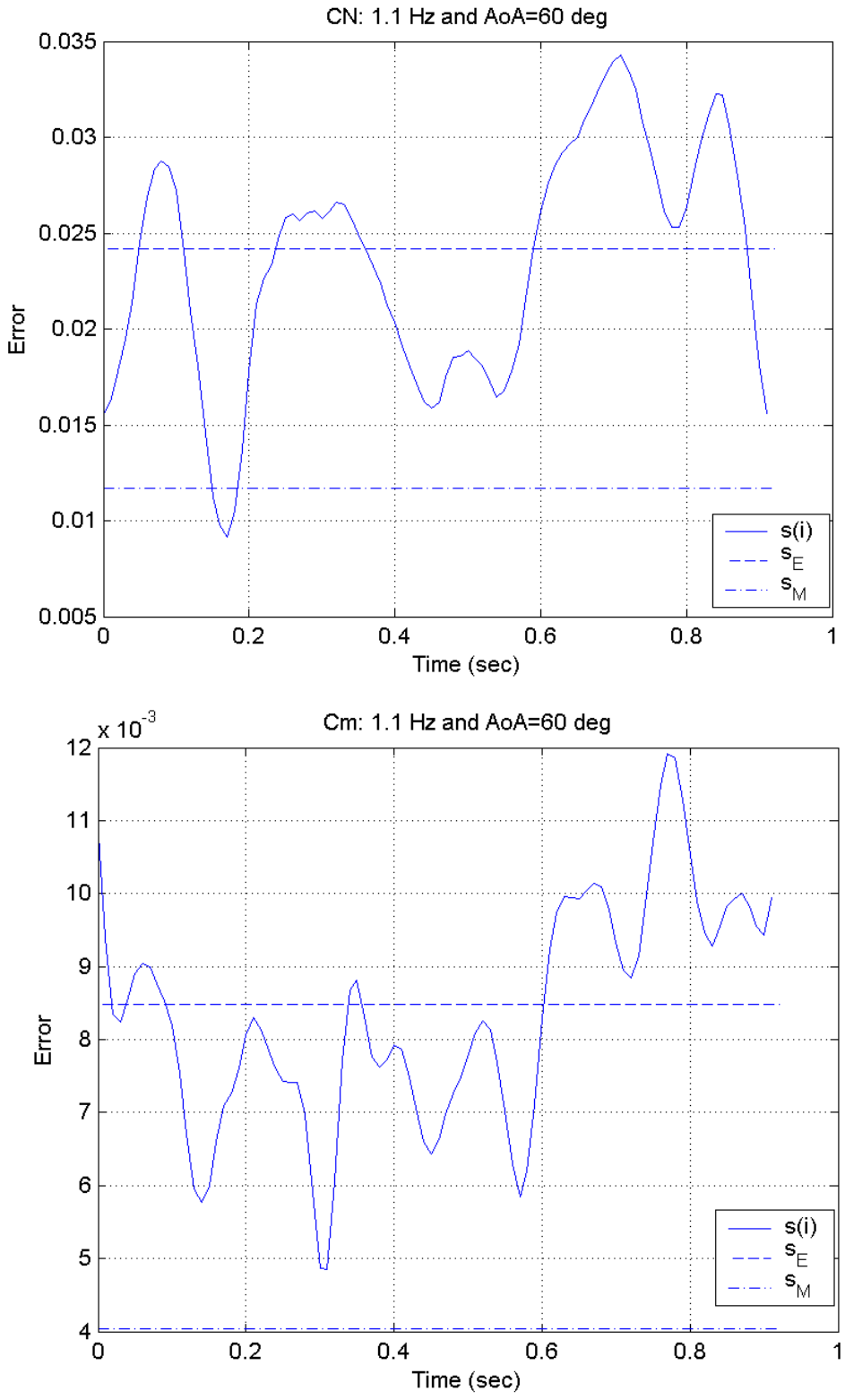

Figure 36. Error Plots for C_N and C_m.

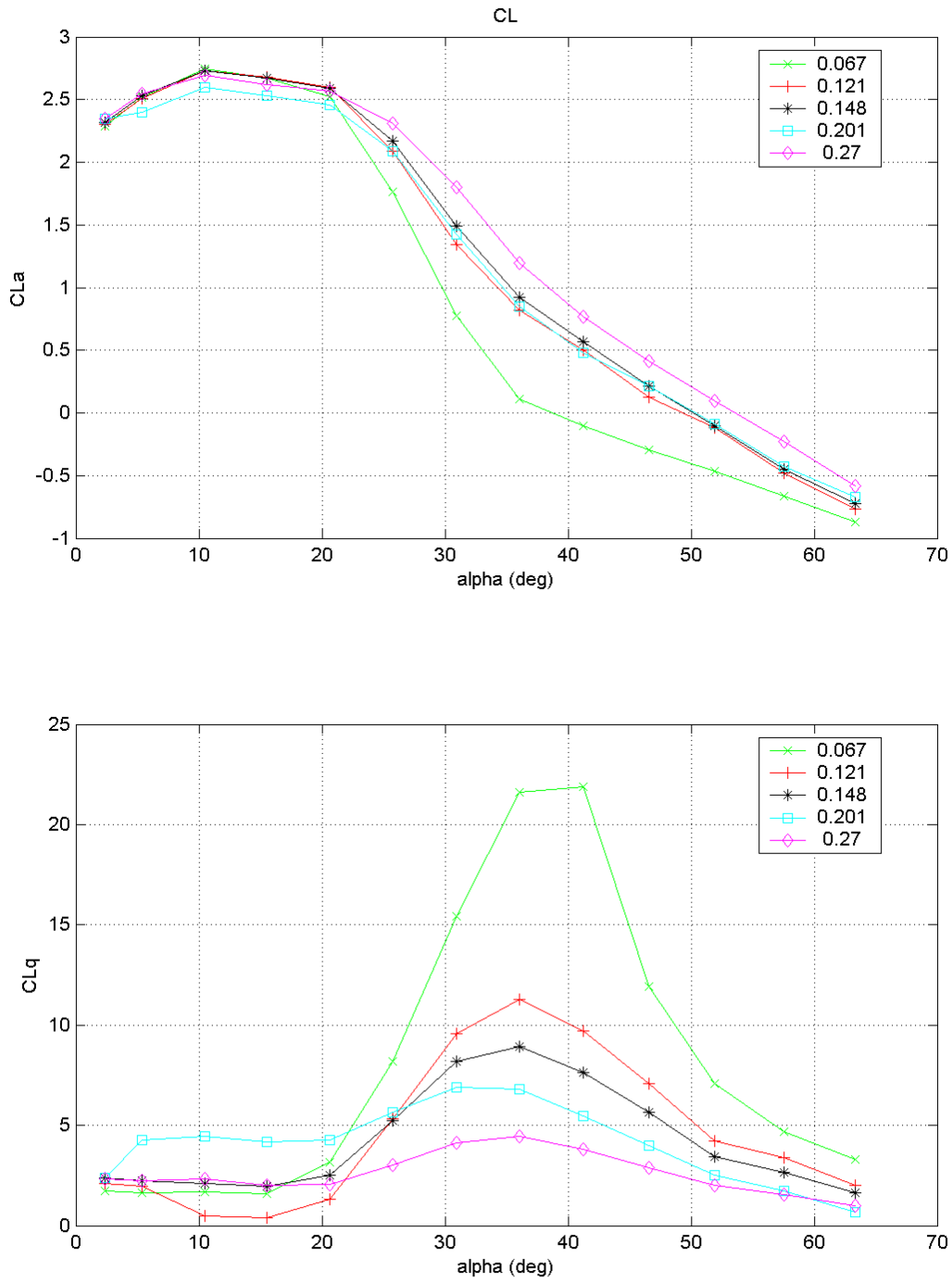

Figure 37. Variation of in-phase and out-of-phase components of C_L with angle of attack variation for different values of reduced frequency.

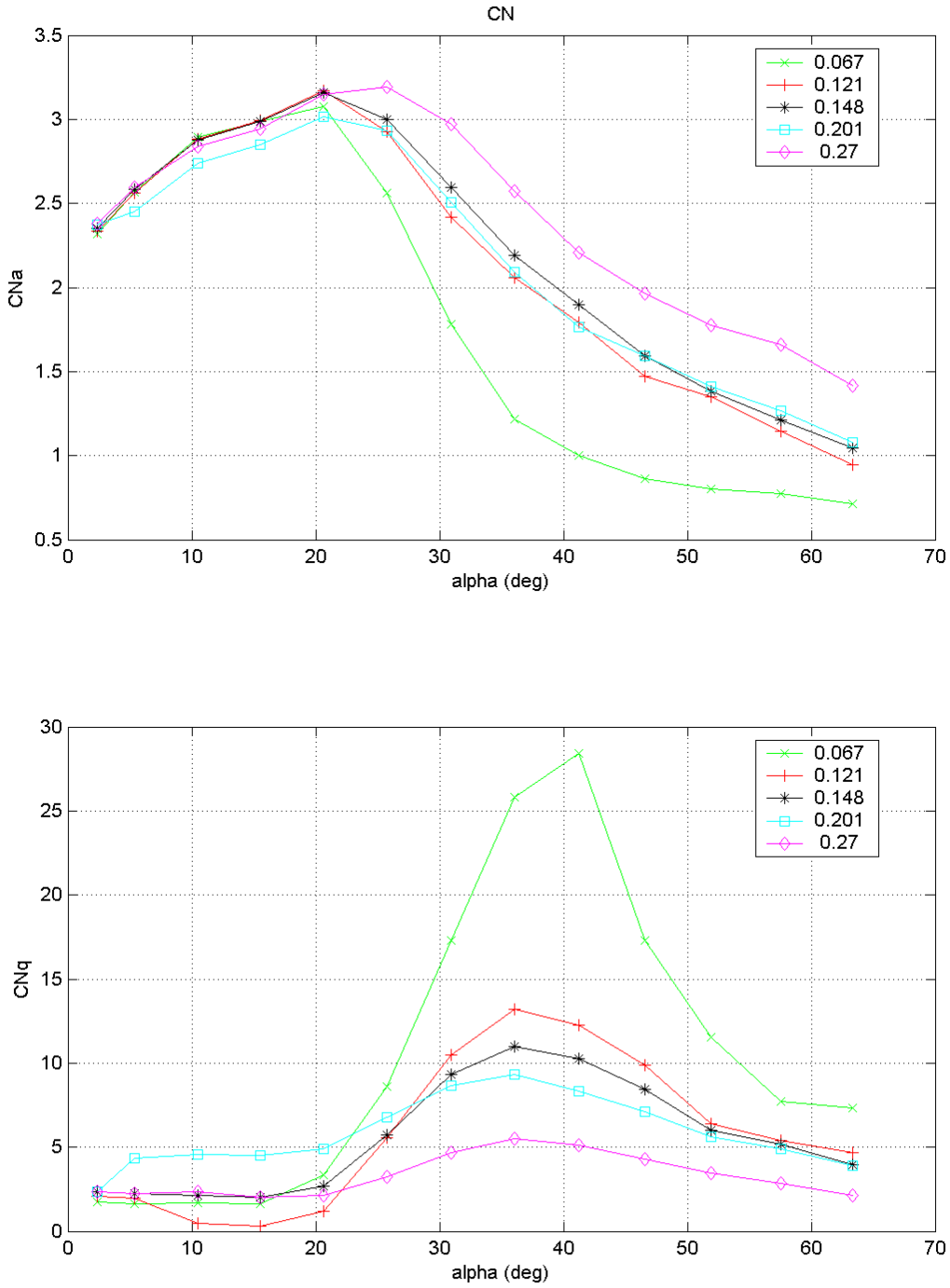

Figure 38. Variation of in-phase and out-of-phase components of C_N with angle of attack variation for different values of reduced frequency.

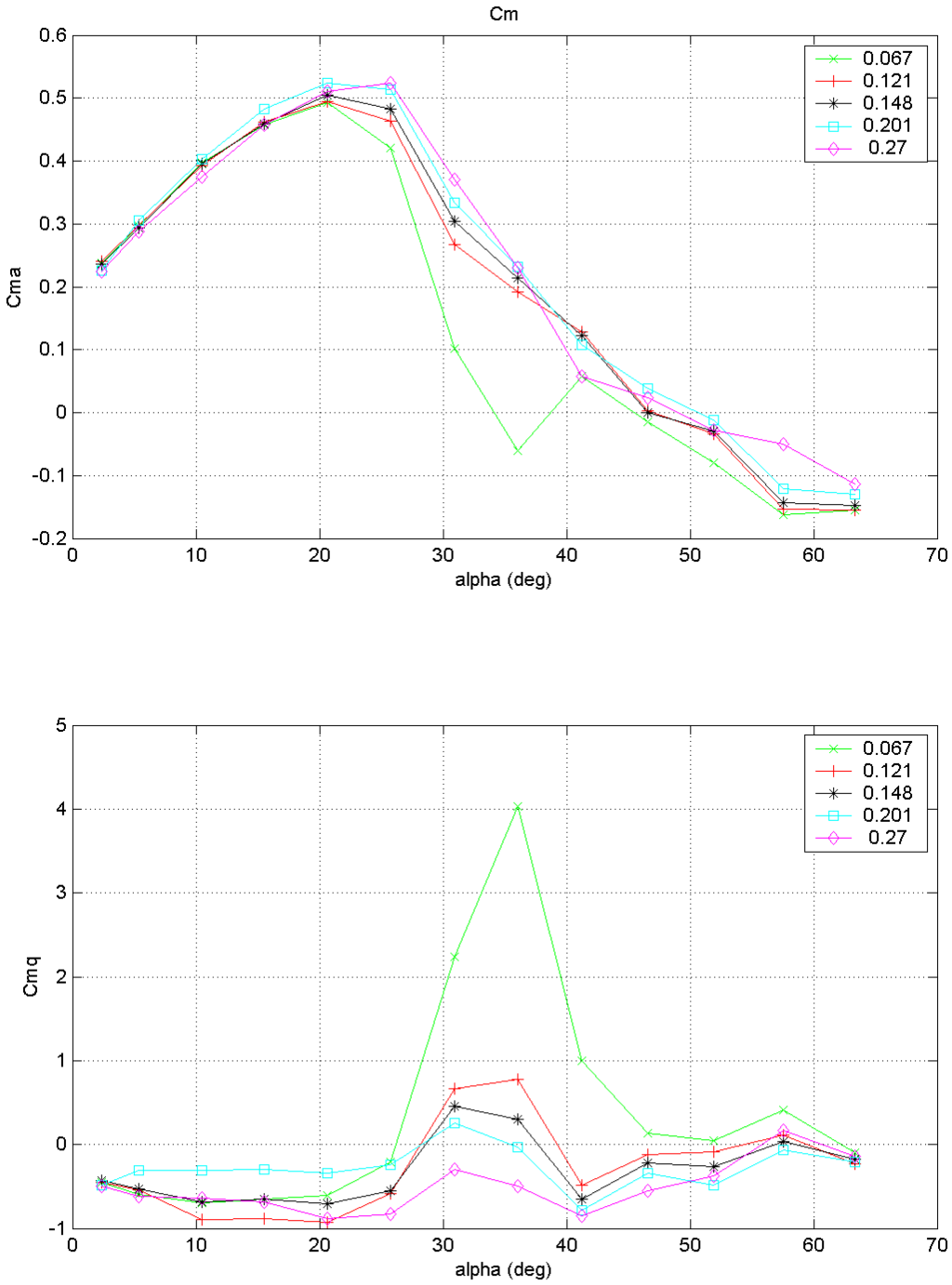

Figure 39. Variation of in-phase and out-of-phase components of C_m with angle of attack variation for different values of reduced frequency.

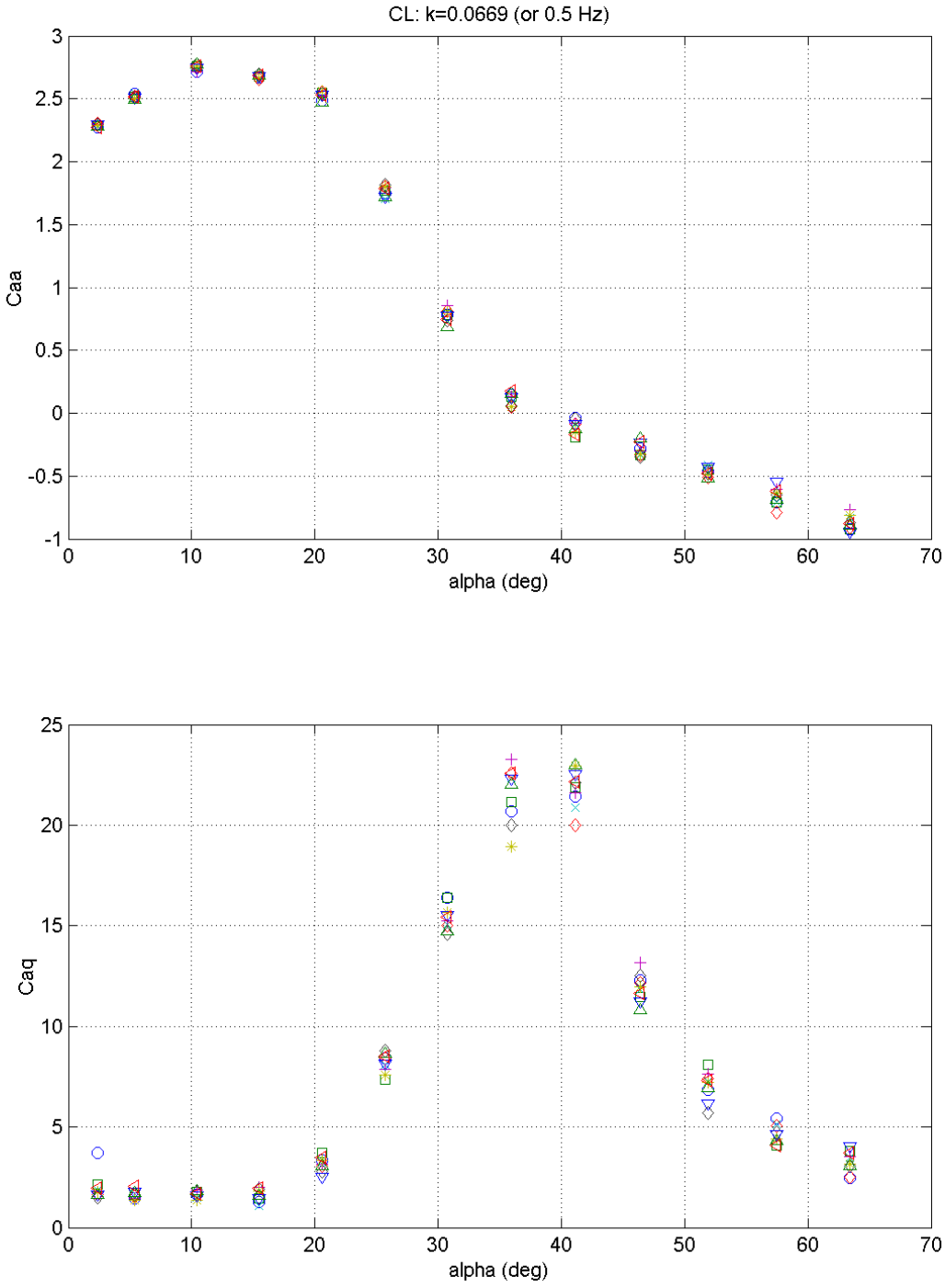

Figure 40. Each single-run's variation of in-phase and out-of-phase components of C_L with angle of attack variation for f=0.5 Hz.

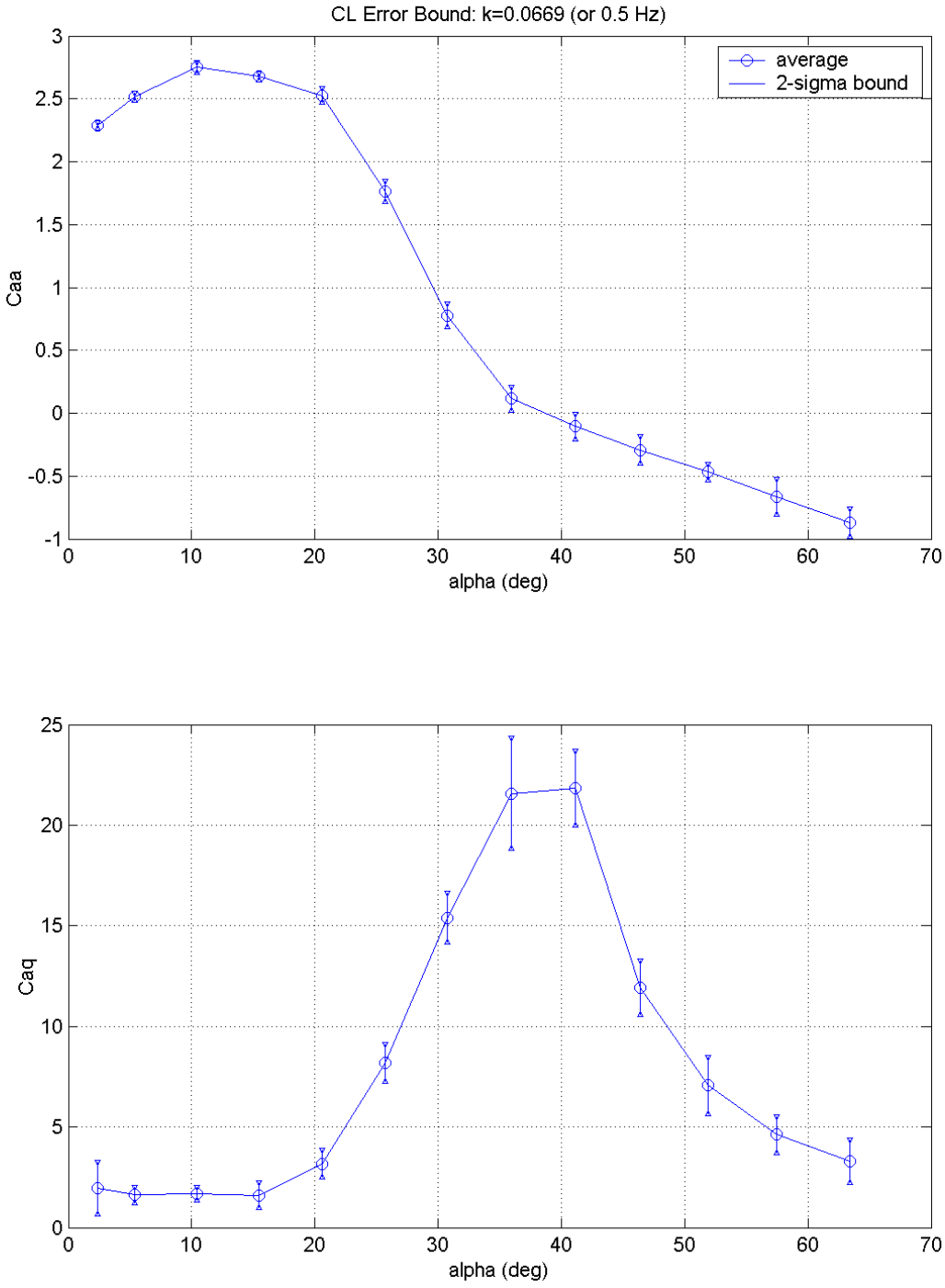

Figure 41. Mean values with 2σ bounds of in-phase and out-of-phase components of C_L with angle of attack variation for f=0.5 Hz.

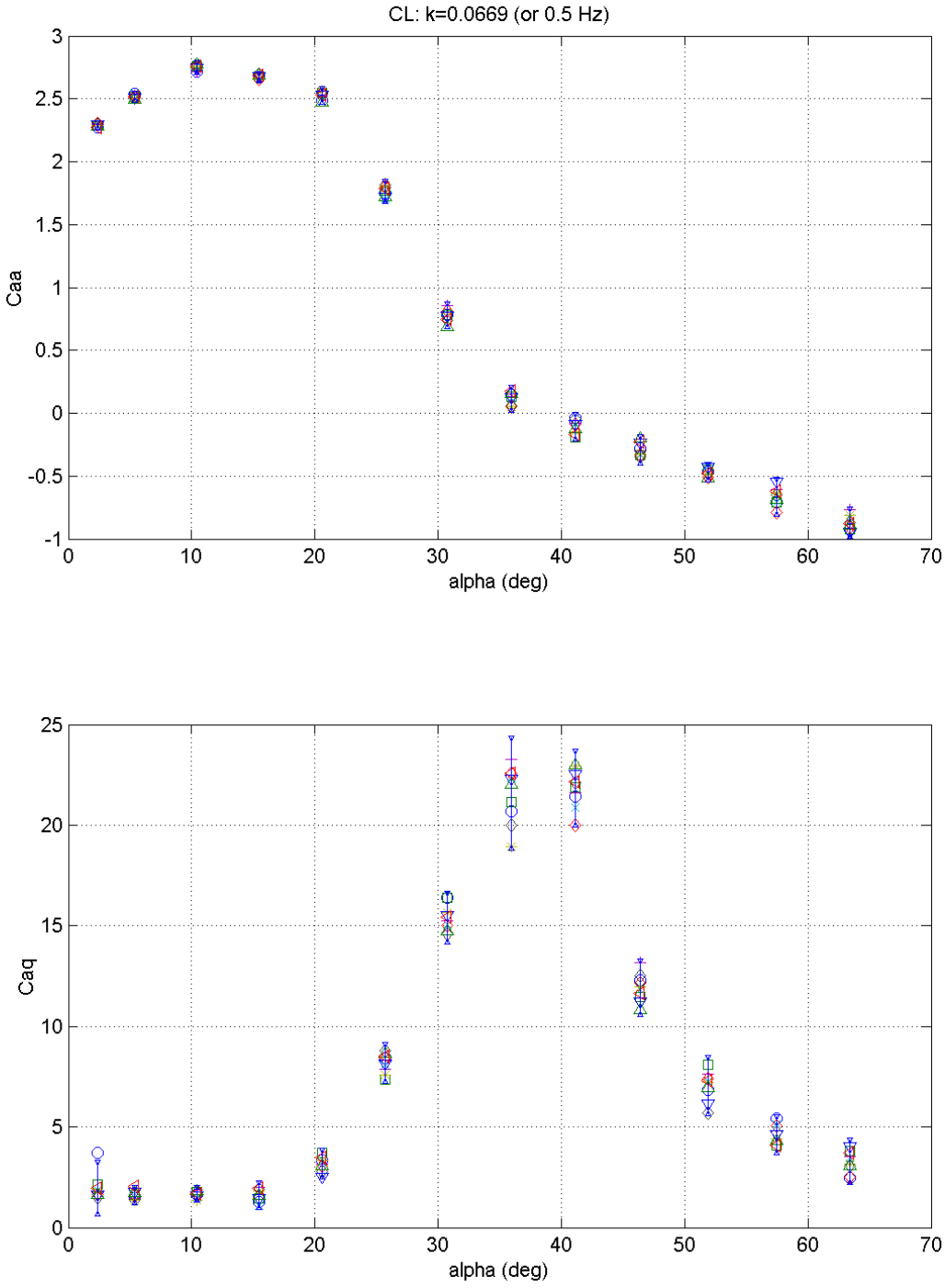

Figure 42. Co-plot of 10 single-runs with 2σ bounds of in-phase and out-of-phase components of C_L with angle of attack variation for f=0.5 Hz.

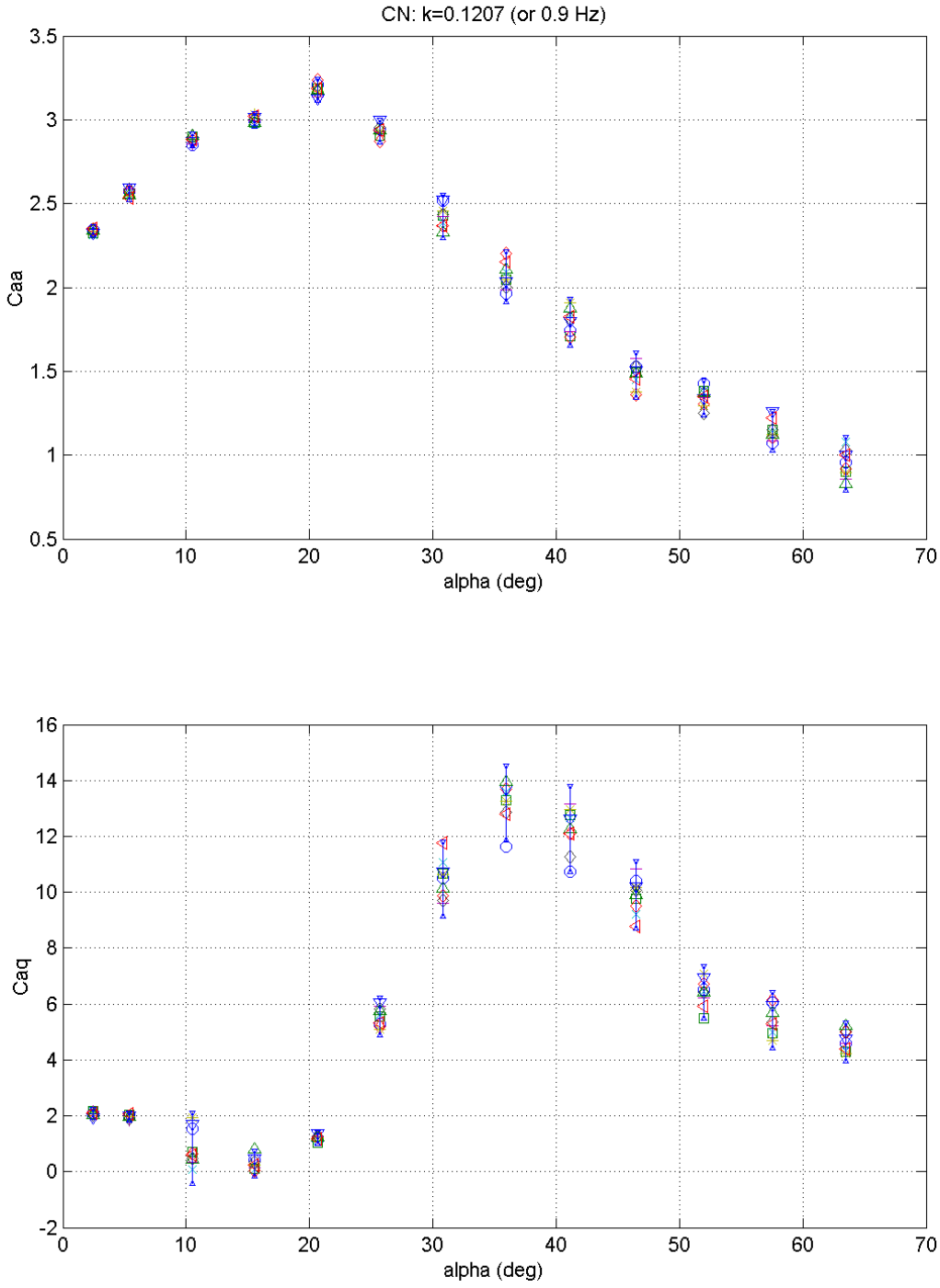

Figure 43. Co-plot of 10 single-runs with 2σ bounds of in-phase and out-of-phase components of C_N with angle of attack variation for f=0.9 Hz.

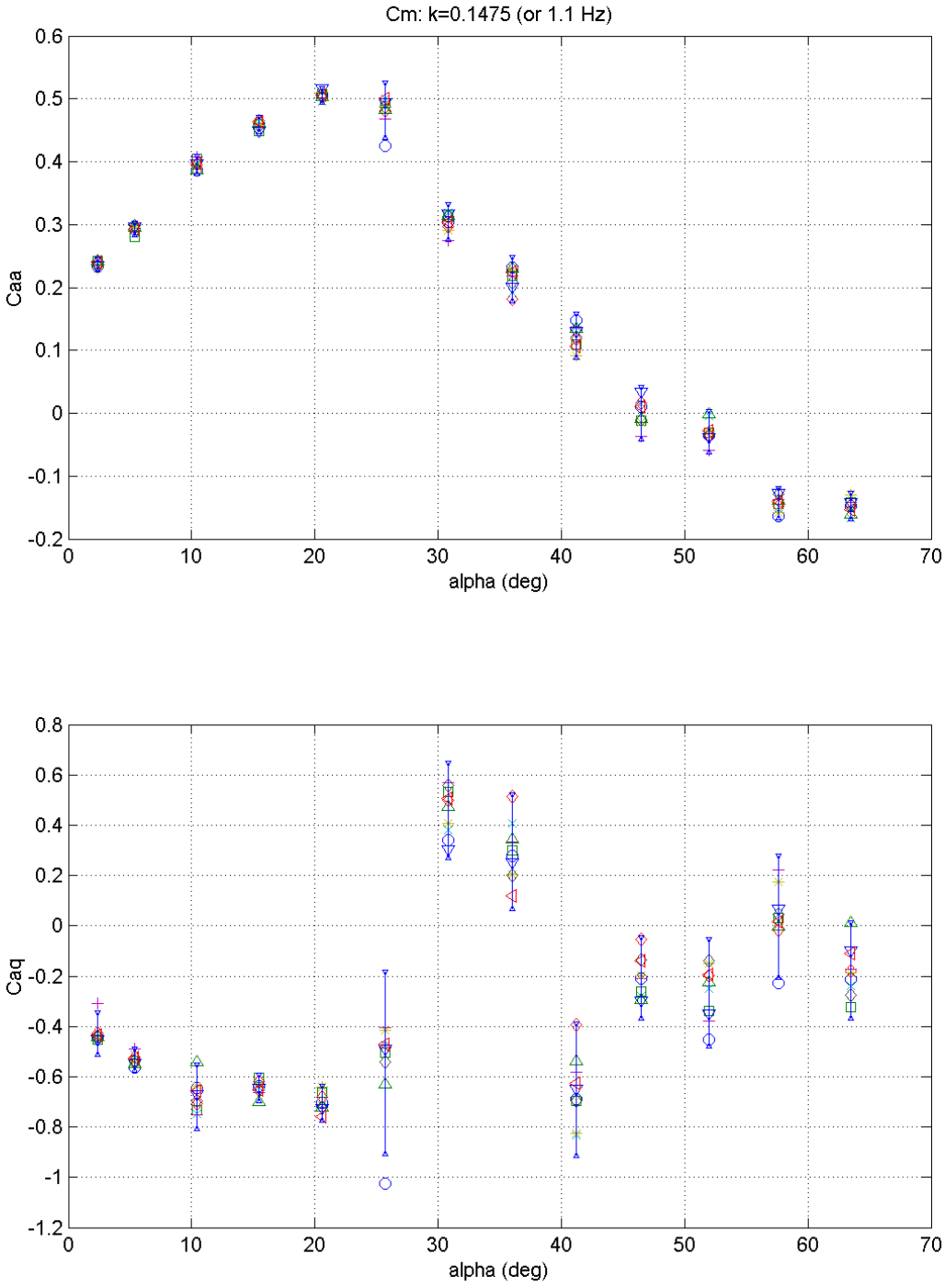

Figure 44. Co-plot of 10 single-runs with 2σ bounds of in-phase and out-of-phase components of C_m with angle of attack variation for f=1.1 Hz.

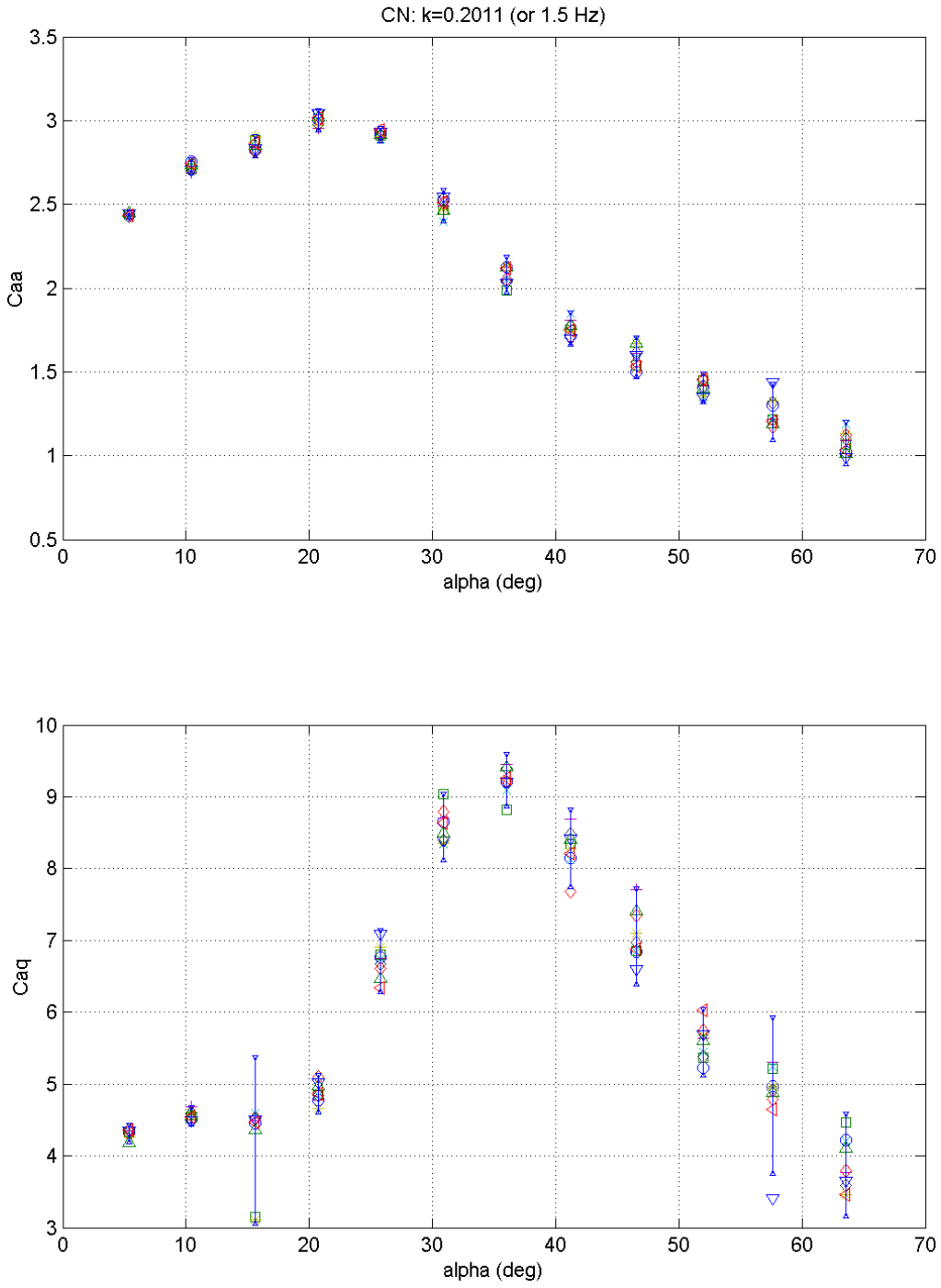

Figure 45. Co-plot of 10 single-runs with 2σ bounds of in-phase and out-of-phase components of C_N with angle of attack variation for f=1.5 Hz.

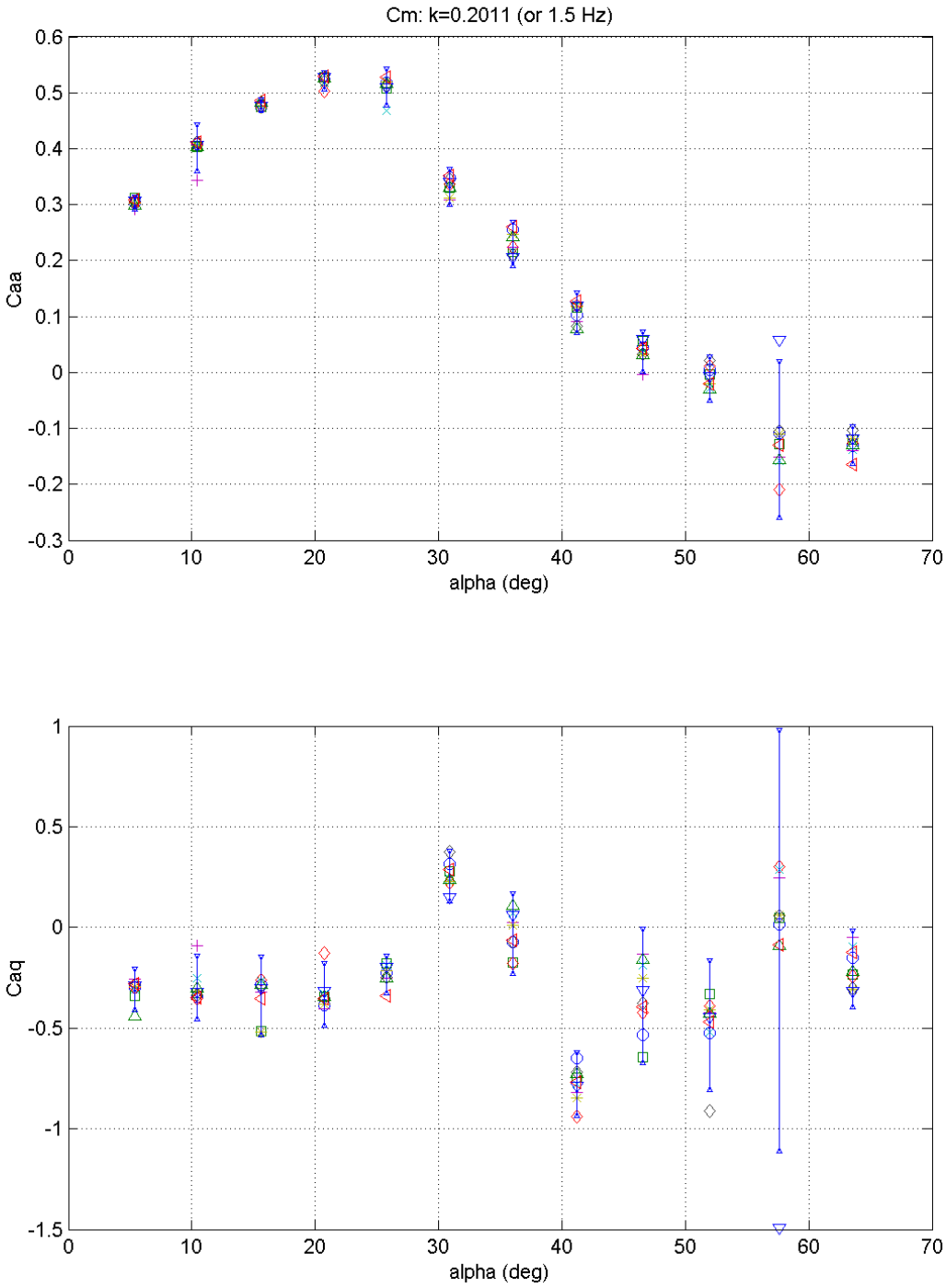

Figure 46. Co-plot of 10 single-runs with 2σ bounds of in-phase and out-of-phase components of C_m with angle of attack variation for f=1.5 Hz.

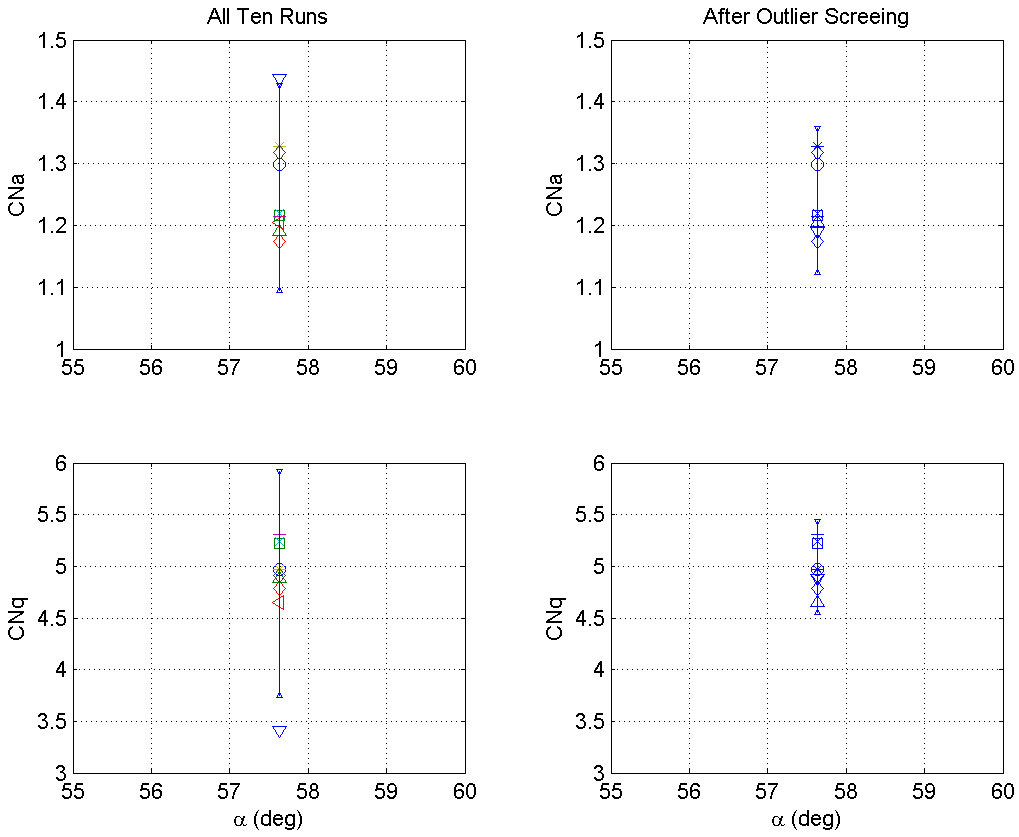

Figure 47. Outlier Screening (All runs (left) vs. Selected runs (right)): Individual Runs (symbols) with 2σ confidence range (vertical lines).

REPORT DOCUMENTATION PAGE

Form Approved
OMB No. 0704-0188

1. REPORT DATE *(DD-MM-YYYY)*	2. REPORT TYPE	3. DATES COVERED *(From - To)*
01- 06 - 2004	Technical Memorandum	

4. TITLE AND SUBTITLE

Evaluation and Analysis of F-16XL Wind Tunnel Data From Static and Dynamic Tests

5a. CONTRACT NUMBER

5b. GRANT NUMBER

5c. PROGRAM ELEMENT NUMBER

6. AUTHOR(S)

Kim, Sungwan; Murphy, Patrick C.; and Klein, Vladislav

5d. PROJECT NUMBER

5e. TASK NUMBER

5f. WORK UNIT NUMBER

762-20-41-03

7. PERFORMING ORGANIZATION NAME(S) AND ADDRESS(ES)

NASA Langley Research Center
Hampton, VA 23681-2199

8. PERFORMING ORGANIZATION REPORT NUMBER

L-18380

9. SPONSORING/MONITORING AGENCY NAME(S) AND ADDRESS(ES)

National Aeronautics and Space Administration
Washington, DC 20546-0001

10. SPONSOR/MONITOR'S ACRONYM(S)

NASA

11. SPONSOR/MONITOR'S REPORT NUMBER(S)

NASA/TM-2004-213234

12. DISTRIBUTION/AVAILABILITY STATEMENT

Unclassified - Unlimited
Subject Category 02
Availability: NASA CASI (301) 621-0390 Distribution: Standard

13. SUPPLEMENTARY NOTES

Kim and Murphy: NASA Langley Research Center, Hampton, Virginia; Klein: The George Washington University, Hampton, Virginia.
An electronic version can be found at http://techreports.larc.nasa.gov/ltrs/ or http://ntrs.nasa.gov

14. ABSTRACT

A series of wind tunnel tests were conducted in the NASA Langley Research Center as part of an ongoing effort to develop and test mathematical models for aircraft rigid-body aerodynamics in nonlinear unsteady flight regimes. Analysis of measurement accuracy, especially for nonlinear dynamic systems that may exhibit complicated behaviors, is an essential component of this ongoing effort. In this report, tools for harmonic analysis of dynamic data and assessing measurement accuracy are presented. A linear aerodynamic model is assumed that is appropriate for conventional forced-oscillation experiments, although more general models can be used with these tools. Application of the tools to experimental data is demonstrated and results indicate the levels of uncertainty in output measurements that can arise from experimental setup, calibration procedures, mechanical limitations, and input errors.

15. SUBJECT TERMS

Wind tunnel testing; Static and dynamic data; Harmonic analysis; Measurement accuracy

16. SECURITY CLASSIFICATION OF:			17. LIMITATION OF ABSTRACT	18. NUMBER OF PAGES	19a. NAME OF RESPONSIBLE PERSON
a. REPORT	b. ABSTRACT	c. THIS PAGE			STI Help Desk (email: help@sti.nasa.gov)
					19b. TELEPHONE NUMBER *(Include area code)*
U	U	U	UU	86	(301) 621-0390